NASA CONTRACTOR REPORT

NASA CR-851

NASA CR-851

THERMAL AND HYDRAULIC PERFORMANCE OF POTASSIUM DURING CONDENSATION INSIDE SINGLE TUBES

by S. G. Sawochka

Prepared by
GENERAL ELECTRIC
Cincinnati, Ohio
for Lewis Research Center

NATIONAL AERONAUTICS AND SPACE ADMINISTRATION • WASHINGTON, D. C. • AUGUST 1967

NASA CR-851

THERMAL AND HYDRAULIC PERFORMANCE OF POTASSIUM DURING CONDENSATION INSIDE SINGLE TUBES

By S. G. Sawochka

Prepared under Contract No. NAS 3-2528 by
GENERAL ELECTRIC
Missile and Space Division
Cincinnati, Ohio

for Lewis Research Center

NATIONAL AERONAUTICS AND SPACE ADMINISTRATION

For sale by the Clearinghouse for Federal Scientific and Technical Information
Springfield, Virginia 22151 – CFSTI price $3.00

FOREWORD

The work described in this report is part of an alkali metal boiling and condensing heat transfer program conducted by the General Electric Company for the National Aeronautics and Space Administration under NASA Contract NAS 3-2528. The work was done under the technical management of Mr. F. E. Tippets, Missile and Space Division General Electric Company, and Miss Ruth N. Weltmann, Space Power Systems Division, NASA-Lewis Research Center.

PRECEDING PAGE BLANK NOT FILMED.

ABSTRACT

Forced convection heat transfer and pressure change data for condensation of potassium in vertical downflow inside single tubes are presented. These data, obtained at saturation temperatures from 1100°F to 1400°F, inlet vapor Mach numbers from about 0.1 to near 1.0 and local heat fluxes up to 300,000 Btu/hr-ft^2, provide a reasonable basis for thermal design of forced convection potassium condensers applicable to space power systems.

PRECEDING PAGE BLANK NOT FILMED.

TABLE OF CONTENTS

LIST OF FIGURES

LIST OF FIGURES (Cont'd)

LIST OF FIGURES (Cont'd)

LIST OF TABLES

NOMENCLATURE

A	Area, ft^2
a, b	Constants in wall temperature least squares equation
c_p	Liquid specific heat, $Btu/lb_m-°F$
D	Hydraulic diameter, ft
E	Probable error in condensing heat transfer coefficient
E'	Flowmeter output, millivolts
e	Thermocouple error, °F
F	Flux density of magnet, gauss
f	Darcy-Weisbach friction factor, dimensionless
G	Mass flux, lb_m/ft^2-hr
G_e	Mass flux of condensing vapor normal to heat transfer surface, lb_m/ft^2-hr.
G_m	Molecular mass flux
g	Acceleration of gravity, ft/hr^2
g_o	Conversion factor, 4.16×10^8 lb_m-ft/lb_f-hr^2
h	Heat transfer coefficient, $Btu/hr-ft^2-°F$
J	Conversion Factor, 778 ft lb_f/Btu
K	Vapor to liquid velocity ratio, dimensionless
k	Liquid thermal conductivity, Btu/hr-ft-°F
$\bar{k}_w$	Average wall thermal conductivity, Btu/hr-ft-°F
K_E, K_1, K_2, K_3	Flowmeter constants, dimensionless
ℓ	Length, ft
L	Condensing Length, ft.
M	Molecular weight, lb_m/lb mole
N	Number of tubes
N_o	Summation limit
N_{Nu}	Liquid Nusselt number
N_{Nuc}	Nusselt condensing ratio
N_{Pe}	Liquid Peclet number
N_{Pr}	Liquid Prandtl number
N_{Re}	Liquid Reynolds number

N_{Ref}	Reynolds number of film
P	Saturation pressure, lb_f/ft^2
p	Helical insert pitch
Q	Volume flow rate of condensate per unit circumference, $ft^3/hr\text{-}ft$
q"	Heat Flux, $Btu/hr\text{-}ft^2$
q'	Heat transfer per unit tube length, $\frac{Btu}{hr\text{-}ft}$
q	Heat transfer rate, Btu/hr, KW
R	Radius, ft
$\bar{R}$	Gas constant, ft lb_f/lb mole °R
R'	Ratio of fluid to wall electrical resistivity, dimensionless
T	Temperature, °F and °R
U	Overall heat transfer coefficient, $Btu/hr\text{-}ft^2\text{-}°F$
u	Velocity in axial direction, ft/hr
V	Velocity, ft/hr
W	Flow rate, lb_m/hr
X	Quality
Y	Condensing circumference, ft.
y	Linear distance from condensing wall, ft.
Γ	Flow rate per unit circumference, lb/ft-hr
Δ	Finite difference; also thermocouple error, °F
δ	Liquid film thickness, ft.
θ	Determinant
λ	Latent heat of vaporization of potassium, Btu/lb_m
μ	Absolute viscosity, $lb_m/ft\text{-}hr$
ρ	Density, lb_m/ft^3
$\hat{\rho}$	Density of two-phase mixture lb_m/ft^3
σ_c	Condensation coefficient, dimensionless
σ_e	Evaporation coefficient, dimensionless
τ	Shear stress, lb/ft^2
τ^*_v	Dimensionless shear stress
ν	Liquid kinematic viscosity, ft^2/hr

ϕ_{ℓ}	Local two-phase friction Pressure Drop Multiplier,
ϕ_{1-O}	Two-phase friction pressure Drop Multiplier Integrated from X = 1 to X = 0

Subscripts

A	Air
AC	Air cooler
B	Bottom station
C	Condensing
Ca	Calorimeter
CB	Centerbody
D	Tube inside diameter
d	Thermocouple drift
DCB	Insert centerbody diameter
E	Experimental value
f	Liquid
fr	Friction
h	Heat transfer coefficient
I	Inlet
i	Inside
j	Summation index
K	Potassium
ℓ	Local
L	Loss
LM	Log mean
m	Molecular
M	Mean
MOM	Momentum
Na	Sodium
NaK	Sodium-Potassium alloy
O	Outlet
o	Outside

P	Calculated value
q"	Heat flux
sat	Saturation
S	Liquid film surface
SH	Shell
T	Top station
TK	Potassium temperature
TPF	Two-phase friction
Tw	Wall temperature
v	Vapor
w	Wall
wi	Inside wall surface
wo	Outside wall surface
z	Axial component
θ	Aximuthal component

SUMMARY

Tests to measure local condensing heat transfer coefficients and two-phase pressure change for potassium in forced convection were done in a stainless steel test rig at condensing temperatures from 1100°F to 1400°F, inlet vapor Mach numbers from about 0.1 to nearly 1.0, local vapor qualities of about 0.2 and 0.8, respectively, and local heat fluxes up to about 300,000 Btu/hr-ft^2. The tests were conducted using 36-inch long single tubes, cooled by sodium in counterflow, with the potassium in vertical downflow. Two different tube sizes were used, 3/8-inch and 5/8-inch ID. The tests were conducted both with and without inserts in the tubes.

The local condensing potassium heat transfer coefficients were found to be relatively high, typically above 10,000 Btu/hr-ft^2-°F. The data indicate that this value of the coefficient is a reasonably conservative design choice for forced convection condensing of potassium in tubes over the range of variables tested.

The measured condensing heat transfer coefficients are generally lower than condensing potassium coefficients calculated by considering only the thermal resistance due to heat conduction through the liquid film, thus indicating the presence of an additional thermal resistance. It was possible to correlate the data by assuming the additional resistance was at the vapor-liquid interface and using an approach based on kinetic gas theory. This treatment resulted in an empirical value of 0.2 for the condensation coefficient associated with the resistance at the interface.

Pressure change data was obtained by relating the measured potassium temperatures in the condenser to the corresponding saturation pressures. Although the pressure changes were quite small, in the order of less than 1-psi, reasonably good agreement was found between the experimental overall two-phase friction

pressure drop multipliers obtained from these measurements and those estimated using the conventional Martinelli flow model modified for potassium.

The experimental results and associated analyses presented in this report provide a reasonable basis for thermal design of forced convection potassium condensers.

I INTRODUCTION

Design of condensers for Rankine cycle space power systems using potassium as the working fluid requires knowledge of the heat transfer and fluid dynamic characteristics of condensing potassium in forced convection. At the time the work described in this report was initiated there were no data available on forced convection condensing of potassium in tubes. Therefore, the experimental program reported here was conducted to obtain basic data on potassium condensing in single tubes.

The tests were done with the potassium in forced convection vertical downflow over the range of condensing temperatures from 1100°F to 1400°F, inlet vapor Mach numbers from about 0.1 to nearly 1.0 and local heat fluxes up to about 300,000 Btu/hr-ft^2. The test results include pressure change data and measurements of local condensing heat transfer coefficients in 36-inch long tubes of two different sizes, 3/8-inch ID and 5/8-inch ID, both without inserts and with three different inserts in the 5/8-inch ID tube.

Vertical downflow of the condensing potassium was chosen in order to eliminate the effect on the flow patterns in the condenser tube of having a component of the gravity force normal to the tube wall. The condenser tubes were cooled by sodium in counterflow outside the tube, in order to provide means for accurately measuring the total heat transfer rate and to have condensing heat flux distributions similar to those which would occur in a liquid metal cooled tube-in-shell condenser. Local condensing heat transfer coefficients were measured, rather than overall coefficients, in order to obtain better accuracy for the condensing coefficient determinations and to provide basic data which would be useful for development and design of space power condensers.

The experimental results and associated analyses are presented in detail in the following sections of this report.

II SUMMARY OF LITERATURE SURVEY

In general, condensation heat transfer can be considered to occur in one or a combination of three different modes, as follows:

(1) Droplet formation in the vapor stream
(2) Dropwise condensation on the cooling surface
(3) Film condensation on the cooling surface

Due to its wetting characteristics, potassium probably condenses as a liquid on the cooling wall in forced convection flow. Therefore, the following discussion of the literature will treat only this mode of condensation.

Until recent times, data on condensation heat transfer has been available only for fluids with high Prandtl numbers. For these fluids the analytical prediction of Nusselt for a falling film in a stagnant vapor has been found to generally apply (Reference 12). However, more recently available data on condensing heat transfer for liquid metals of low Prandtl number indicate that the simple liquid film analysis proposed by Nusselt is not adequate for these fluids (References 13-20).

A number of analytical investigations (References 21-29) have been undertaken to modify Nusselt's model to include such effects as vapor shear, film turbulence and fluid property variation across the liquid film. However, none of these treatments, for which it is assumed that the liquid film is the only thermal resistance, succeed in bringing the analytical predictions into agreement with measured condensing heat transfer coefficients for the low Prandtl number fluids.

Some evidence of the existence of a substantial additional thermal resistance besides that associated with the liquid film has been presented by Rohsenow and Sukhatme for mercury condensing on the outside of a 3/4-inch OD x 6-inch long tube in a stagnant vapor chamber (Reference 16). Their results for mercury condensing on the outside of this vertical tube were:

(1) The measured liquid film thicknesses are in reasonable agreement with those predicted by the Nusselt model.

(2) The measured condensing heat transfer coefficients are as much as two orders of magnitude lower than those predicted by the Nusselt theory.

On the basis of these observations, Sukhatme and Rohsenow concluded that for mercury and other low Prandtl number fluids there is a significant vapor phase thermal resistance, which is additive to the liquid film resistance. This vapor phase thermal resistance also may be present with high Prandtl number fluids, but for these fluids it would be negligible in comparison with the thermal resistance of the liquid film.

As pointed out by Wilhelm (Reference 30), the presence of a non-condensable gas can lower the condensing heat transfer coefficient. Thus, this is another possible cause of the large difference between measured condensing heat transfer coefficients for low Prandtl number fluids and those calculated using the liquid film analyses.

III TEST APPARATUS

Facility

An isometric drawing of the test facility is presented in Figure 1. Figure 2 shows the facility during initial stages of construction and Figure 3 shows the completed facility prior to initial operation. The entire facility, except the test section, is constructed of Type 316 stainless steel, which was selected on the basis of its strength and compatibility with alkali metals at temperatures to 1600°F.

Potassium vapor was generated in a pot boiler heated by electrical immersion heaters. The pot boiler, shown in Figure 4, was constructed of a 12-inch Schedule 40 pipe tee and caps, with a flat plate serving as the flange for the heaters. Twenty immersion heaters, each rated at 4.7 KW were installed in the boiler, as shown in Figure 5. These heaters were electrically connected so that no single heater could exceed a 3.6 KW electrical input. Two types of artificial nucleating sites were employed in the boiler. The first type, referred to as a "hot finger", consisted of a 1-inch OD Type 316 stainless steel bar containing a 0.040-inch OD hole. Three of these "hot fingers" were located in the bottom of the boiler. Independent electrical heaters maintained the "hot fingers" above the potassium saturation temperature. A second type of artificial nucleator, which was made of one-inch long sleeves shrunk onto the bottom row of immersion heaters, was also provided. No measurable effect of either of these types of nucleators on loop operation was noted.

As indicated in Figure 1, the vapor generated in the boiler flowed through an 8-foot vertical length of two-inch Schedule 40 pipe, a 1½-inch throttle valve, a 10-foot horizontal run of 1-inch Schedule 40 pipe, and then passed down through the sodium-cooled test section where it was condensed. During test operation, the liquid-vapor interface was maintained below the test section in the head tank.

After exiting from the test section and head tank, the liquid condensate passed through a thermal calorimeter, an induction electromagnetic pump and an electromagnetic flowmeter into the boiler. All pipe lines were wrapped with Inconel sheathed Chromel "A" heating wire for preheating.

The sodium loop, an all-liquid loop, was used to cool the test condenser. The sodium flowed vertically upward through the test section annulus where it was heated by the condensing potassium, flowed through 8-foot lengths of 1-inch and 2-inch Schedule 40 pipe, respectively, and then passed through a conduction electromagnetic pump and an electromagnetic flowmeter. The sodium then passed through a tube-in-shell air cooler where heat was rejected, after which the sodium returned to the test section. A dump tank was provided in the loop for storing the sodium during shutdown.

For purification of the potassium, a bypass hot trap, shown in Figure 6, was installed in parallel with the test condenser. The hot trap, which contained approximately 4 lbs of zirconium gettering material, provided hot trapping to remove oxide from the potassium during flushing of the loop prior to the beginning of operation. In the sodium loop, a diffusion cold-trap was provided. This cold-trap was in the form of a cold leg between the sodium pump and dump tank to allow oxide precipitation during operation.

Test Section

A schematic drawing of the condensing test section used in this series of experiments is shown in Figure 7. Potassium condensation occurred inside a thick walled nickel tube which was cooled by a countercurrent sodium flow in the surrounding annulus. Operation was with the condenser tube axis vertical and the potassium in vertical downflow.

During this investigation, experimental data were obtained for five condensing geometries, which are listed below in the chronological order of

testing:

Number	Geometry
1	5/8-inch ID tube with no insert
2	5/8-inch ID tube with an unistrumented tapered pin insert
3	3/8-inch ID tube with no insert
4	5/8-inch ID tube with an instrumented helical insert
5	5/8-inch ID tube with an instrumented 1/4-inch OD tubular insert

The three inserts which were tested are shown in Figure 8.

The condenser tubes were thick-walled and were made of high-purity nickel (99.95%+) which was selected for its high thermal conductivity in combination with its compatability with the alkali metal test environment. The tubes had an active heat transfer length of 36-inches (Figure 7). The potassium flow passage was concentric with the outside surface diameter of the tube to within 0.003-inch.

To calculate the condensing heat transfer coefficients, measurements of the local heat flux, inner wall temperature and vapor temperature are required. These measurements were made at two stations in the condenser, one at about 20% and the other at about 80% of the condensing length measured from the potassium vapor inlet (Figure 7). To determine the inner wall temperature and heat flux at these two measuring stations, thermocouples were located in holes drilled by an electrical discharge process from each end of the thick-walled nickel tube parallel to the axis of the tube. There were five of these holes at each end of the nickel tube, located as shown in Figure 9.

The drilled thermocouple holes were 0.050-inch in diameter and 9-inches deep, and their radial location was held within a tolerance of 0.004-inch over their length, as determined by radiographic examination. Two of the five holes

at each measuring station were located close to the tube inside surface, one hole was located at an intermediate radial position, and two holes were located close to the tube outside surface (Figure 9). One thermocouple was placed in each of the thermocouple holes at the depths for each measuring station indicated in Figure 7. The axial positions indicated in Figure 7 are estimated to be correct within less than $\pm$ 1/16-inch error.

Potassium vapor temperatures were measured only at the test section inlet and outlet with the first three test section geometries. However, with test section geometries No. 4 and No. 5, thermocouples were located in the test section inserts along the condensing length to measure directly the potassium axial temperature distribution.

In addition to the thermocouples located within the nickel tube wall and in the potassium stream, thermocouple wells were provided to measure the sodium inlet and outlet bulk temperature. Figure 10 shows the sodium inlet end of the test section with three thermocouple wells spaced 120° apart for measuring the inlet bulk sodium temperature. A similar arrangement was provided at the sodium exit.

Figure 11 shows one end of the 3/8-inch inside diameter nickel condenser tube with a stainless steel adaptor pipe brazed into place for connection of the nickel condenser tube to the potassium loop piping. Arrangements identical to this were used at both ends of each test section. In addition to the adaptor pipe arrangement shown in Figure 11, each end of the nickel condenser tube was fitted with a 2-inch OD stainless steel tube which was welded to the outside surface of the nickel tube at each end and was used to join the nickel tube to the surrounding sodium-containing shell. The space between the adaptor pipe and the 2-inch OD tube connecting the condenser tube to the shell formed an annulus which was open to the atmosphere, through which the tube wall thermo-

couples were installed. This arrangement, which can be seen in Figure 7, avoided crossing either the sodium or potassium streams with the wall thermocouple leads, thereby avoiding mechanical complexity and undesirable flow disturbances.

The test section outer shell was constructed of $2\frac{1}{2}$-inch Schedule 80 pipe with two enlarged end fittings made from standard pipe reducers and flat plates. Each end of the test section was internally baffled on the sodium side with a perforated disc. Concentricity between the test section shell and the thick walled nickel condenser tube was maintained by small spacers which were attached to each end of the nickel tube. Flexibility to accommodate lengthwise differential thermal expansion between the stainless steel shell and the nickel tube was provided by a guided $3\frac{1}{2}$-inch OD bellows located at the bottom end of the outer shell.

Figure 12 shows a condenser tube with the adaptor pipes attached and shows an assembled condensing test section. The condenser tube is shown adjacent to the assembled test section to indicate its relative length and location within the test section shell.

Figure 13 shows the test section installed in the facility before covering it with thermal insulation. As shown, in the Figure, the test section was surrounded by a structural framework to minimize bending and to maintain a vertical orientation. The supporting structure allowed the test section to expand vertically but prevented deviation from vertical orientation of more than $\pm$ 1/16-inch in the 28-inch length between the supports. The shell thermocouples shown in Figure 13 were used during initial operation with Test Section No. 1 to check on the axial symmetry of the sodium flow. For subsequent operation, two thermocouples were attached to the shell at the sodium inlet, at the sodium outlet and in the middle of the test section.

The first of the three inserts tested consisted of a non-instrumented tapered pin which had diameters of 1/32-inch and 3/8-inch at the test section inlet and outlet, respectively (Figure 8-a). This insert was used to simulate a tapered tube flow geometry by providing a gradually reducing flow cross-section to the condensing potassium stream. The insert was held concentric with the inside diameter of the condensing tube by wire prongs welded at two positions, approximately 11-inches and 30-inches, respectively, from the test section inlet. The tapered pin was also secured in the axial direction by a hairpin shaped yoke attached to the upstream end of the insert and tack-welded to the pipe inside surface above the test section inlet.

The second insert used was an instrumented helical insert of pitch-to-diameter ratio equal to 6 (Figure 8-b). This insert consisted of a single helical ribbon wound around a 1/4-inch outside diameter centerbody tube (Figure 14). The centerbody tube penetrated the potassium loop piping through a fitting located above the test section inlet, as shown in Figure 14. Twelve thermocouples were located in the insert centerbody tube. Three of the thermocouples were located upstream of the active condensing heat transfer length, and the other nine thermocouples were placed at positions about 5-inches apart along the active condensing length (two thermocouples were located together at the potassium outlet). The loop piping penetration for the centerbody tube was made at an enlargement in the potassium loop piping, which consisted of two eccentric reducers welded together back to back. This arrangement was used for two purposes; first, to permit a gradual long radius bend in the insert tube which made insertion and removal of the thermocouples possible without requiring bending of the thermocouples, and secondly, to provide a penetration location which had the proper angle and accessibility for satisfactory welding.

The third insert was similar in arrangement to the one shown in Figure 14, except that instead of being a helix it was a straight 1/4-inch OD tube (Figure 8-c). This straight tubular insert was held concentric with the test section by means of wire prongs and guide vanes. The tubular insert also contained twelve internal thermocouples, which were distributed in a manner similar to that used for the helical insert, to measure the axial temperature distribution of the condensing potassium.

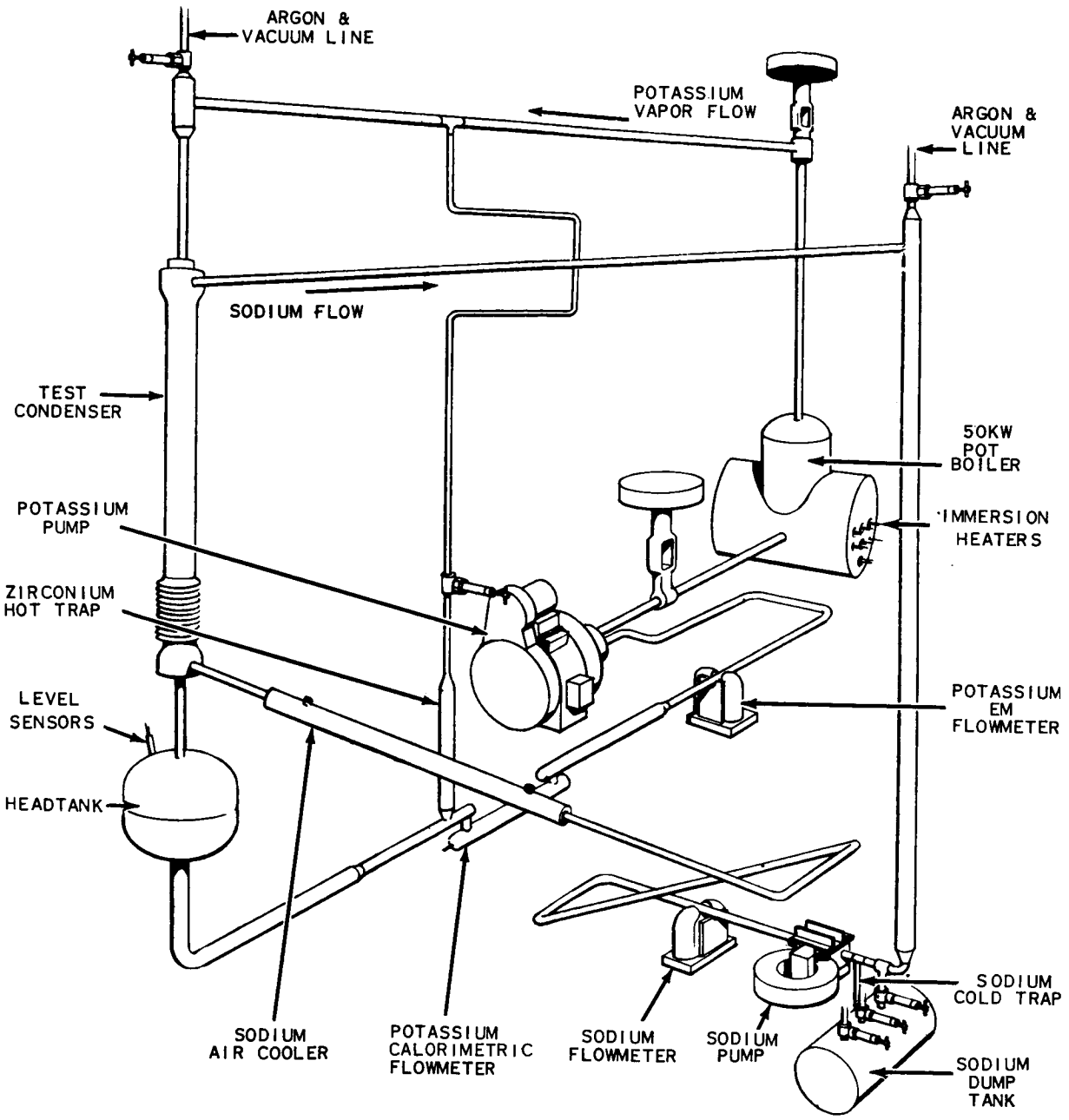

Figure 1, Flow Diagram of Condensing Test Facility

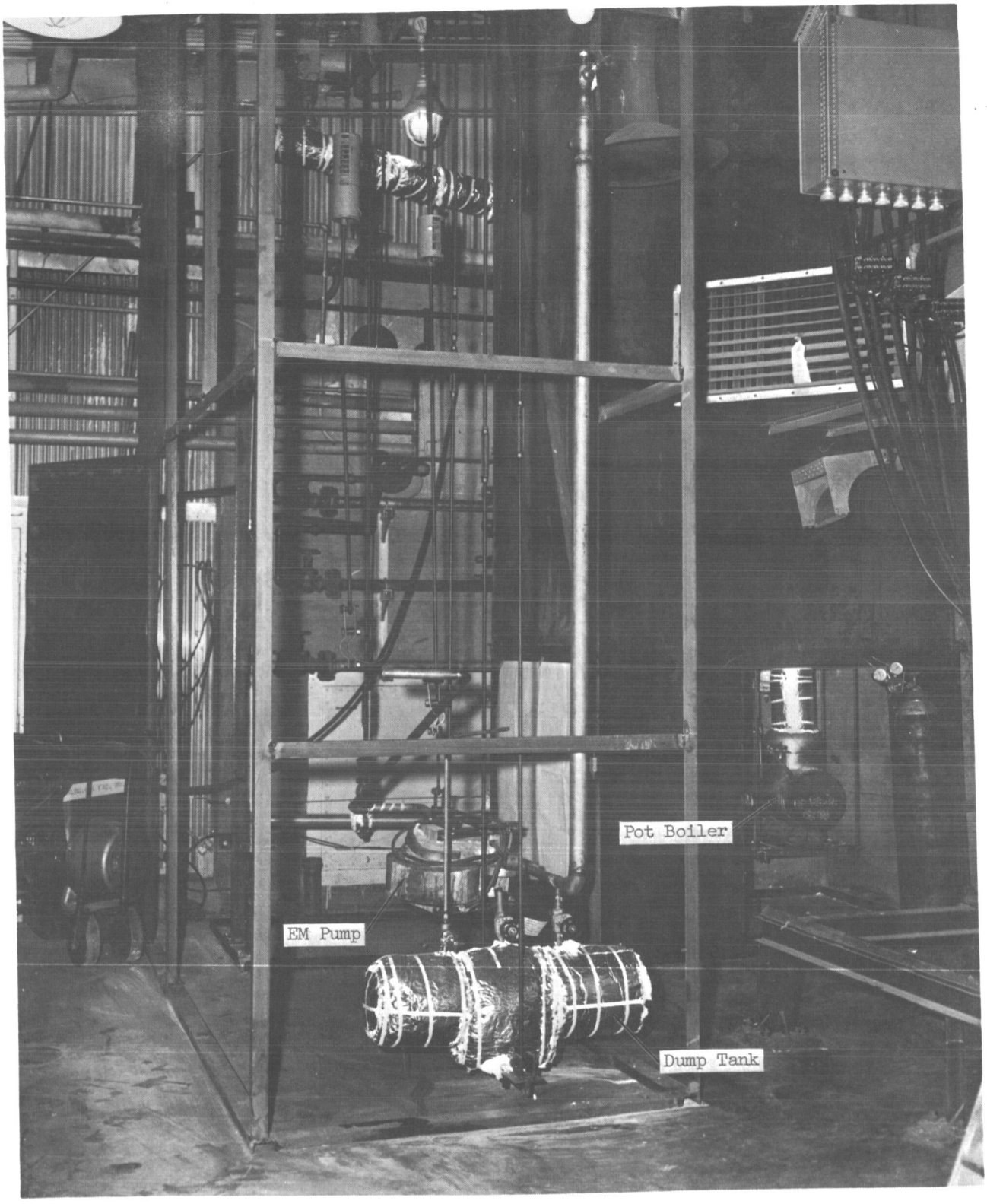

Figure 2. Condensing Test Facility During Construction

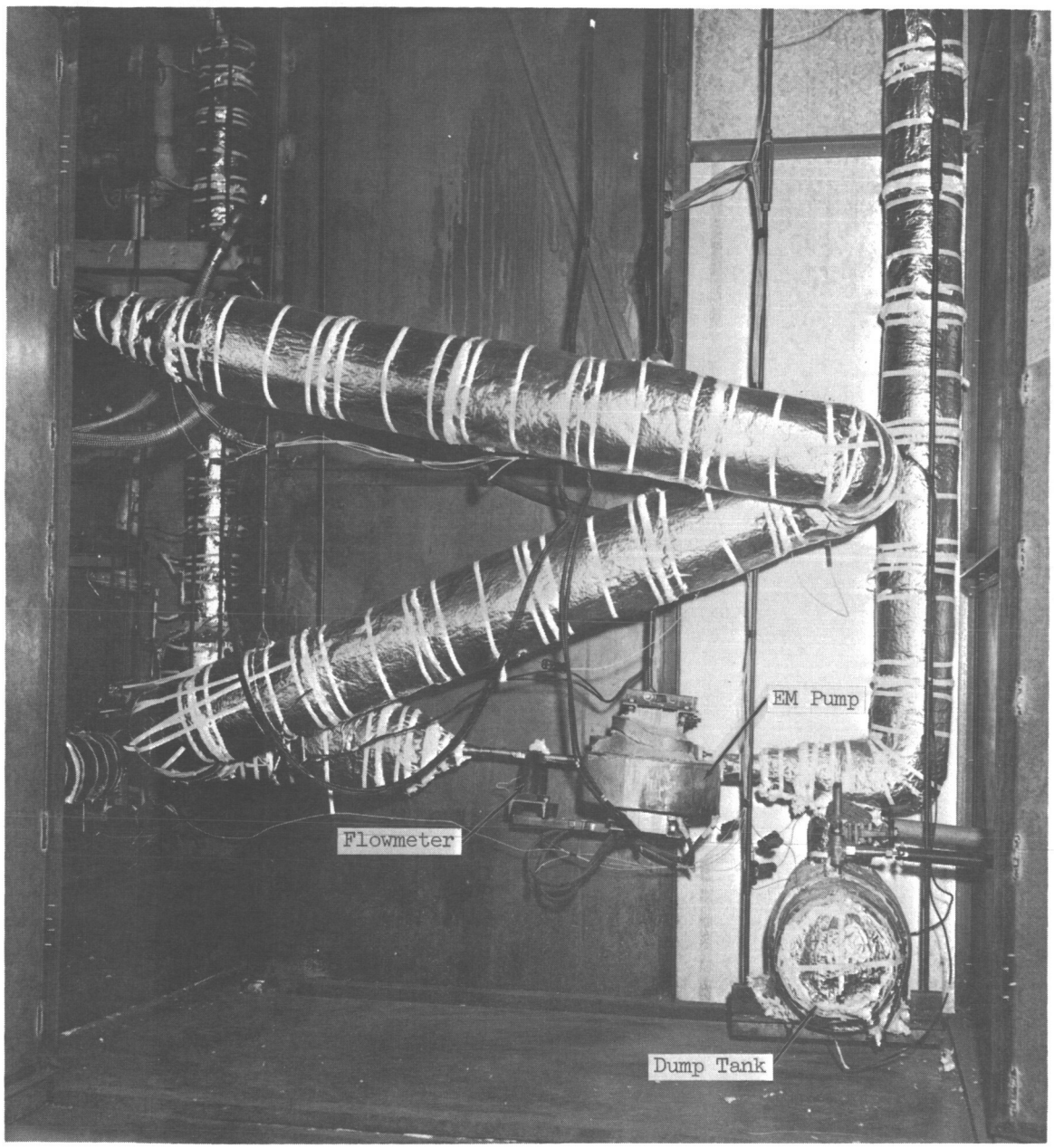

Figure 3. Condensing Test Facility Prior to Initial Startup

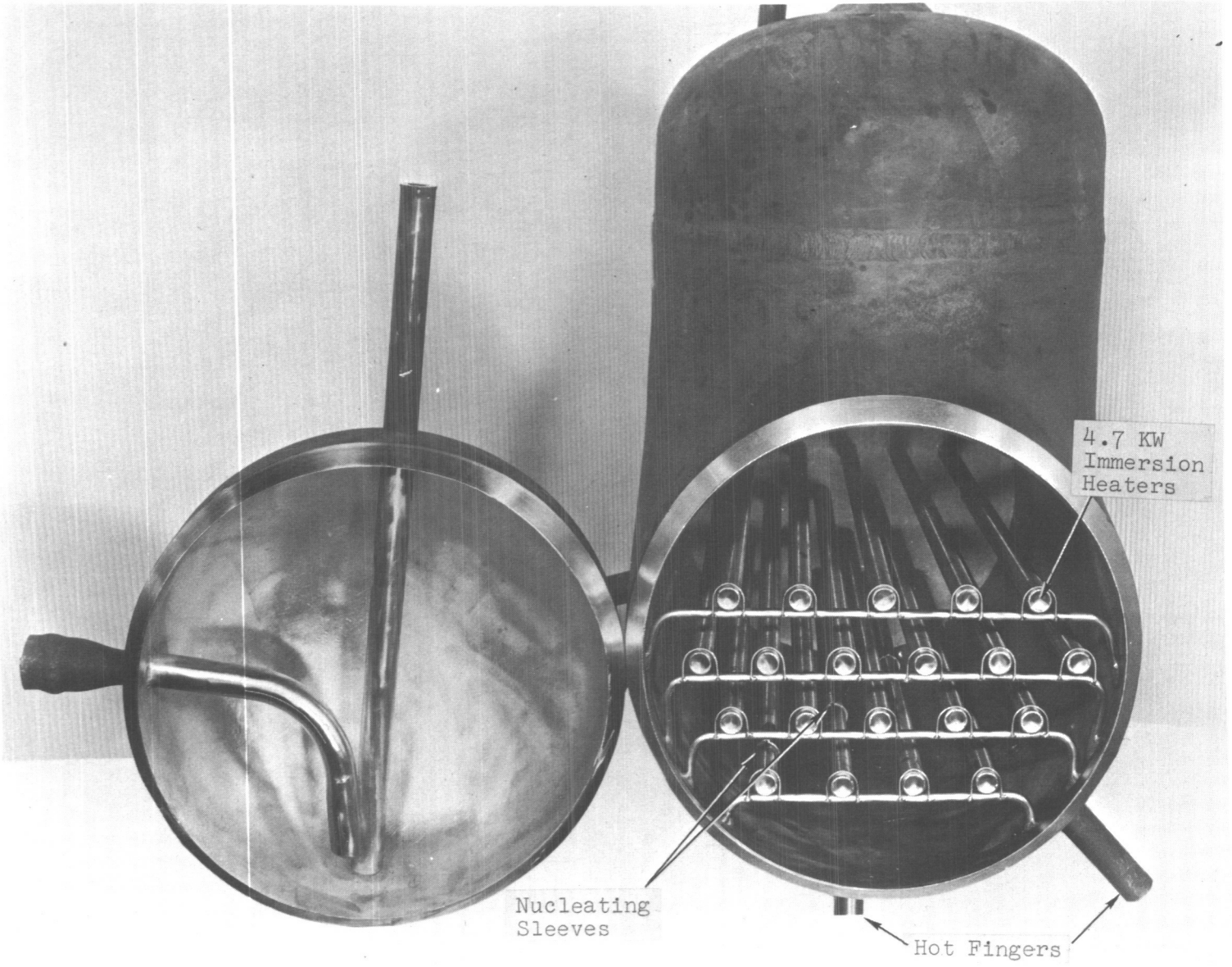

Figure 4. Photograph of Pot Boiler Showing Arrangement of Immersion Heaters and Artificial Nucleators

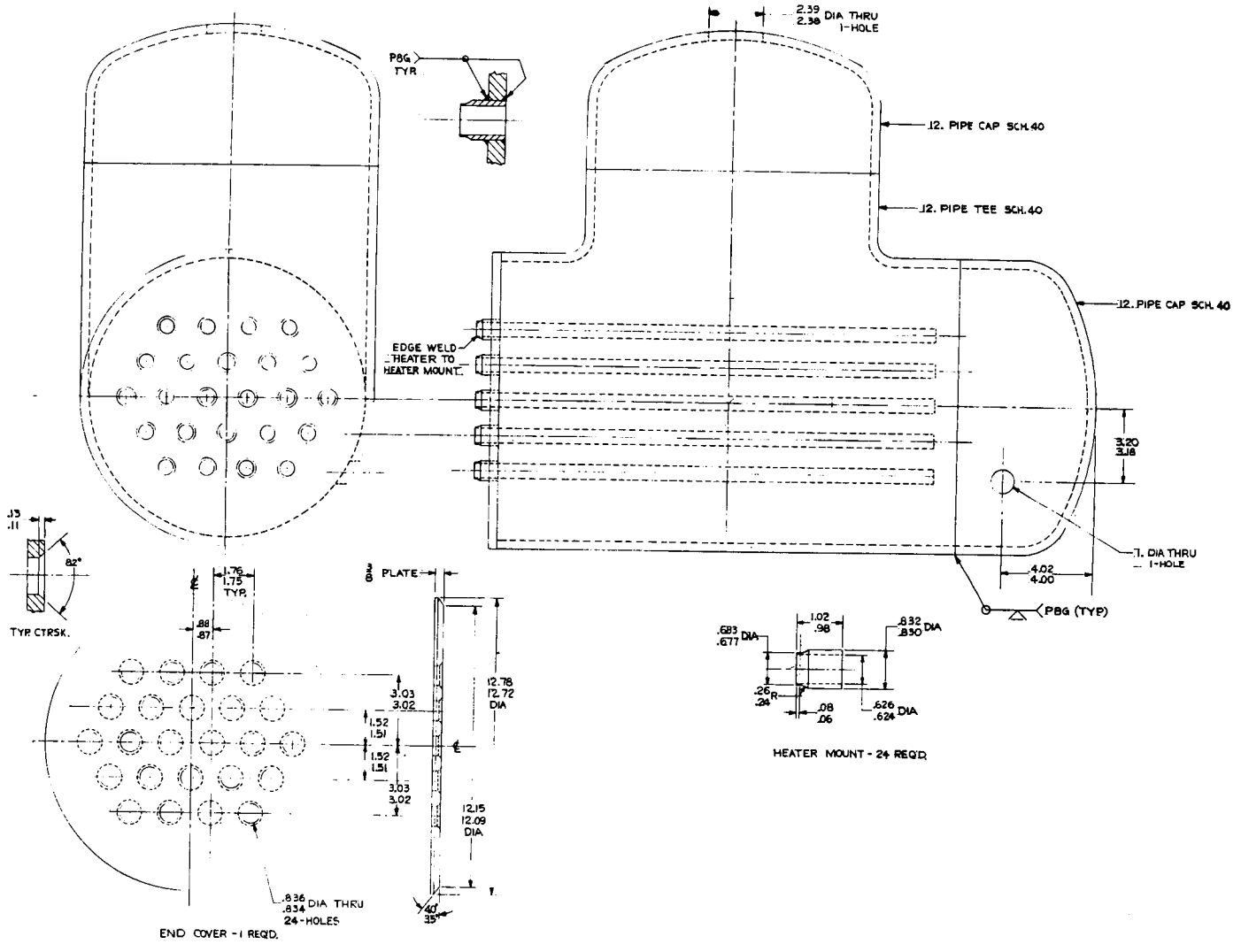

Figure 5. Design Drawing Showing Detail Dimensions of Pot Boiler

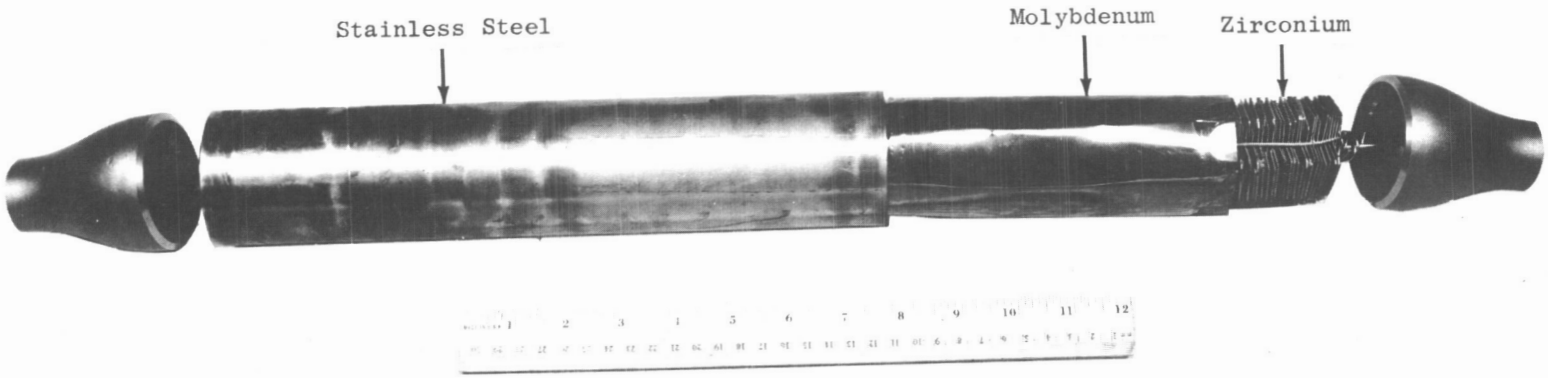

Figure 6. Photograph of Zirconium Hot Trap Used In Condensing Test Facility

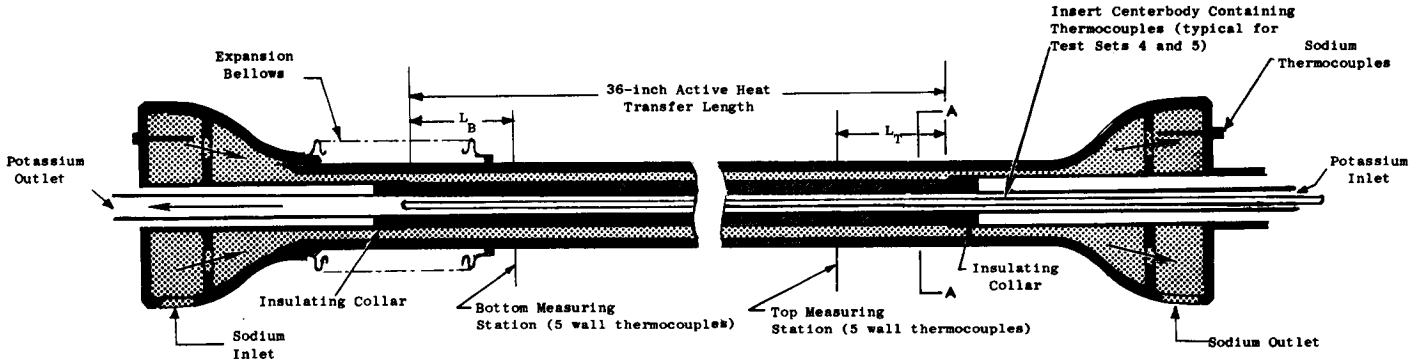

Test Set Number	Tube ID, in.	Tube OD, in.	L_B, in.	L_T, in.	Insert Thermocouples
1-A	0.625	1.72	18	18	None
1-B	"	"	12	12	"
1-C	"	"	7	8	"
1-D	"	"	8	8	"
2	0.627	1.85	8	6	"
3	0.375	"	8	8	"
4	0.627	"	6	6	5-inches apart along active length
5	"	"	6	6	

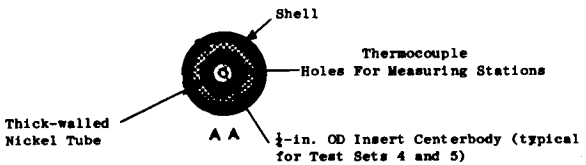

Figure 7. Schematic Drawing of Condensing Test Section

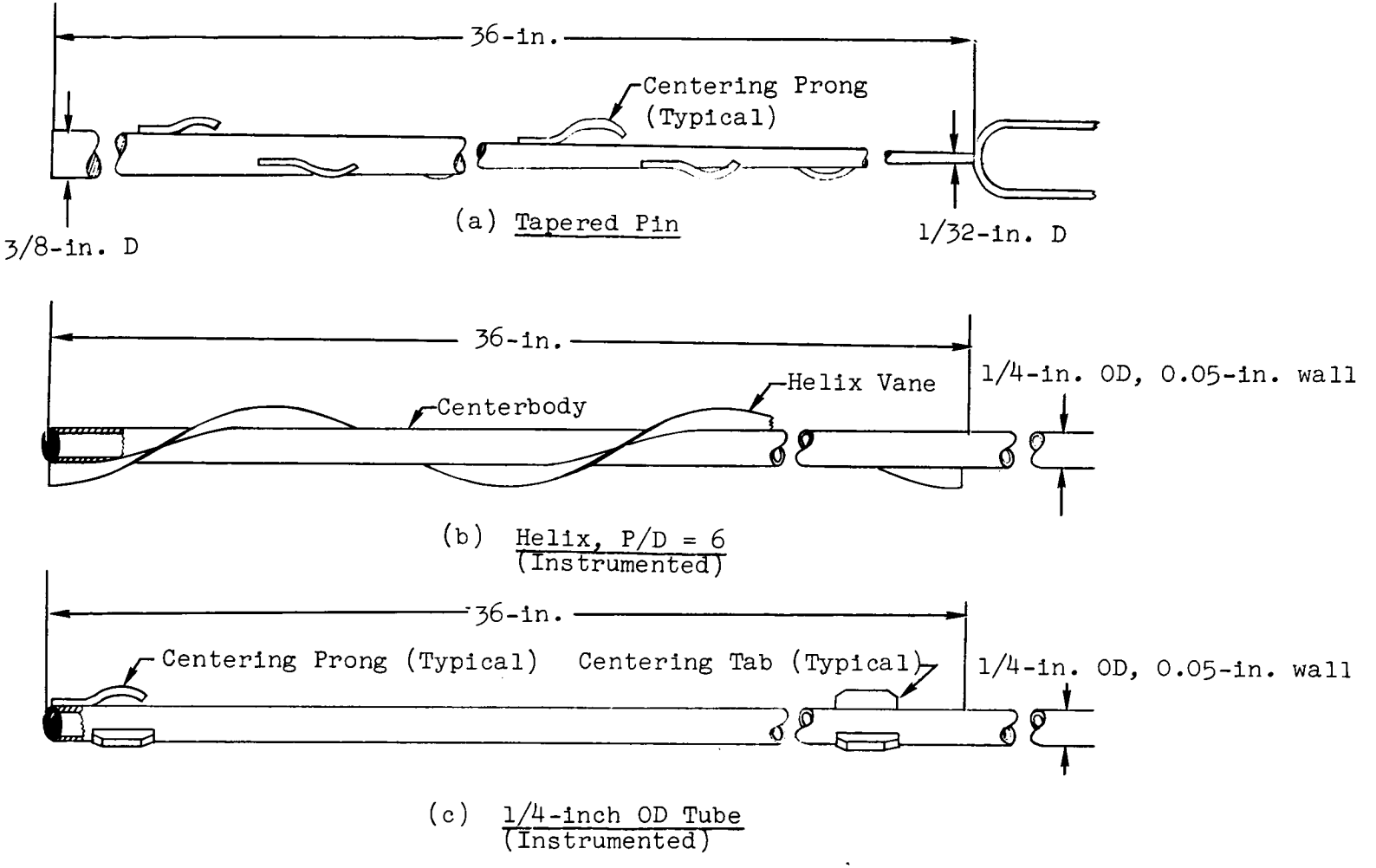

(a) Tapered Pin

(b) Helix, P/D = 6 (Instrumented)

(c) 1/4-inch OD Tube (Instrumented)

Figure 8. Inserts Tested in 5/8-inch ID Condenser Tube

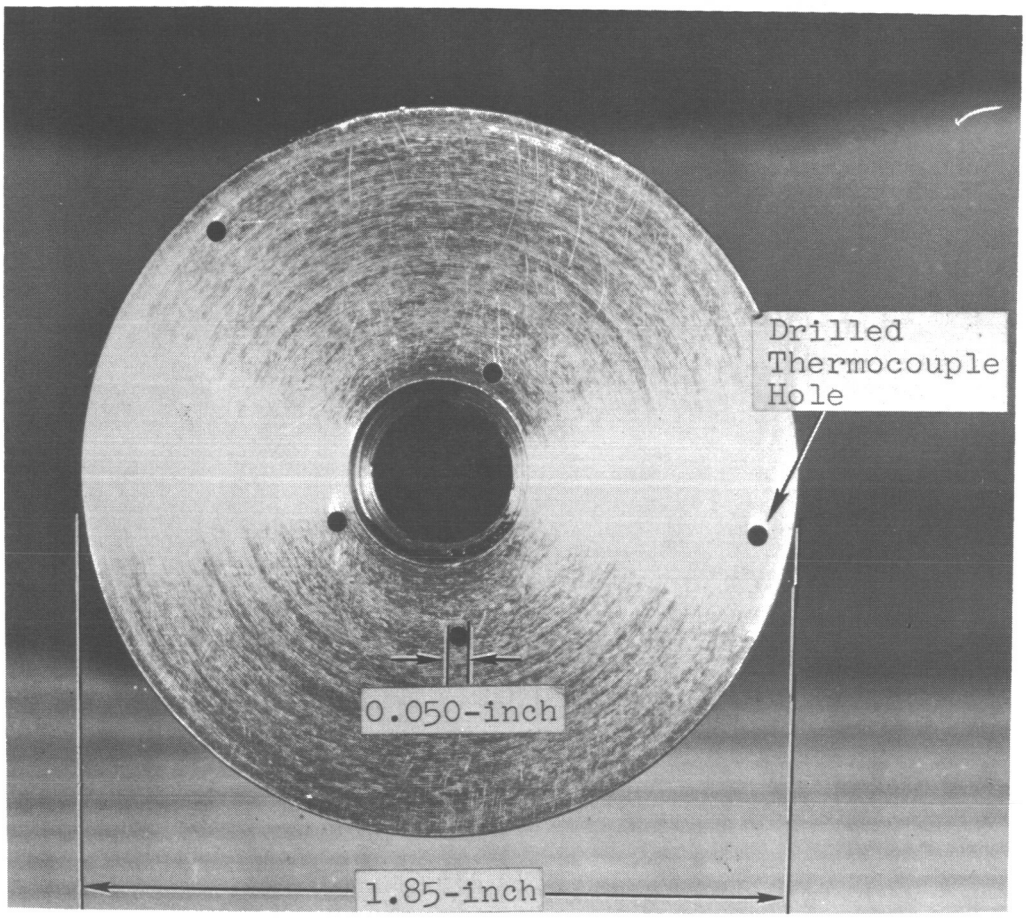

Figure 9. End View of 3/8-inch ID Condenser Tube Showing Drilled Thermocouple Holes

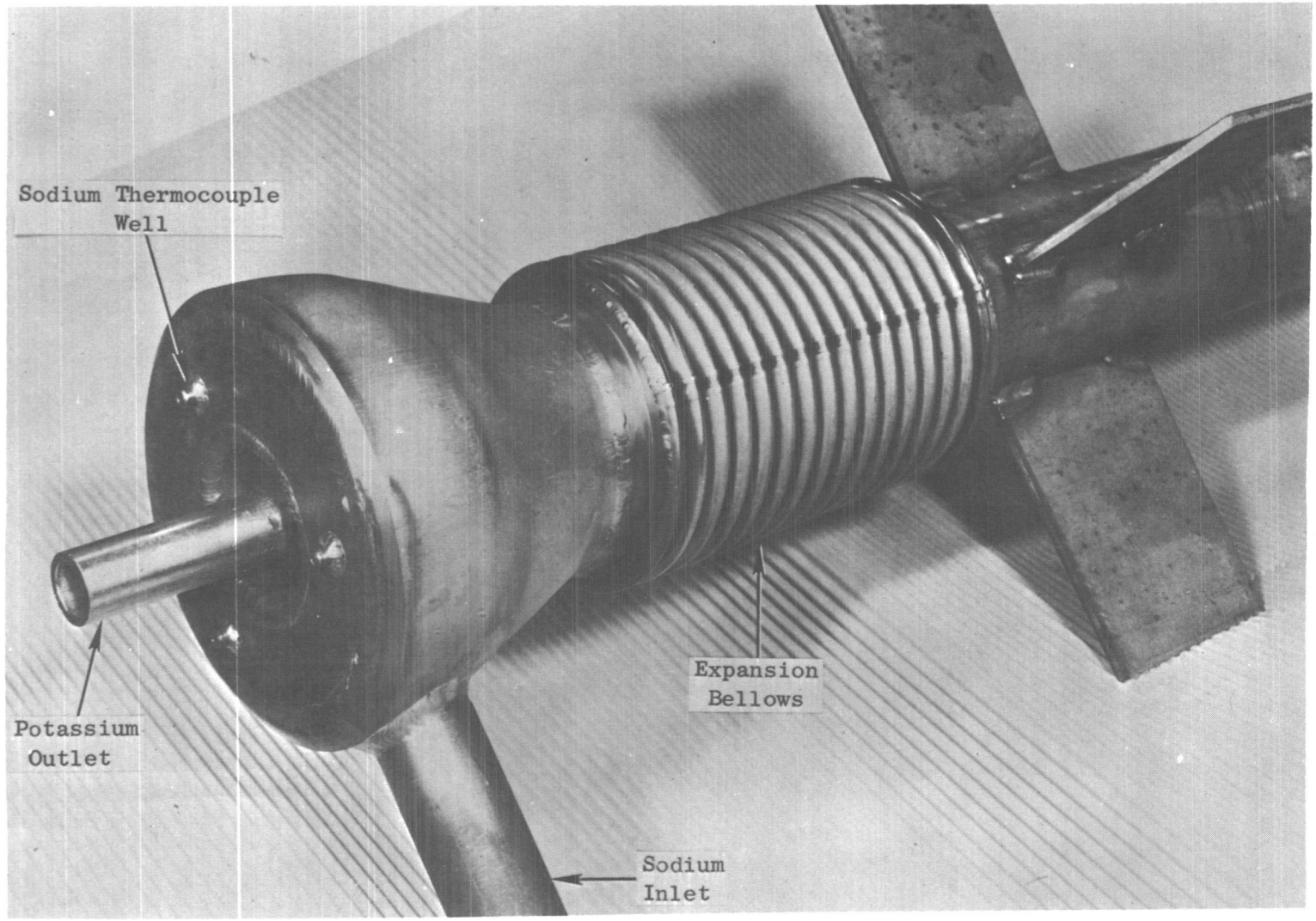

Figure 10. End View of Test Condenser Shell Showing Sodium Inlet Thermocouple Wells

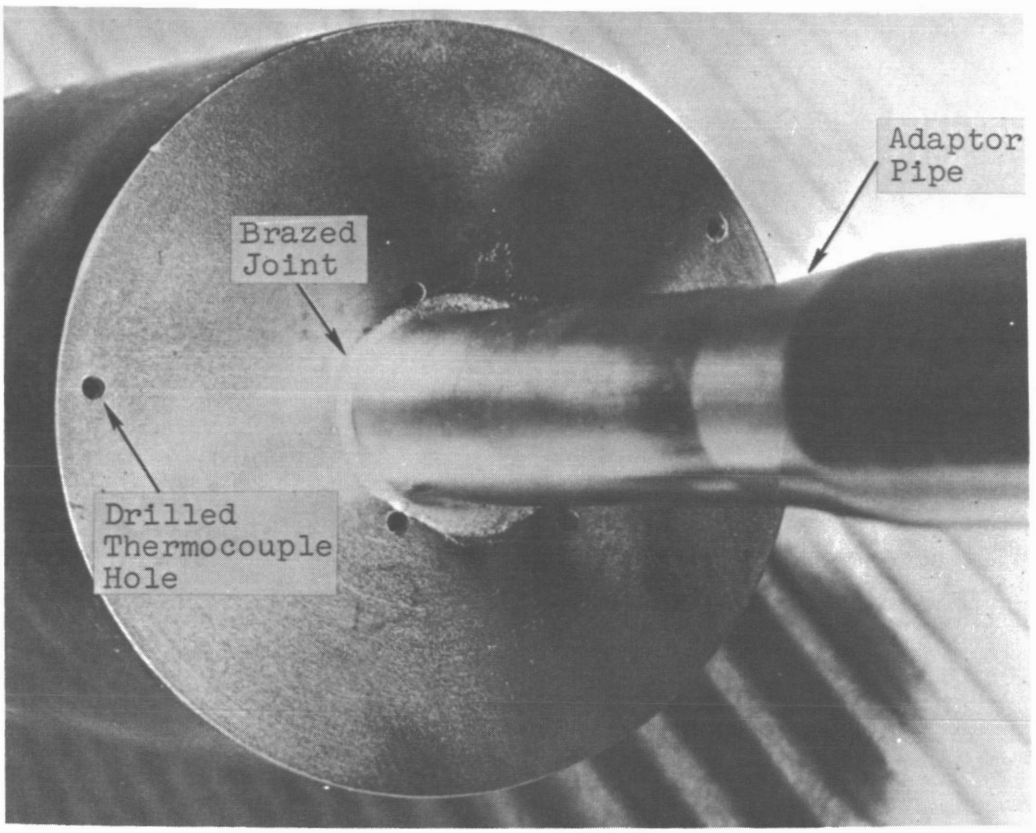

Figure 11. End View of 3/8-inch ID Condenser Tube Showing Potassium Loop Adaptor Pipe and Wall Thermocouple Holes

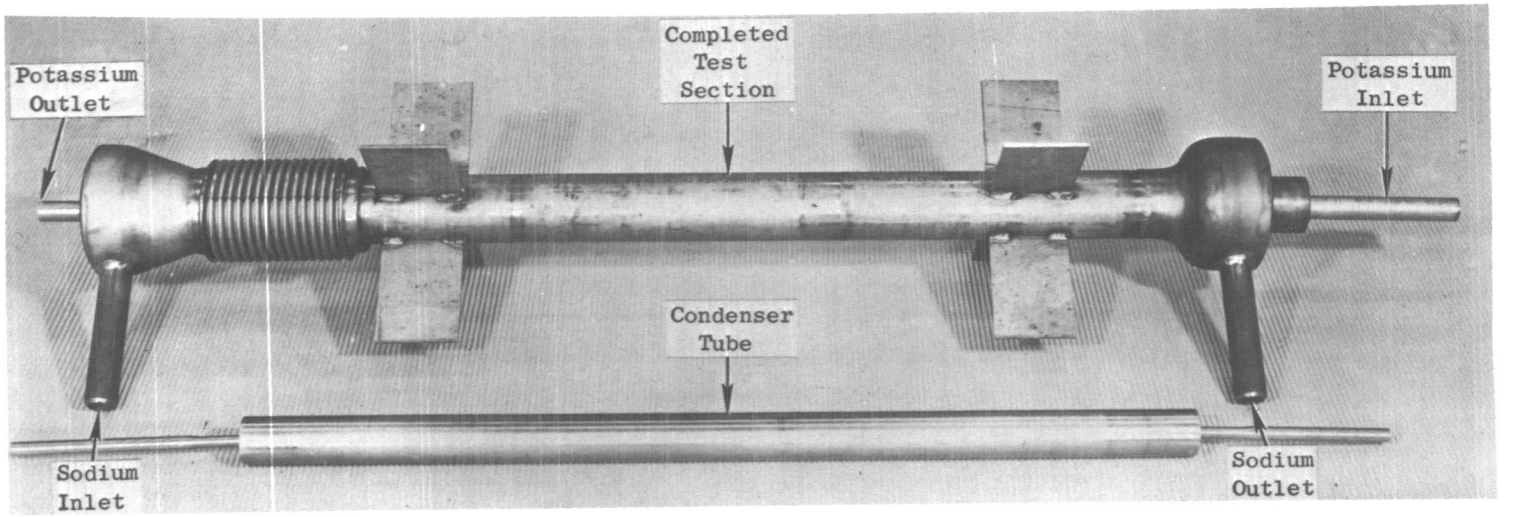

Figure 12. Assembled Test Condenser and Condenser Tube

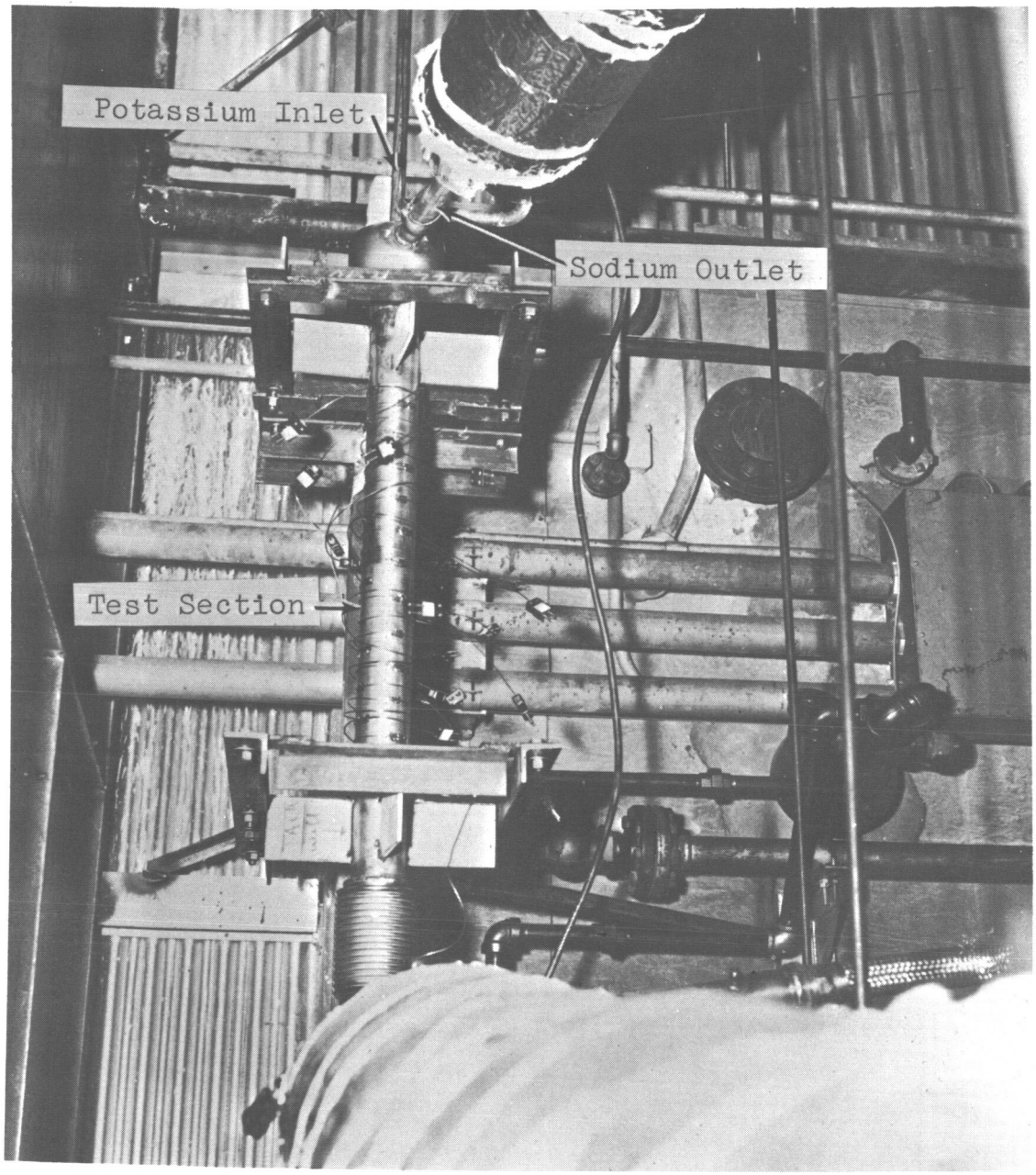

Figure 13. Test Condenser Installed In Condensing Test Facility (Shell thermocouples shown were used during initial operation with Test Section No. 1 to check symmetry of sodium flow).

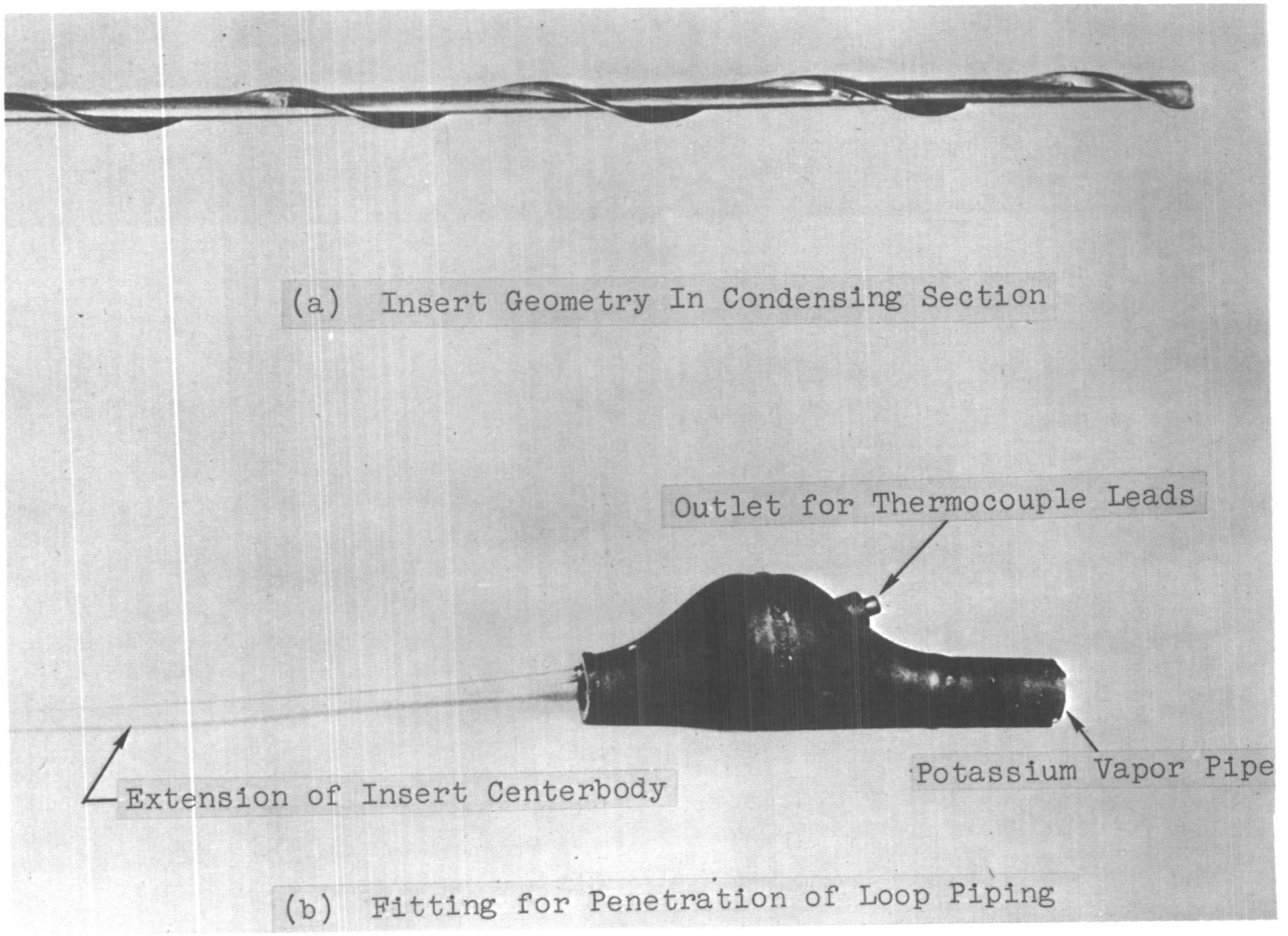

Figure 14. Helical Insert Used In 5/8-inch ID Condenser Test Section

IV EXPERIMENTAL TECHNIQUE

Test Procedure

During two-phase operation, the independent parameters in the Condensing Test Facility were:

1. Boiler power, q_b
2. Air flow rate to sodium air cooler, W_A
3. Sodium flow rate, W_{Na}
4. Auxiliary heat input

The dependent parameters are:

1. Potassium flow rate, W_K
2. Potassium vapor temperature, T_K
3. Sodium temperature, T_{Na}
4. Test section inlet quality, X_I

Auxiliary heat input and heat losses are assumed to be negligible, and the potassium is assumed to be 100% saturated vapor at the test section inlet. With these assumptions the potassium vapor flow rate is related to the boiler power, as expressed by Equation (1) and Sketch a.

$$W_K = \frac{q_b}{\lambda} \qquad (1)$$

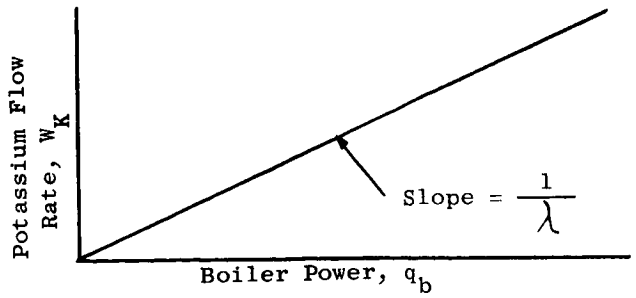

Sketch-a

Neglecting heat losses, the boiler heat input is equal to the heat rejected to the sodium coolant in the test condenser, as expressed by Equation (2).

$$q_b = q_C = W_{Na}\ Cp_{Na}\ (T_{NaO} - T_{NaI}) \qquad (2)$$

The coupling between the sodium and potassium loops occurred in the test condenser and can be expressed in terms of U the overall heat transfer coefficient, A_c the test condenser heat transfer area, $(T_K - T_{Na})_{LM}$ the log mean temperature difference, and q_C the test section heat input, as given by Equation (3).

$$q_C = U\ A_C\ (T_K - T_{Na})_{LM} \qquad (3)$$

The heat transfer resistance of the thick-walled nickel tube was large compared to the sodium and potassium thermal resistances. Thus, the overall heat transfer coefficient was approximately constant during testing. The liquid level was maintained below the test section exit. Thus, the condensing heat transfer area was constant and was equal to the total area of the test condenser. Therefore, the coupling between the sodium and potassium loops expressed by Equation (3), was as illustrated by Sketch-b and Sketch-c.

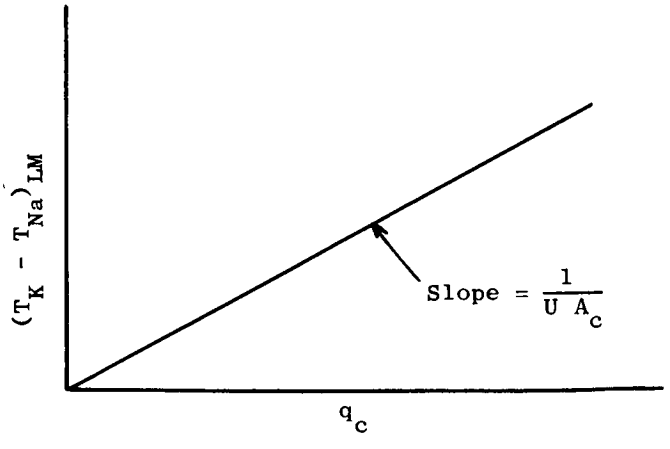

Sketch-b

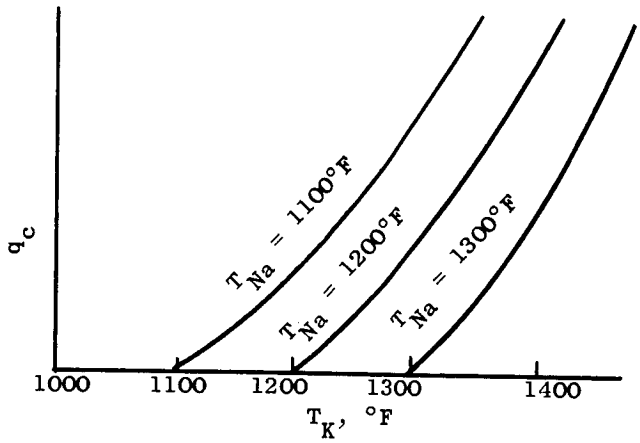

Sketch-c

The heat gained by the sodium in the test section was rejected to air in the sodium loop air cooler (Figure 1). The heat rejection rate is given by Equation (4), for which it is assumed the air-side heat transfer coefficient h_A is controlling. Sketch-d illustrates the functional relationship between the heat rejection rate and the sodium temperature.

$$q_C = q_A = h_A A_{AC} (T_{Na} - T_A)_{LM} \qquad (4)$$

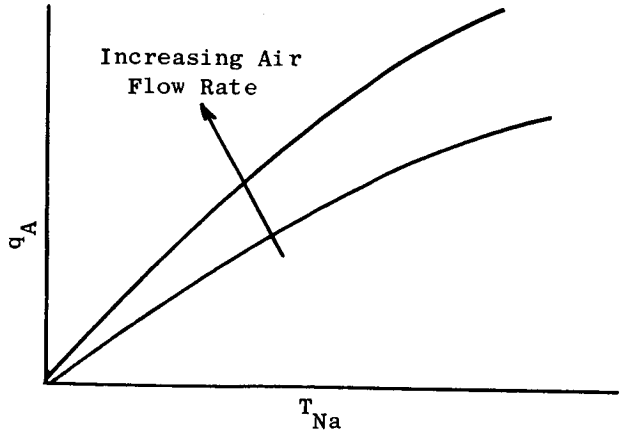

Sketch-d

The sodium flow rate was maintained constant at its maximum value during testing. Thus, the sodium flow rate was not employed as a test parameter.

The system response to an increase of boiler power will now be discussed. An increase of boiler power results in a corresponding increase in potassium vapor temperature, in order to enable rejection of the additional heat input in the test section. With a constant air flow rate to the sodium cooler, the sodium temperature also increases to allow rejection of the additional heat rate to the air, as indicated in Sketch-d. When steady-state is reached, the potassium temperature will have increased more than the sodium temperature increase, since, as indicated in Sketch-b the test section log mean temperature difference between the potassium and the sodium must also increase in order to allow an increase in the condenser heat transfer rate. The potassium flow rate will have increased also, due to the increased boiler power, as shown in Sketch-a. If the air flow rate is increased at fixed boiler power, the sodium temperature will decrease, thereby lowering the potassium condensing temperature, as indicated in Sketch-c. Thus, at fixed boiler power the potassium condensing temperature can be controlled by adjusting the air flow rate to the sodium cooler. These characteristics of the system formed the basis of the condensing test procedure. The sequence of steps used in the operating procedure was as follows:

1. The potassium loop was first evacuated at 600°F to a pressure of approximately 25 microns. The difference between liquid and vapor temperatures in the boiler was used to check for the partial pressure of inert gases in the system. If a substantial difference (greater than 10°F) between those temperatures was obtained, the loop was re-evacuated and the process was repeated to the extent required.

2. Next, sodium flow was established, a boiler power was set, and the temperature of the sodium was adjusted using the air cooler and line heat to bring the potassium vapor at the test section inlet to the desired temperature.

3. Tests were conducted at constant boiler power by systematically varying the sodium temperature to obtain data for potassium vapor inlet temperatures over the range from 1100 to 1400°F.

4. When a group of tests was completed at a given boiler power, the boiler power was changed, and then step-3 was repeated.

This procedure was repeated to provide condensing heat transfer data, with condenser heat transfer rate and condensing temperature as parameters, for each of the five test section geometries. Figure 15 shows the range of operating capability of the Condensing Test Facility, within which the condensing tests were conducted. Line CD is the 1600°F temperature limit of the facility and line AE sets the lowest temperature of interest at 1100°F. Line AB sets the boiler power limit for choked flow in the test condenser. Line BC sets the maximum boiler power at 50 KW. Line DE sets the minimum net boiler power at 4 KW for a minimum condensing heat flux of 30,000 Btu/hr-ft^2 for a 36-inch long 5/8-inch ID condenser.

Prior to the beginning of condensing test operation for Test Set No. 1, liquid tests were made to obtain operating experience with the test facility and to gain familiarity with the test section instrumentation. Potassium liquid heat transfer coefficients were calculated from these data. These data are presented in Appendix A.

Flow Rate Measurement

The potassium and sodium flow rates were measured using electromagnetic

flowmeters. A calorimetric method was used to calibrate the flowmeters, as described in Appendix B.

Temperature Measurement

Sheathed, capped, 0.040-inch diameter, chromel-alumel thermocouples were selected for the temperature measurements, on the basis of their stability and relatively high emf output in the 1100-1400°F temperature range. The high output of the chromel-alumel thermocouples, approximately 23 micro-volts/°F, minimized temperature errors due to instrumentation noise. The instrumentation noise was generally less than ± 3 micro-volts, which correspond to ± 0.13°F.

During the early stages of the program it became evident that the condensing heat transfer coefficient for potassium was relatively high, in the order of 10,000 Btu/hr-ft^2-°F. Thus, accurate calibration of the test section thermocouples became necessary. For the calculation of the condensing heat transfer coefficient a difference between the vapor and wall temperatures is needed. Therefore, it was not necessary to calibrate each thermocouple on an absolute basis, but only to obtain accurate in-place calibration of the test section thermocouples relative to each other.

Both before and after each test set, the thermocouples in the potassium fluid and in the nickel tube wall were calibrated in-place relative to one of the potassium thermocouples, at temperatures of 1200 and 1300°F, as discussed in detail in Appendix C. On the basis of these calibrations each thermocouple was assigned a temperature correction as a function of temperature. The sodium well thermocouples were also calibrated in-place relative to one of the inlet sodium well thermocouples using a technique described in Appendix C.

Early calibration attempts were hampered by inhomogeneities in the chromel-alumel sheathed thermocouples, which were caused by small bends made during installation. These inhomogeneities were detected by moving a soldering iron at about 700°F along the exposed thermocouple length, after installation,

and observing the thermocouple reading. In the early stages of the program it was not uncommon to obtain outputs due to inhomogeneities as great as 500 micro-volts (20°F). Thermocouples for which the homogeneity check indicated an output greater than 50 micro-volts were replaced. In addition, individual ice junctions were used for each thermocouple to reduce errors caused by junction emf's.

As a further effort to assess temperature measurement accuracy, the magnitude of distortion of the temperature field in the thick-walled nickel tube caused by the axial thermocouple holes was estimated analytically. The results of this study are discussed in Appendix D.

To calculate the condensing heat transfer coefficient, the potassium saturation temperature, heat flux, and inner wall temperature had to be determined. During reduction of the condensing data, the inner wall temperature and heat flux at each measuring station were obtained from the nickel tube wall radial temperature profile. The method used is discussed in Appendix E, which describes the condensing data reduction in detail. Figure 16 shows two typical radial temperature profiles (obtained during Test Set No. 5). As discussed in Appendix E, a least squares procedure was employed to fit the measured temperature within the nickel tube wall using the integrated Fourier conduction equation. The local inner wall heat flux, q/A_i, was obtained from the slope of the radial wall temperature profile.

For the five test sets, two different methods were used to determine the local potassium temperature at the measuring stations. For the first three test sets, which included the 5/8-inch and 3/8-inch ID plain tubes without inserts and the 5/8-inch ID tube with tapered pin insert, only the potassium inlet and outlet temperatures were measured. For these data the local potassium temperature at the measuring stations was estimated by linear interpolation between the measured inlet and outlet temperatures, with correction for friction pressure drop in the inlet pipe from the temperature measuring point to the test section inlet. For the last two test sets, which consisted of the

5/8-inch ID tube with the instrumented helical insert (Test Section No. 4) and with the instrumented tubular insert (Test Section No. 5), the local potassium temperature was measured directly with the insert thermocouples.

In Figure 17 are shown two potassium axial temperature distributions and corresponding saturation pressures at an inlet temperature of 1150°F for two mass velocities which were measured in the 5/8-inch ID tube with tubular insert. The pressure profiles indicate that in both cases the frictional pressure drop near the test section inlet exceeds the pressure rise due to momentum reduction, but is less than the momentum pressure rise near the test section exit. A net pressure increase is indicated over the condensing length for both cases. A larger pressure rise across the test section was obtained at the higher mass velocity.

In Figure 18 are shown two potassium axial temperature distributions and corresponding saturation pressures for inlet temperatures of 1300°F and 1400°F at a superficial mass velocity of approximately 13 $lb/sec\text{-}ft^2$, which were also measured in the 5/8-inch ID tube with tubular insert. For the lower inlet temperature, a larger momentum pressure increase was obtained. This is caused by the larger inlet vapor velocity at the lower temperature for the same flow rate. The precision of the insert thermocouples is indicated by examination of Figure 18b. As can be seen, the total temperature variation between the test section inlet and outlet was less than 2°F, and the maximum scatter of the measured temperatures is less than 0.5°F at 1400°F. Included in Figure 18 are the measurements of the last two of the three thermocouples which were located in the vapor inlet pipe upstream of the condensing heat transfer section. These thermocouples show that the pressure in the inlet vapor pipe decreases as a function of length, due to friction pressure drop.

Figure 19 shows two typical potassium temperature distributions measured

using the instrumented helical insert (Test Set No. 4), one for a mass velocity of 7.4 lbs/sec-ft^2 and the other for a mass velocity of 14 lbs/sec-ft^2 at an inlet vapor temperature of 1200°F. As can be seen from Figure 19, there was a net pressure drop across the condenser with the helical insert, due to the friction pressure drop being larger than the momentum pressure rise. Increasing the mass velocity tended to increase the net pressure drop (compare Figure 19b with Figure 19a).

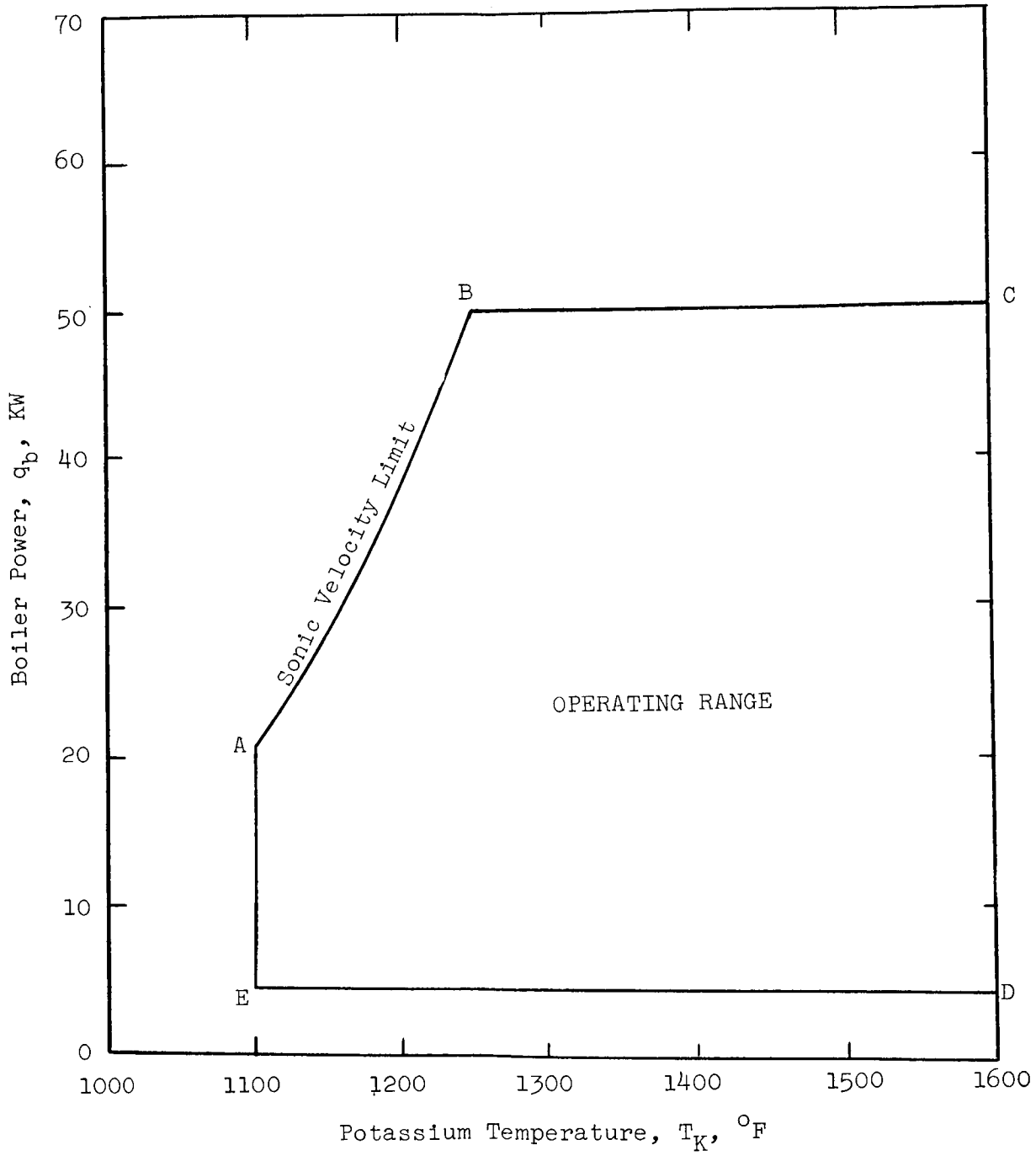

Figure 15. Condensing Facility Operating Range

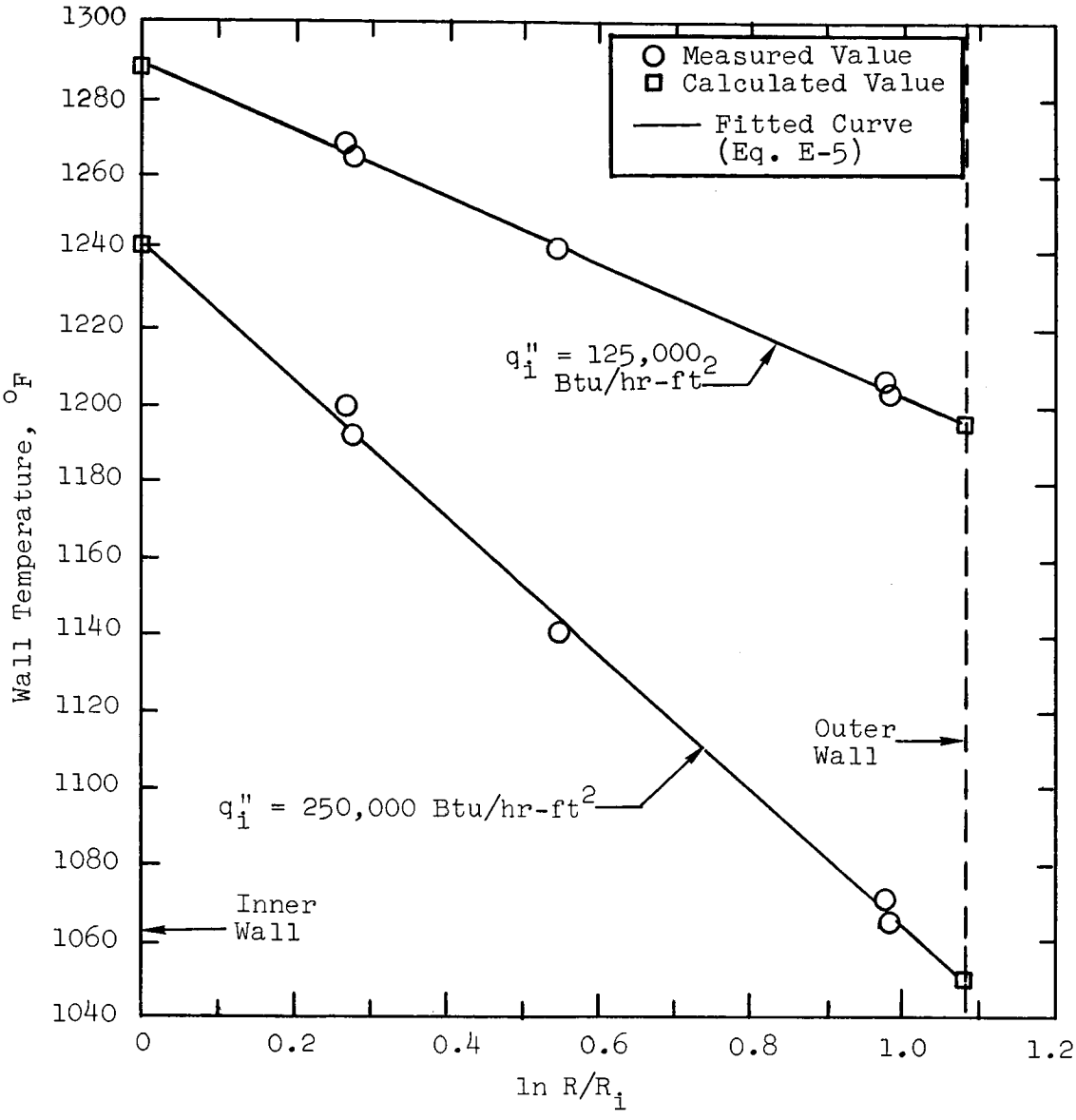

Figure 16. Typical Radial Temperature Distributions In Thick-Walled Nickel Condenser Tube.

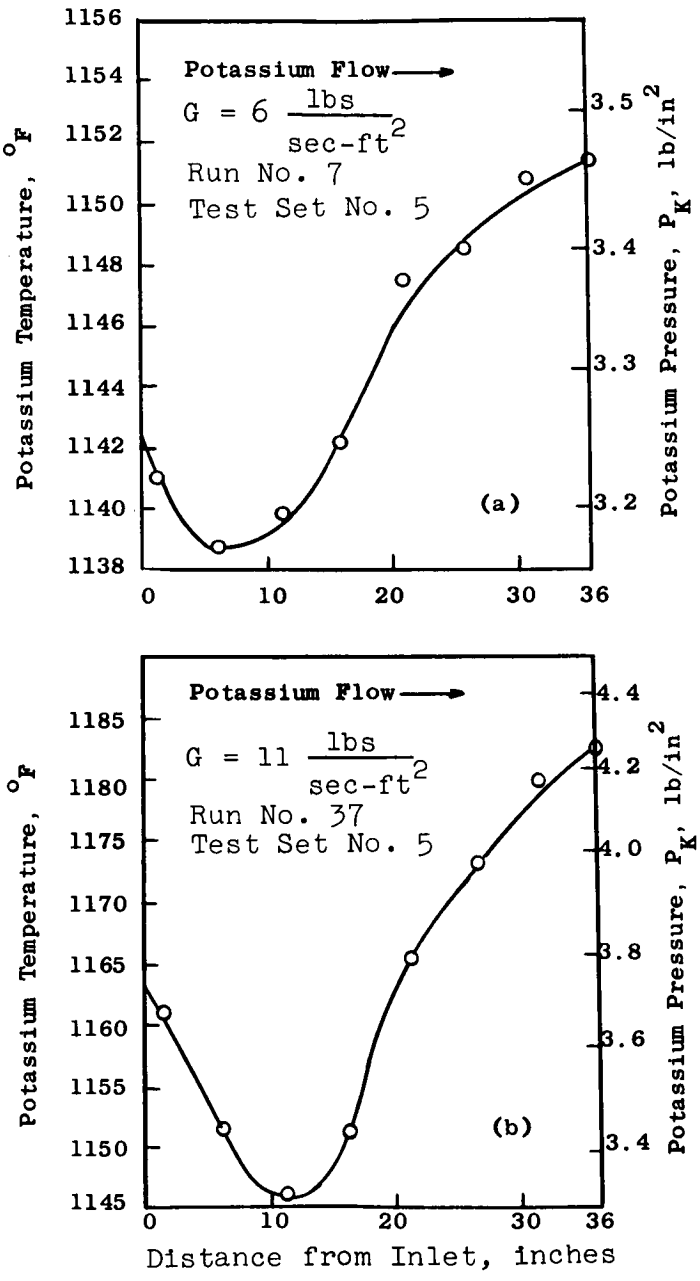

Figure 17. Potassium Axial Temperature Distributions and Corresponding Saturation Pressures For Two Different Mass Velocities At About 1150°F Inlet Temperature (5/8-inch ID tube with 1/4-inch OD Instrumented Tubular Insert)

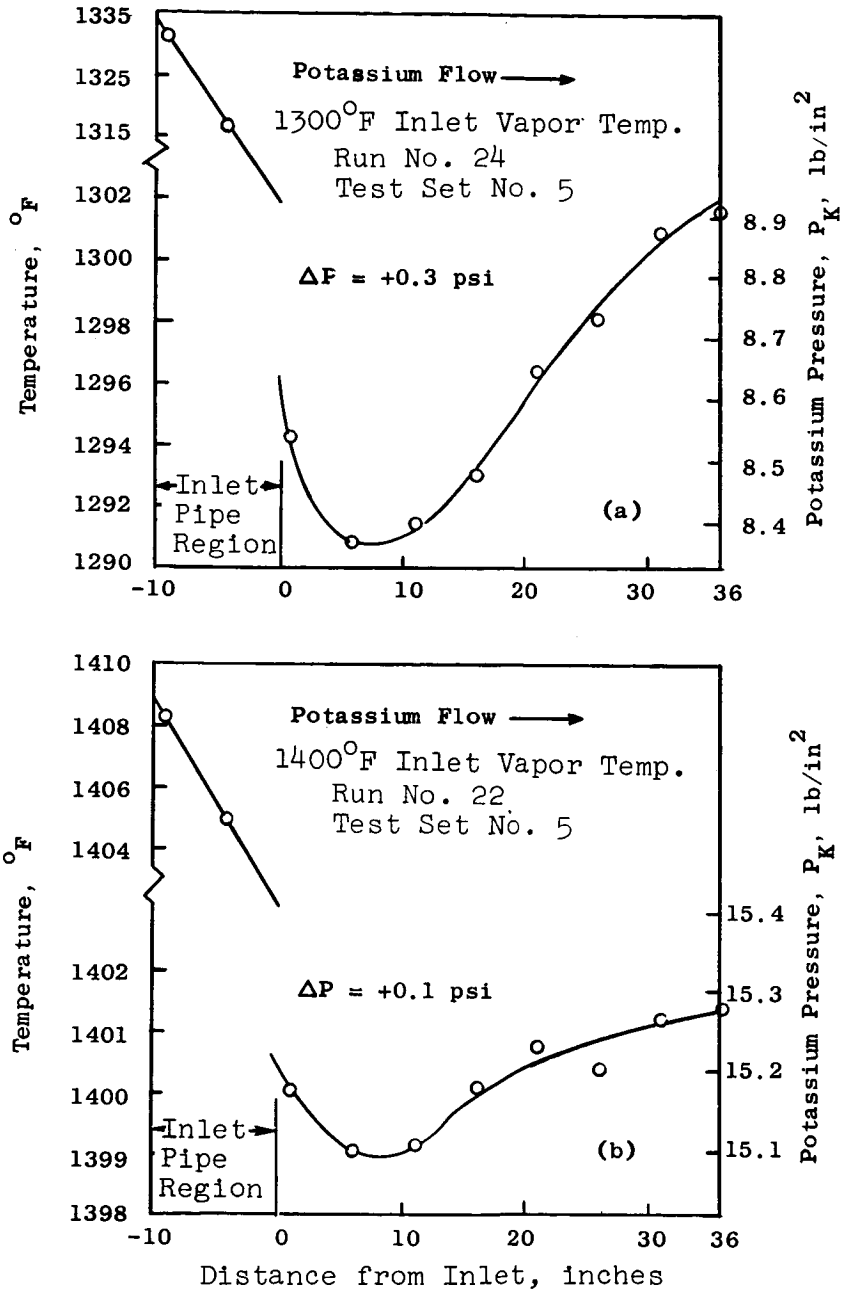

Figure 18. Potassium Axial Temperature Distributions and Corresponding Saturation Pressures For Two Different Inlet Temperatures at G = 13 lb/sec-ft^2 (5/8-inch ID Tube with 1/4-inch OD Instrumented Tubular Insert)

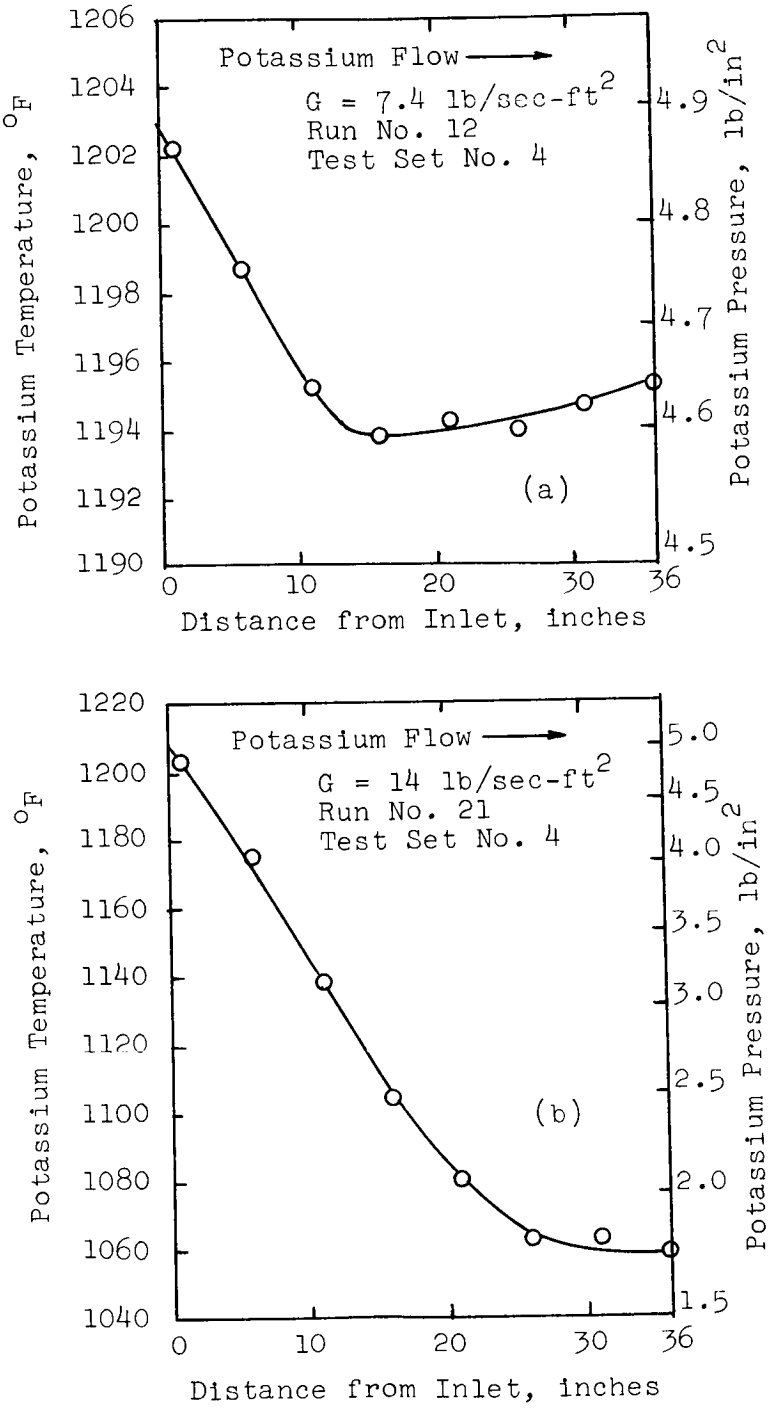

Figure 19. Potassium Axial Temperature Distributions and Corresponding Saturation Pressures for Two Different Mass Velocities at About 1200°F Inlet Temperature (5/8-inch ID Tube with Instrumented Helical Insert, $p/D_i = 6$)

V CONDENSING POTASSIUM HEAT TRANSFER RESULTS

A summary of the test conditions used with each of the five condenser test section geometries is given in Table 1. The experimental condensing heat transfer data obtained are given in Tables 2 to 6. The data reduction procedures employed are described in Appendix E. A discussion of estimated errors in determination of the condensing heat transfer coefficients is given in Appendix F.

For purposes of discussion, the results from Test Set No. 4 (5/8-inch ID tube with instrumented helical insert, $P/D_i = 6$) and Test Set No. 5 (5/8-inch ID tube with instrumented 1/4-inch OD tubular insert) are presented together. These data, given in Tables 2 and 3, are the most reliable of the data obtained for the five test sections because the local potassium temperature was measured directly using thermocouples in the inserts. The results from Test Sets No. 1, 2 and 3, for which the local potassium temperatures were estimated by linear interpolation from measurements at the test section inlet and outlet, are presented as a second group.

Results From Test Sets No. 4 and 5

The heat transfer results obtained using an instrumented helical insert in a 5/8-inch ID tube (Test Set No. 4) and an instrumented 1/4-inch OD tubular insert in the same 5/8-inch ID tube (Test Set No. 5) are presented in Figures 20 and 21 and in Tables 2 and 3. The two sets of data are presented together for comparison in Figure 22. Calculated values of the condensing heat transfer coefficients at 1300°F, calculated using Nusselt's laminar film model (Reference 12) and Seban's turbulant film model (Reference 21), are also shown in the Figures for comparison with the data.

The tubular insert data from Test Set No. 5 are based directly on the local measurements of the potassium temperature obtained from the insert thermocouples.

The helical insert data from Test Set No. 4 are based on the local measurements of the potassium temperature obtained from the insert thermocouples, corrected to account for the increased pressure and saturation temperature at the tube wall due to the radial acceleration caused by the helical insert. The analysis on which this correction is based is given in Appendix E.

The local vapor qualities for each of the data points taken with an instrumented tubular insert in Test Set No. 5, listed in Table 3, were calculated by energy balance using the measured fluid temperatures and flow rates, as discussed in Appendix E. The approximate local vapor qualities at the top and bottom measuring stations, respectively, indicated in Table 2 for the helical insert data of Test Set No. 4 were estimated by linear interpolation assuming 100% vapor at the test section inlet and 0% vapor at the test section outlet. As discussed in Appendix E, this procedure results in an estimated error of about 5% in local quality at the measuring stations, compared to vapor qualities calculated by energy balance. This amount of error is not significant in determination of the condensing coefficients. A more detailed calculation of the local vapor quality is not justified for the helical insert data because of the uncertainties inherent in correcting for radial acceleration effects due to the helical flow.

Examination of Figures 20-22 shows that:

(1) The condensing heat transfer coefficients are in the order of magnitude of 10,000 Btu/hr-ft^2-°F or more (Figures 20 and 21).

(2) The data from the bottom measuring stations (ℓ/D_i = 48) where the vapor quality is least ($X \approx 0.20$) have slightly lower heat transfer coefficients than those from the top measuring station (ℓ/D_i = 10) where the vapor quality is higher ($X \approx 0.88$). As can be seen from the Figures, this experimental trend is in general agreement with the trend of reduced heat transfer coefficient with increased liquid film Reynolds Number predicted by theory (References 12 and 21).

(3) The measured condensing heat transfer coefficients are less than those calculated by the Nusselt and Seban models.

(4) Agreement between the helical insert data from Test Set No. 4 and the tubular insert data from Test Set No. 5 is within the scatter of the data (Figure 22).

The local condensing heat transfer coefficient data taken with an instrumented 1/4-inch OD tubular insert in a 5/8-inch ID tube (Test Set No. 5) are plotted in Figure 23 versus local potassium saturation temperature, mass velocity and local heat flux. As can be seen in Figure 23, the condensing heat transfer coefficient is approximately independent of heat flux, mass velocity and saturation temperature over the ranges of conditions tested.

Three of the data points shown in Figure 23 were taken at condensing temperatures in the range from about 880°F to 1060°F. As shown in Figure 23, the heat transfer coefficients for these three data points are significantly less than for the other data, which were taken at saturation temperatures in the range from 1100°F to 1400°F. It is possible that this is due to a trend of decreased heat transfer coefficient with decreasing temperature which might exist at the lower temperatures but is not evident in the higher range of temperatures in which the rest of the data were taken. It is also possible that these three points have lower coefficients because of some undetermined experimental error which occurred when they were being taken. Excepting these three lower temperature data points, nearly all the other Test Set No. 5 data have condensing coefficients that are larger than 10,000 Btu/hr-ft^2-°F, as shown in Figure 23.

The characteristic of the measured condensing heat transfer coefficients being generally less than those calculated using the liquid film models of Nusselt (Reference 12) and Seban (Reference 21), as shown in Figures 20-22, suggests the possibility of an additional thermal resistance besides that associated with conduction through the liquid film. An investigation of this was done by treating the Test Set No. 5 data (5/8-inch ID tube with instrumented 1/4-inch OD tubular insert) using an analytical model based on the concept of there being a vapor phase thermal resistance that is additive to the resistance due to conduction through the liquid film, as suggested by Rohsenow and Sukhatme (Reference 16). The analysis is presented in detail in Appendix G. Major steps

in the treatment of the Test Set No. 5 data to determine the vapor phase thermal resistance and corresponding vapor phase coefficients are as follows.

First, the liquid film thickness δ was calculated using Dukler's model (Reference 28) for each of the Test Set No. 5 data points. Using these values of δ the heat transfer coefficient corresponding to conduction through the liquid film was calculated employing Equation (5).

$$h_f = k_f/\delta \tag{5}$$

The vapor-phase thermal resistances ($1/h_v$) were then determined by subtracting the calculated liquid film thermal resistance ($1/h_f$) from the experimental values of the total condensing thermal resistance ($1/h_c$) measured for each of the Test Set No. 5 data points, using Equation (6).

$$\frac{1}{h_v} = \frac{1}{h_c} - \frac{1}{h_f} \tag{6}$$

In order to compare with theory the values of h_v calculated from the experimental heat transfer data using Equation (6), an analysis was done based on kinetic gas theory following a procedure suggested by the work of Schrage (Reference 32). The analysis, given in Appendix G, results in Equation (7) for the vapor phase coefficient h_v as a function of vapor saturation properties, absolute temperature and condensation coefficient σ_c.

$$h_v = \sigma_c \lambda \left[\frac{M g_o}{2 \pi \bar{R} T}\right]^{\frac{1}{2}} \left(\frac{dP}{dT} - \frac{P}{2T}\right) \tag{7}$$

The vapor-phase heat transfer coefficients obtained from the Test Set No. 5 data using Equation (6) are presented in Figure 24, together with calculated values from Equation (7) for $\sigma_c = 0.2$. The selected value of $\sigma_c = 0.2$ gives an approximate best fit to the data (average deviation less than $\pm$ 25%). The vapor-phase heat transfer coefficients obtained for each of the Test Set No. 5

data points and the corresponding values of σ_c calculated for each data point using Equation (7) are listed in Table 4.

As shown in Figure 24, the selected value of $\sigma_c = 0.2$ results in fair agreement between the vapor-phase heat transfer coefficients calculated using Equation (7) and those obtained from the Test Set No. 5 data using Equation (6). Vapor-phase coefficients obtained from the data of Engelbrecht (Reference 19) using Equation (6), shown in Figure 24, are in order-of-magnitude agreement with values calculated using Equation (7) with $\sigma_c = 0.2$ for saturation temperatures down to 700°F. A trend of decreasing vapor-phase heat transfer coefficient with decreased saturation temperature is calculated using Equation (7) with $\sigma_c = 0.2$, as shown in Figure 24.

Results From Test Sets No. 1, 2 and 3

The heat transfer results obtained using a 5/8-inch ID tube without insert (Test Set No. 1), a 5/8-inch ID tube with non-instrumented tapered pin insert (Test Set No. 2) and a 3/8-inch ID tube without insert (Test Set No. 3) are presented in Figures 25-27 and Tables 5-7, respectively. Calculated values of the condensing heat transfer coefficients at 1300°F, calculated using Nusselt's laminar film model (Reference 12) and Seban's turbulent film model (Reference 21), are also shown in the Figures for comparison with the data.

For Test Sets No. 1, 2 and 3 the local potassium temperatures at the measuring stations, on which the local condensing heat transfer coefficients are based, were estimated by linear interpolation between the measured potassium inlet and outlet temperatures, with correction for pressure drop in the vapor inlet pipe between the upstream bulk thermocouple station and the condensing section inlet. As discussed further in Appendix H, this procedure for estimating the local potassium temperature at the measuring stations probably contributed to the increased scatter evident in the data obtained from Test Sets No. 1, 2 and 3.

The approximate local vapor qualities at the measuring stations indicated in Tables 5-7 for Test Sets No. 1, 2 and 3, respectively, were estimated by

linear interpolation assuming 100% vapor at the test section inlet and 0% vapor at the test section outlet. Based on the calculated quality distribution comparisons given in Appendix E this procedure results in an estimated error of about 5% in local quality at the measuring stations. This amount of error is not significant in determination of the condensing coefficients.

Examination of Figure 25 shows that the heat transfer coefficient data from Test Set No. 1 (5/8-inch ID tube without insert) have more scatter but are in order-of-magnitude agreement with the Test Set No. 5 data (5/8-inch ID tube with instrumented 1/4-inch OD tubular insert) shown in Figure 21. Most of the Test Set No. 1 data have coefficients larger than 10,000 Btu/hr-ft^2-°F, but all of the coefficients are lower than values calculated using the Nusselt laminar film model (Reference 12) and the Seban turbulent film model (Reference 21), as shown in Figure 25.

The Group-D data listed under Test Set No. 1 in Table 1, comprised of forty-one data points taken in a 5/8-inch ID tube without insert, are not included in Figure 25 and Table 5. This group of data was taken at approximately the same conditions as the other data from Test Set No. 1 given in Figure 25 and Table 5 and is reported in Reference 8. The majority of the Group-D data had indicated coefficients that were negative due to excessive thermocouple errors and possible mal-distribution of the sodium flow in the condenser shell, as discussed in Reference 8. Thus, the Group-D data are not useable. These sources of experimental error were corrected for the other tests.

The data from Test Set No. 2 (5/8-inch ID tube with non-instrumented tapered pin insert), are shown in Figure 26. The coefficients have more scatter and are higher than the data from Test Sets No. 1 and 5, and they are higher than values calculated using the Nusselt model and the Seban model. Examination of Table 6 shows that about half of the data points taken during Test Set No. 2 have indicated coefficients that are negative, primarily at the top measuring station (not plotted in Figure 26), indicating excessive experimental errors in the data. Thus, the

Test Set No. 2 data are not reliable and in consequence no definite conclusions can be drawn regarding the effect of the tapered pin insert on the condensing heat transfer coefficient.

Figure 27 shows the data from Test Set No. 3 (3/8-inch ID tube without insert). The coefficients have large scatter, both above and below values calculated using the Nusselt and Seban models, especially at the top measuring station ($\ell/D_i = 21$). Examination of Table 7 shows that some of the data from the top measuring station have indicated coefficients that are negative (not included in Figure 27). Due to the large scatter in the data shown in Figure 27, no definite conclusions can be drawn regarding the effect on the condensing coefficient of a smaller tube size (3/8-inch ID) in comparison with coefficients measured in the 5/8-inch ID tubes (Test Sets No. 1 and 5).

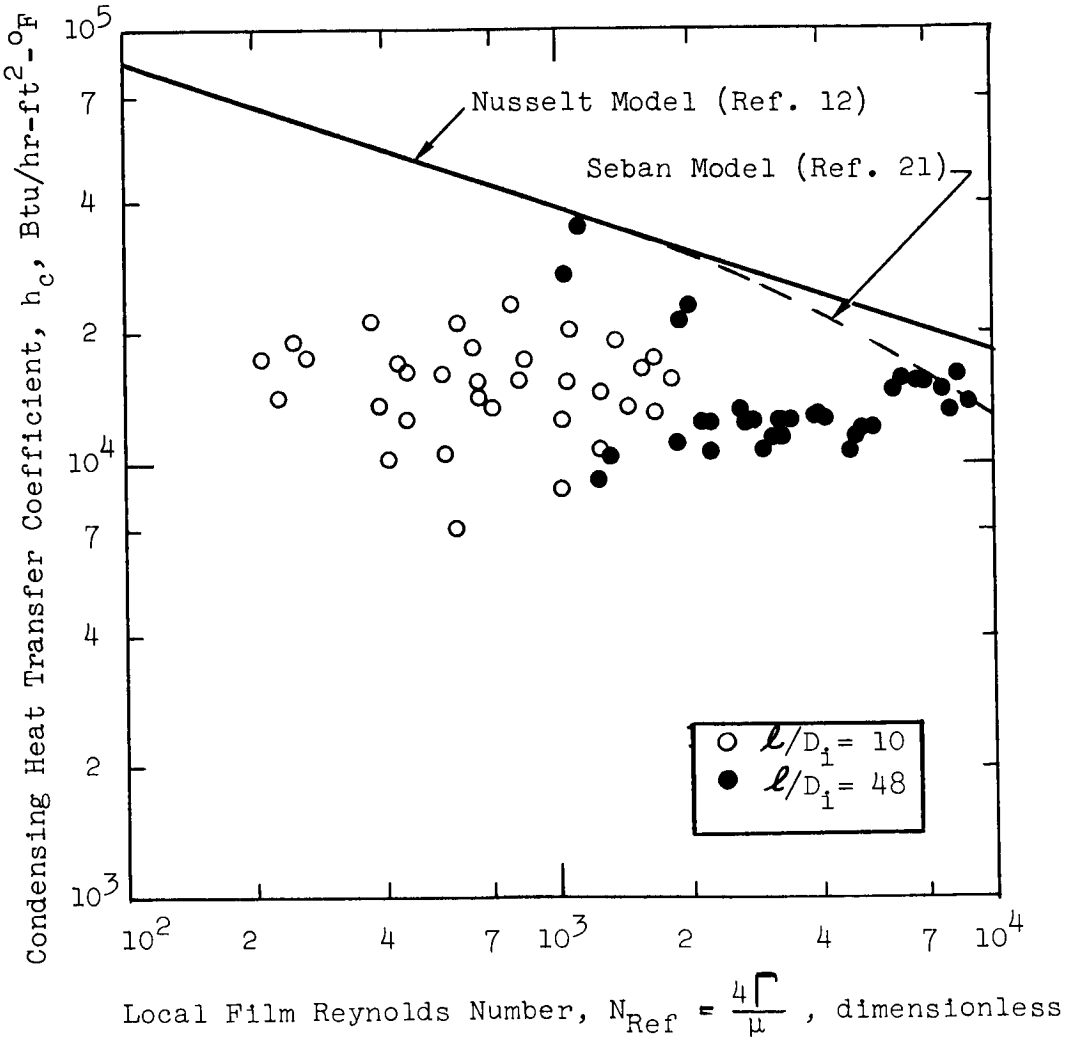

Figure 20. Local Condensing Heat Transfer Coefficients From Test Set No. 4, 5/8-inch ID Tube with Instrumented Helical Insert (p/D_i = 6)

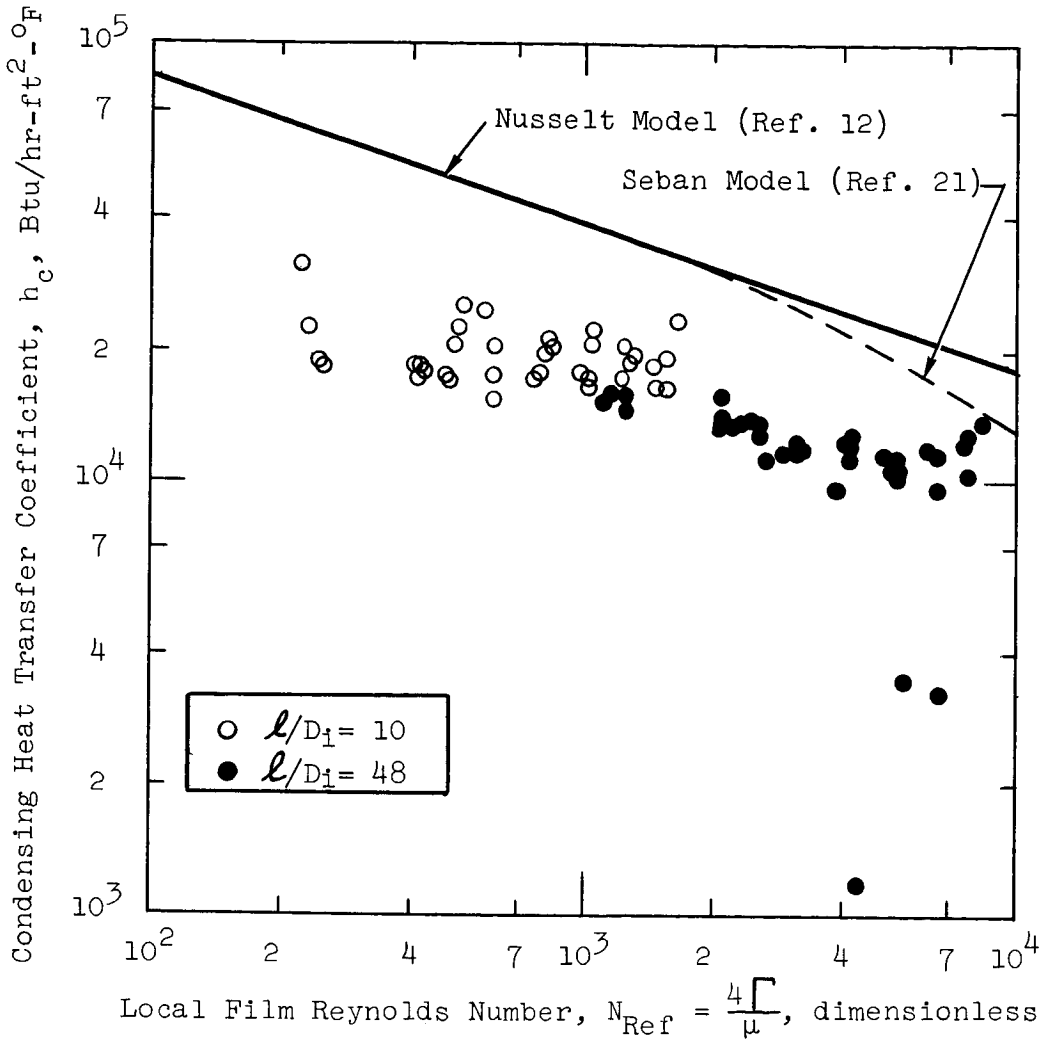

Figure 21. Local Condensing Heat Transfer Coefficients From Test Set No. 5, 5/8-inch ID Tube with Instrumented 1/4-inch OD Tubular Insert.

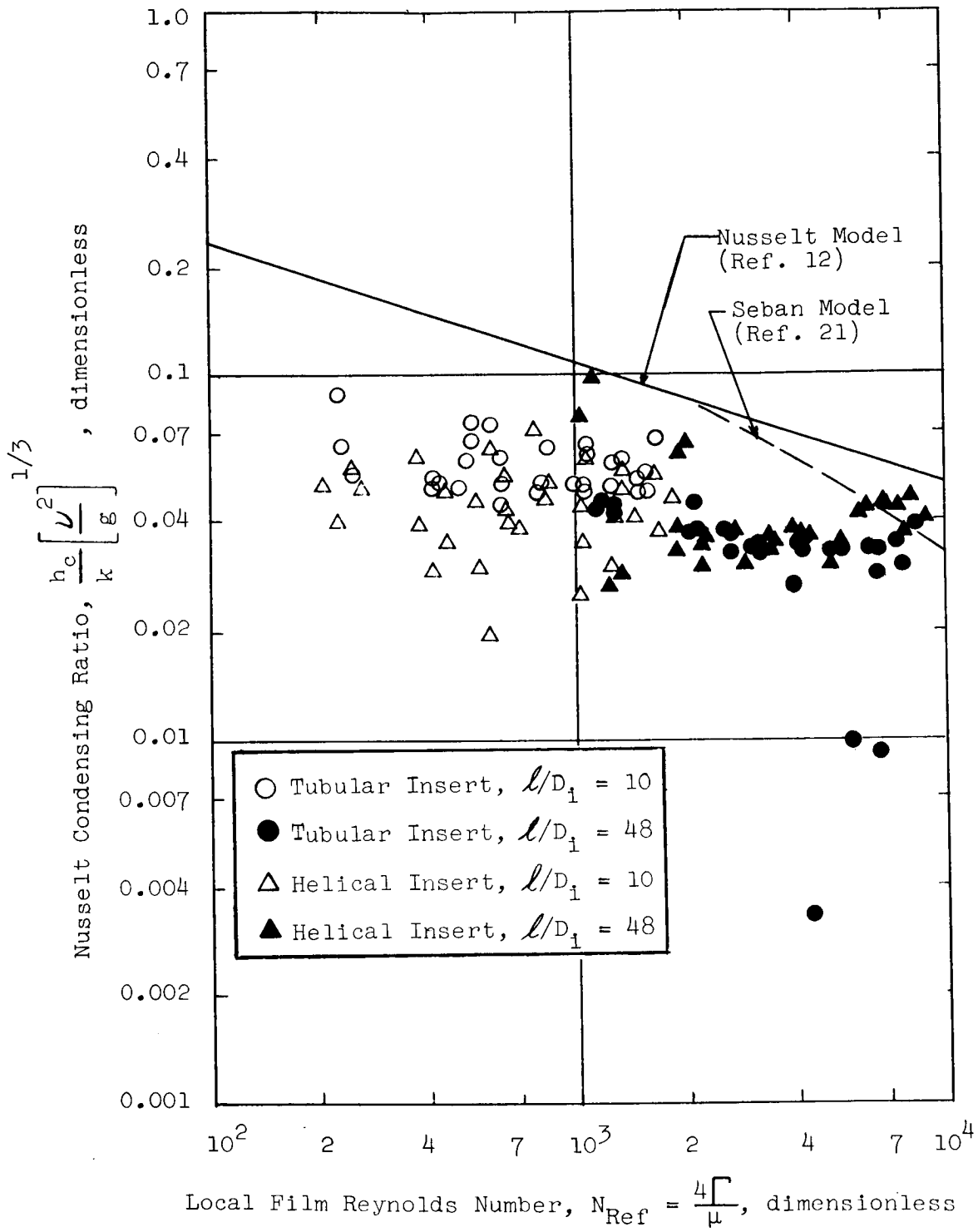

Figure 22. Local Condensing Heat Transfer Results from Test Sets No. 4 and 5, 5/8-inch ID Tube with Instrumented Inserts

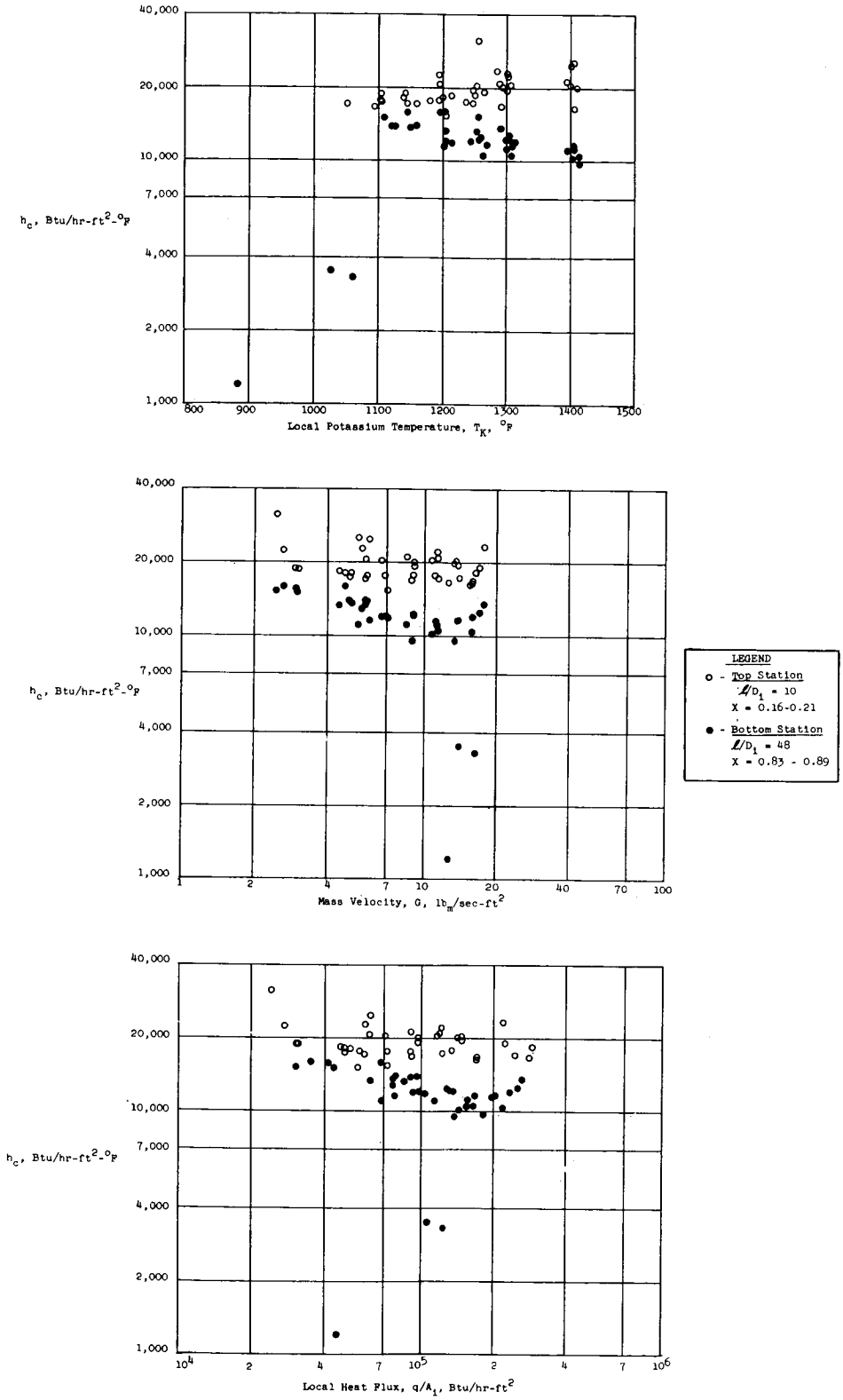

Figure 23. Variation of Local Potassium Condensing Heat Transfer Coefficient with Saturation Temperature, Mass Velocity and Heat Flux (5/8-inch ID Tube with 1/4-inch OD Instrumented Tubular Insert).

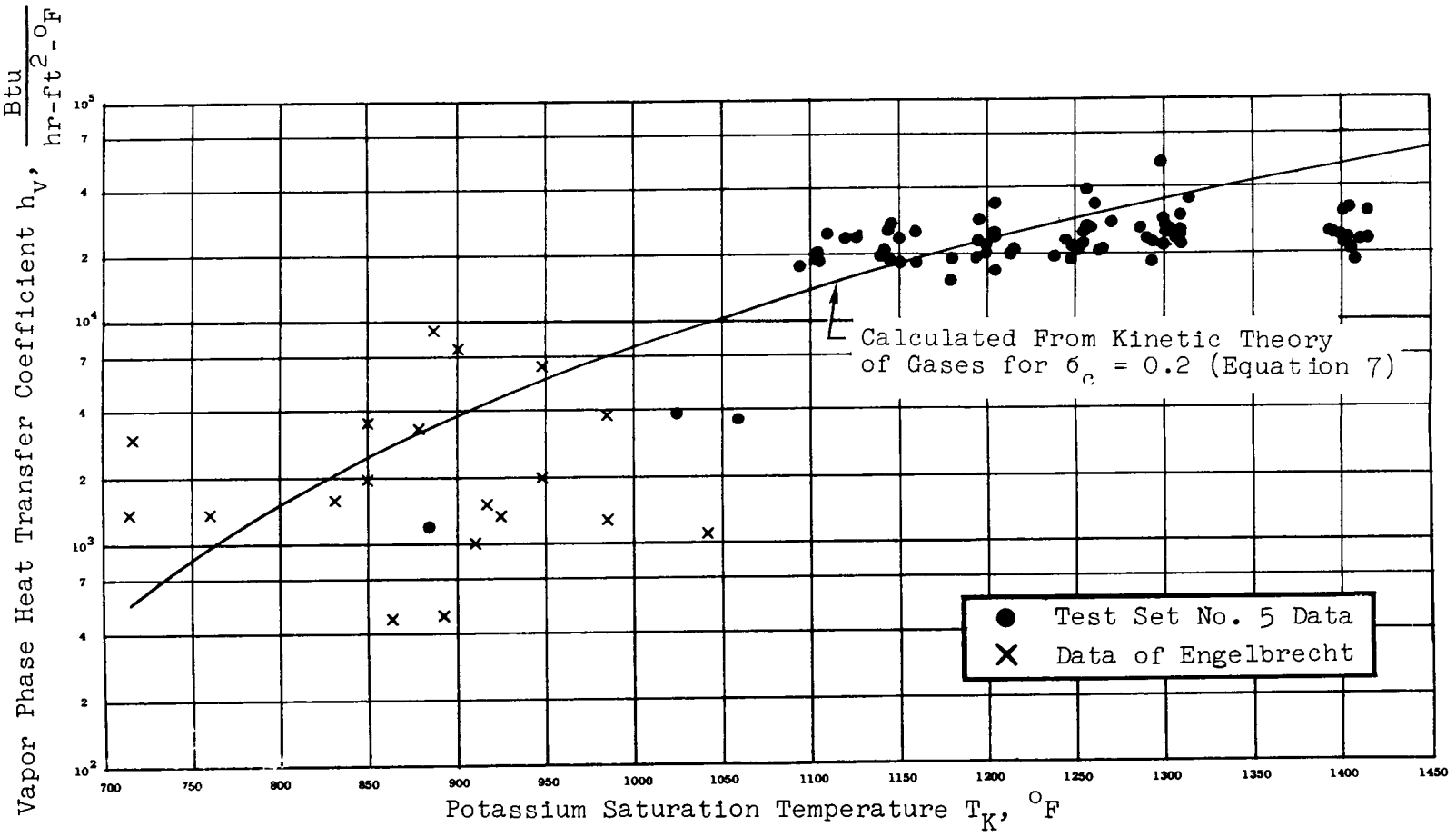

Figure 24. Experimental Potassium Vapor Phase Heat Transfer Coefficients, Defined by Equation (6), Compared With Values Calculated From Kinetic Theory of Gases Using Equation (7) With σ_c = 0.2 For Test Set No. 5 Data and Data of Engelbrecht (Reference 19).

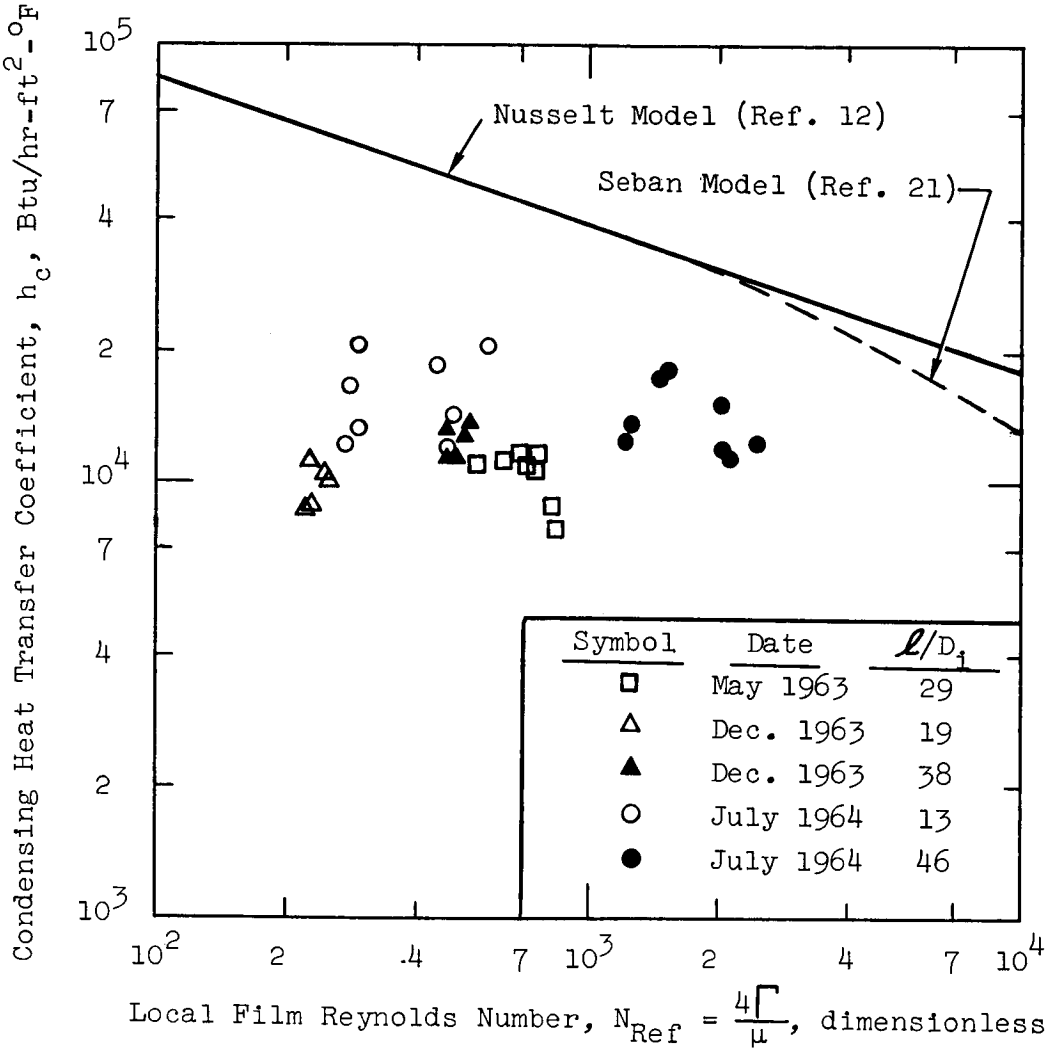

Figure 25. Local Condensing Heat Transfer Coefficients from Test Set No. 1, 5/8-inch ID Tube Without Insert

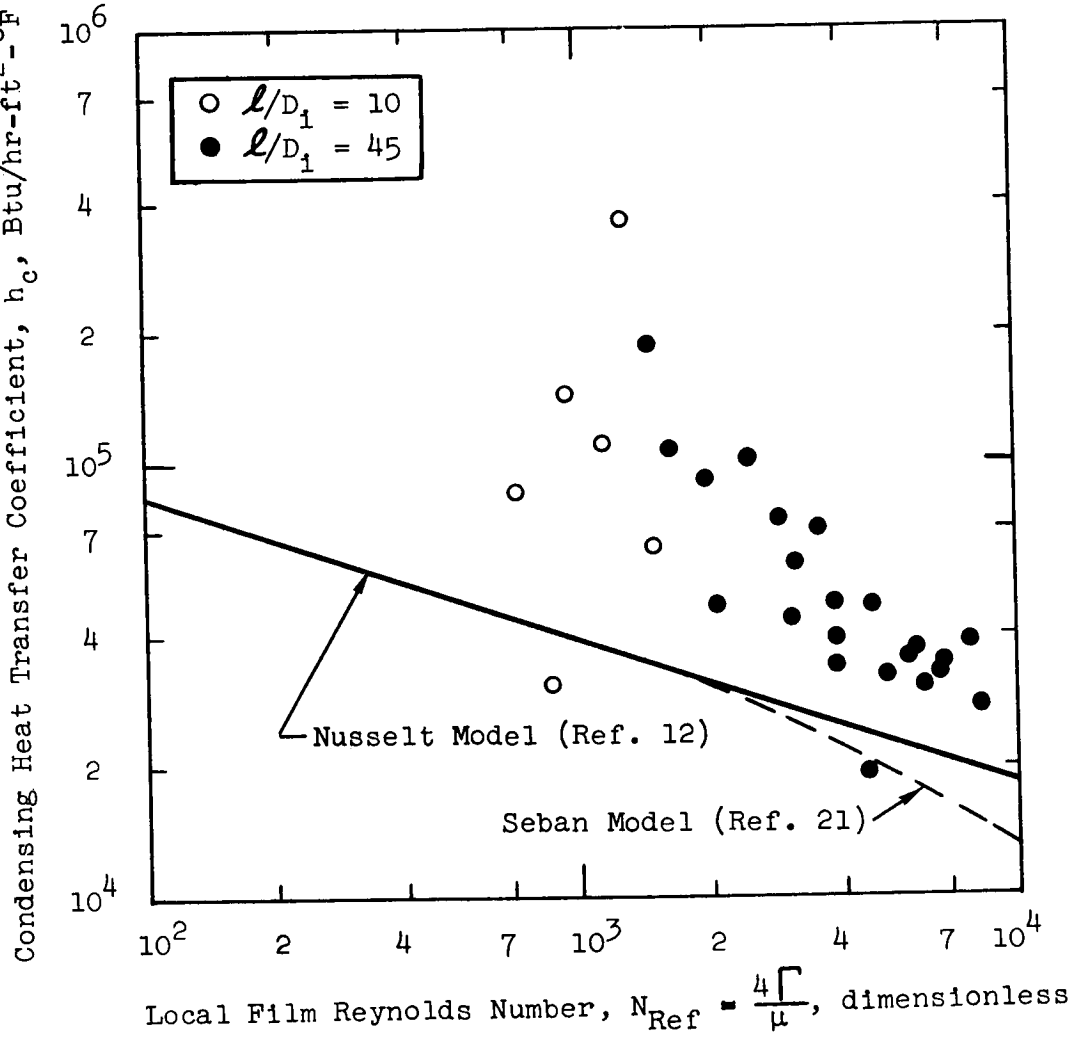

Figure 26. Local Condensing Heat Transfer Coefficients From Test Set No. 2, 5/8-inch ID Tube With Non-Instrumented Tapered Pin Insert.

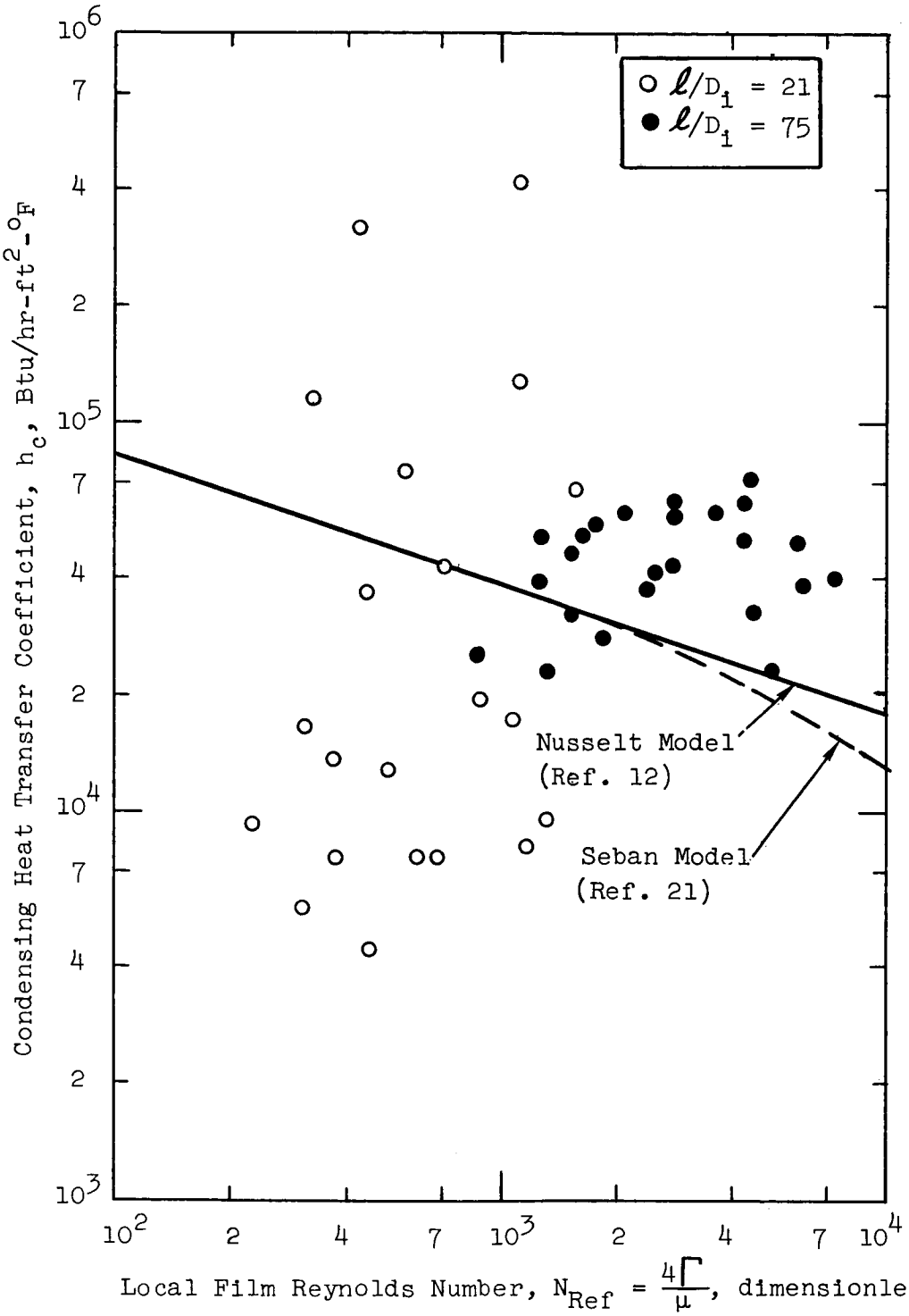

Figure 27. Local Condensing Heat Transfer Coefficients From Test Set No. 3, 3/8-inch ID Tube Without Insert.

VI CONDENSING POTASSIUM PRESSURE CHANGE RESULTS

In this section the experimental two-phase pressure change data obtained during the condensing tests are presented and briefly compared with predictions using the homogeneous flow model (K = 1) and the Martinelli model (Reference 31) modified for application to potassium (Reference 6). The experimental data presented include: overall pressure change across the condensing test section as a function of flow rate; integrated or overall two-phase friction pressure drop multiplier as a function of saturation temperature; and local two-phase friction pressure drop multiplier as a function of saturation temperature. The pressure change data in each case are based on measurements of the two-phase potassium temperatures. The saturated temperature-pressure properties given in Reference 69 were used to relate the measured two-phase temperatures to the corresponding saturation pressures.

Pressure Change Versus Flow Rate

Assuming that at the condenser inlet the potassium is dry saturated vapor (X = 1.0), the pressure change between the inlet and a position at distance ℓ downstream from the inlet where the local vapor quality is X is given by

$$P_\ell - P_I = \frac{G^2}{\rho_f g_o} \left[\frac{\rho_f}{\rho_v} - \frac{\rho_f}{\hat{\rho}} - \frac{f\ell}{2D} \phi_{1-x} \right] \tag{8}$$

where

$$\frac{1}{\hat{\rho}} = \left[\frac{K}{\rho_f} (1-X) + \frac{X}{\rho_v} \right] \left[\frac{1-X}{K} + X \right] \tag{9}$$

For total condensation from X = 1 at the test section inlet to X = 0 at the outlet ($\ell = L_c$), the corresponding pressure change, from Equation (8), is

$$P_O - P_I = \frac{G^2}{\rho_f g_o} \left[\frac{\rho_f}{\rho_v} - 1 - \frac{fL_c}{2D} \phi_{1-0} \right] \tag{10}$$

The integrated two-phase friction multiplier in Equation (10), ϕ_{l-o}, was calculated for this portion of the data treatment using the local two-phase friction multiplier based on the homogeneous flow model (K-1), which is (Reference 6).

$$\phi_{\ell} = \frac{(dP/d\ell)_{TPF}}{(dP/d\ell)_{Liquid}} = \frac{1 + X\left[(\rho_f/\rho_v) - 1\right]}{1 + X\left[(\mu_f/\mu_v) - 1\right]}^{\frac{1}{4}} \qquad (11)$$

The integration of Equation (11) to obtain

$$\phi_{l-o} = \frac{1}{L_c} \int_0^{L_c} \phi_{\ell} \left[x(\ell) \right] d\ell \qquad (12)$$

is done assuming a linear variation of quality with length from the condenser inlet, which can be expressed simply as

$$X = 1 - \frac{\ell}{L_c} \qquad (13)$$

The assumption of a linear variation in vapor quality is an approximation to the actual distribution. The comparison of calculated quality distributions given in Appendix E indicates that the error in local quality due to this approximation is a maximum of about 10% to 15% at the middle of the test section and about 5% at the measuring stations, compared to qualities calculated by energy balance.

Overall condensing pressure change results obtained from Test Set No. 5 (5/8-inch ID tube with instrumented 1/4-inch OD tubular insert) are given in Figures 28 and 29 for vapor inlet temperatures of 1200°F and 1300°F, respectively. Overall pressure changes from condenser inlet to outlet calculated using Equation (10) are also shown in the Figures for comparison with the data. The analytical and experimental results are in good agreement for potassium flow

rates up to about 70 lbs/hr, which corresponds to vapor inlet velocities of 1000 ft/sec at 1200°F and 600 ft/sec at 1300°F for Test Set No. 5. The deviation between the experimental and calculated pressure changes becomes larger as the potassium flow rate increases.

At the highest flow rates, for both 1200°F and 1300°F inlet vapor temperatures, the data show an overall pressure drop from condenser inlet to outlet, rather than the pressure increase calculated using Equation (10). The pressure drop across the condenser increases with increasing flow rate. At the lower flow rates, below about 70 lb/hr for 1200°F (Figure 28) and below 100 lb/hr for 1300°F (Figure 29), the experimental data show an overall pressure rise across the condenser, which is in reasonably good agreement with the trend calculated using Equation (10).

Overall Two-Phase Friction Pressure Drop Multipliers

Equation (10) can be rearranged into Equation (14), which gives the overall or integrated two-phase friction pressure drop multiplier ϕ_{1-O} as a function of the measured overall pressure change from condenser inlet to outlet ($P_O - P_I$) and the other flow variables.

$$\phi_{1-O} = \frac{2D}{fL}\left[\frac{\rho_f}{\rho_v} - 1 - \frac{P_O - P_I}{G^2/\rho_f\, g_o}\right] \qquad (14)$$

Experimental overall two-phase friction pressure drop multipliers calculated using Equation (14) from the data of Test Sets No. 4 and 5 are presented in Tables 8 and 9, respectively, and are plotted in Figure 30. Two-phase friction pressure drop multipliers calculated using Equation (14) from the data of Test Set No. 1 are presented in Table 10 and are plotted in Figure 31. The potassium properties for these calculations are those given in Reference 69 evaluated at the arithmetic average temperature between the test section inlet and outlet. The following smooth-tube

friction factor equation of Blasius was used for calculation of the single-phase liquid friction factor (Reference 61).

$$f = 0.316/(N_{Re})^{\frac{1}{4}} \qquad (15)$$

As suggested in Reference 10, the maximum helical velocity and maximum helical path length were used in the calculations for the helical insert geometry of Test Set No. 4.

Also shown on Figures 30 and 31 are values of the integrated two-phase friction multiplier calculated using the homogeneous flow model of Reference 6, given by Equations (11-13) and values obtained from the Martinelli model (Reference 31) as modified for potassium in Reference 6. Referring first to Figure 30, it is apparent that reasonably good agreement exists between calculated values using the Martinelli model and experimental values of the overall two-phase friction multiplier for both the helical insert data of Test Set No. 4 and the tubular insert data of Test Set No. 5. The experimental two-phase multipliers in general are higher than those calculated using the homogeneous model (K = 1).

The experimental two-phase friction multipliers obtained from the Test Set No. 1 data (5/8-inch ID tube without insert) are in good agreement with values calculated from both the Martinelli model and the homogeneous model, as shown in Figure 31. Nearly all of these data are in between the values calculated using the two analytical models.

Local Two-Phase Friction Pressure Drop Multipliers

Local friction pressure drop multipliers were evaluated from measured potassium axial temperature distributions of Test Sets No. 4 and 5. The local pressure gradients were determined from the measured potassium temperature

gradients using the potassium saturation pressure-temperature properties given in Reference 69. This was done for both the top and the bottom measuring stations in the test section. The local pressure gradients were determined using in each case the potassium temperatures measured with insert thermocouples at three positions bracketing the measuring station, and a least-squares procedure was used to calculate a best fit gradient through the three temperatures.

The local friction pressure gradient $(dP/d\ell)_{fr}$ was estimated for each data point by subtracting a calculated local pressure gradient due to momentum change $(dP/d\ell)_{MOM}$ from the measured pressure gradient $(dP/d\ell)$, as expressed by Equation (16).

$$\left(\frac{dP}{d\ell}\right)_{fr} = \frac{dP}{d\ell} - \left(\frac{dP}{d\ell}\right)_{MOM} \tag{16}$$

The local momentum pressure gradient can be expressed as

$$\left(\frac{dP}{d\ell}\right)_{MOM} = \frac{G^2}{g_o} \frac{d}{d\ell} \left(\frac{1}{\hat{\rho}}\right) \tag{17}$$

where $\frac{1}{\hat{\rho}}$ is given by Equation (9).

Homogeneous flow (K = 1) was assumed for the calculations, for which Equation (17), combined with Equation (9), reduces to

$$\left(\frac{dP}{d\ell}\right)_{MOM} = \frac{G^2}{g_o} \left(\frac{1}{\rho_v} - \frac{1}{\rho_f}\right) \frac{dX}{d\ell} \tag{18}$$

The local vapor quality gradient $dX/d\ell$ for use in Equation (18) was calculated from an energy balance using the flow rate and the local heat flux at each measuring station.

The local two-phase friction pressure gradients $(dP/d\ell)_{fr}$, calculated from Equation (16), were then used in the following Equation (19) to estimate the corresponding local two-phase friction pressure drop multipliers ϕ_ℓ :

$$\phi_\ell = \frac{2\, g_o\, D\, \rho_f}{f G^2} \left(\frac{dP}{d\ell}\right)_{fr} \qquad (19)$$

The single-phase liquid friction factor f was calculated from Equation (15). For the helical insert data of Test Set No. 4, the maximum helical velocity was used, as suggested in Reference 10.

Values of the local two-phase friction pressure drop multipliers ϕ_ℓ calculated from the data of Test Sets No. 4 and 5 using Equation (19) are presented in Tables 8 and 9 and Figures 32 and 33 respectively. Values of ϕ_ℓ calculated using the homogeneous flow model (K = 1), given by Equation (11), and the Martinelli flow model, modified for potassium (Reference 6), are shown on the Figures for comparison with the data.

As can be seen from Figures 32 and 33 the experimental values of ϕ_ℓ scatter widely and agreement with calculated values using either of the two flow models is poor. In general, the experimental values of ϕ_ℓ for the bottom measuring station where the vapor quality was low are higher than the values calculated from the two flow models, but at the top measuring station where the vapor quality was higher agreement with the calculated values is better. The vapor qualities indicated in Figures 32 and 33, X = 0.2 at the bottom station and X = 0.8 at the top station, are within about 10% of the qualities calculated by energy balance (Appendix E), which is sufficiently accurate for purposes of comparing multipliers calculated theoretically with those obtained from the data.

The large scatter in the data shown in Figures 32 and 33 indicate that the errors in determining the local multipliers are too large for the data to be useful other than to show order-of-magnitude trends.

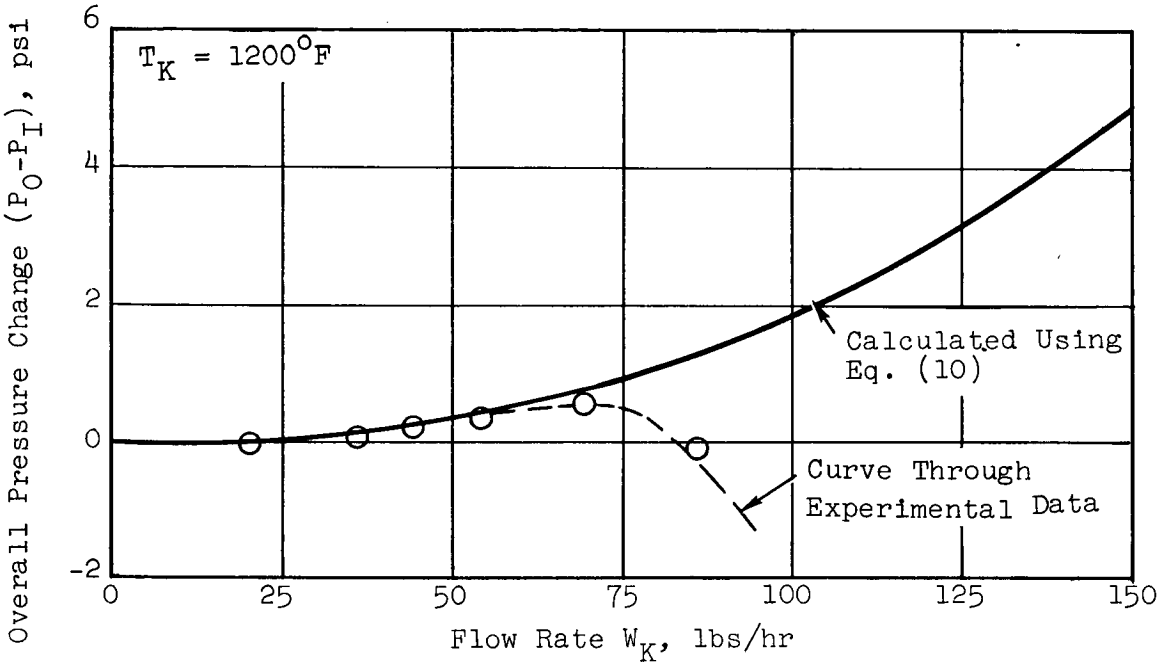

Figure 28. Overall Condensing Pressure Change Versus Flow Rate For Test Set No. 5 At Potassium Vapor Inlet Temperature of 1200°F (5/8-inch ID Tube With 1/4-inch OD Tubular Insert)

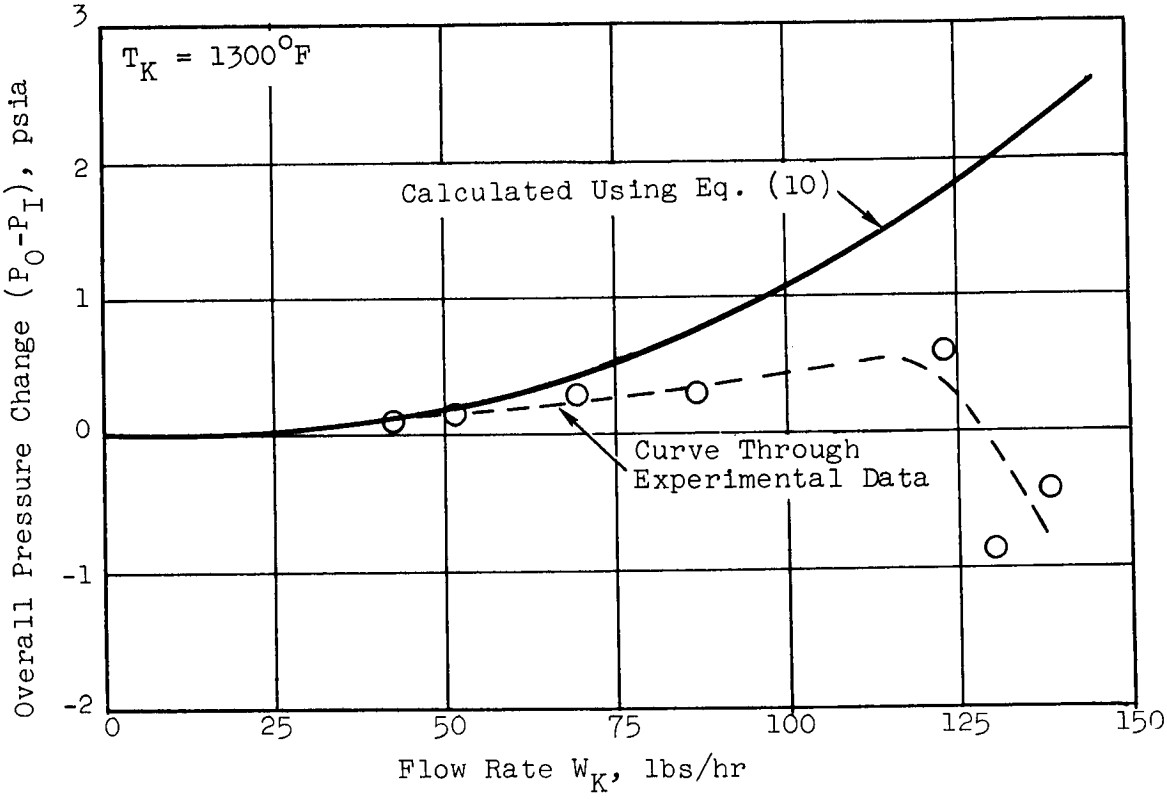

Figure 29. Overall Condensing Pressure Change Versus Flow Rate for Test Set No. 5 at Potassium Vapor Inlet Temperature of 1300°F (5/8-inch ID Tube With 1/4-inch OD Tubular Insert)

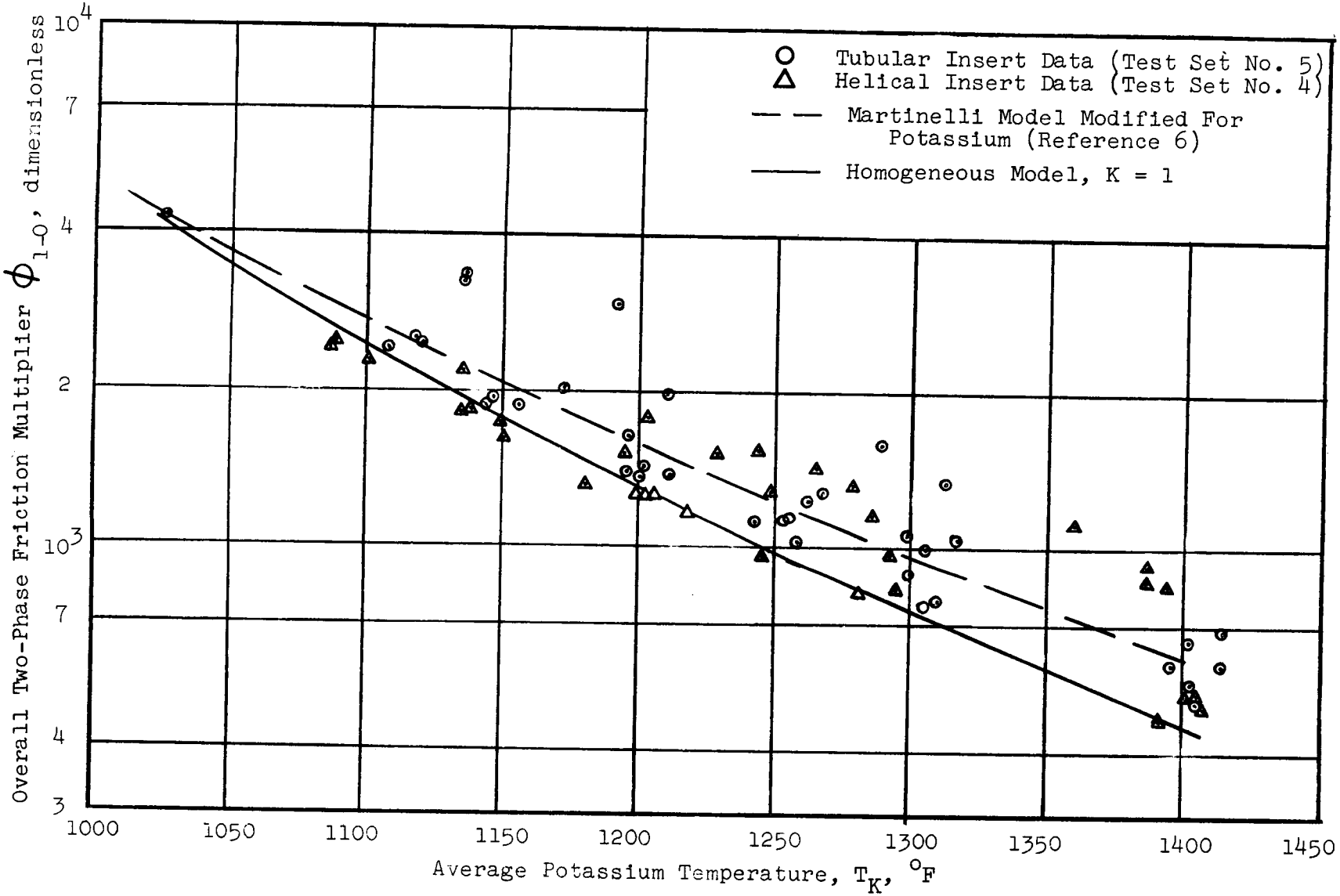

Figure 30. Overall Two-Phase Friction Pressure Drop Multipliers For Condensing From Approximately 100% to 0% Quality As A Function of Potassium Temperature Calculated From Data Of Test Sets No. 4 and 5 Using Equation (14)

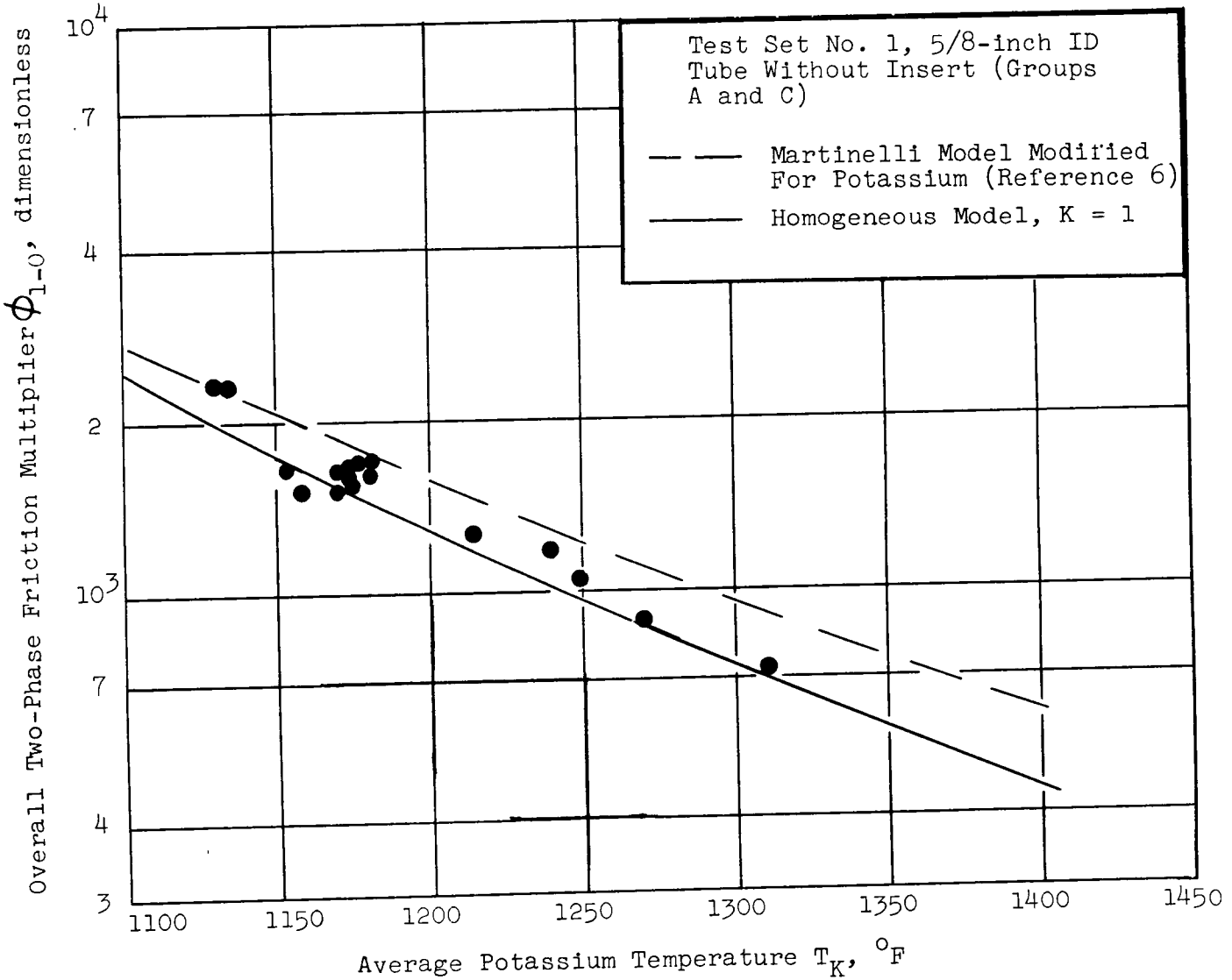

Figure 31. Overall Two-Phase Friction Pressure Drop Multipliers For Condensing From Approximately 100% to 0% Quality As A Function of Potassium Temperature, Calculated From Data of Test Set No. 1, Using Eq. (14)

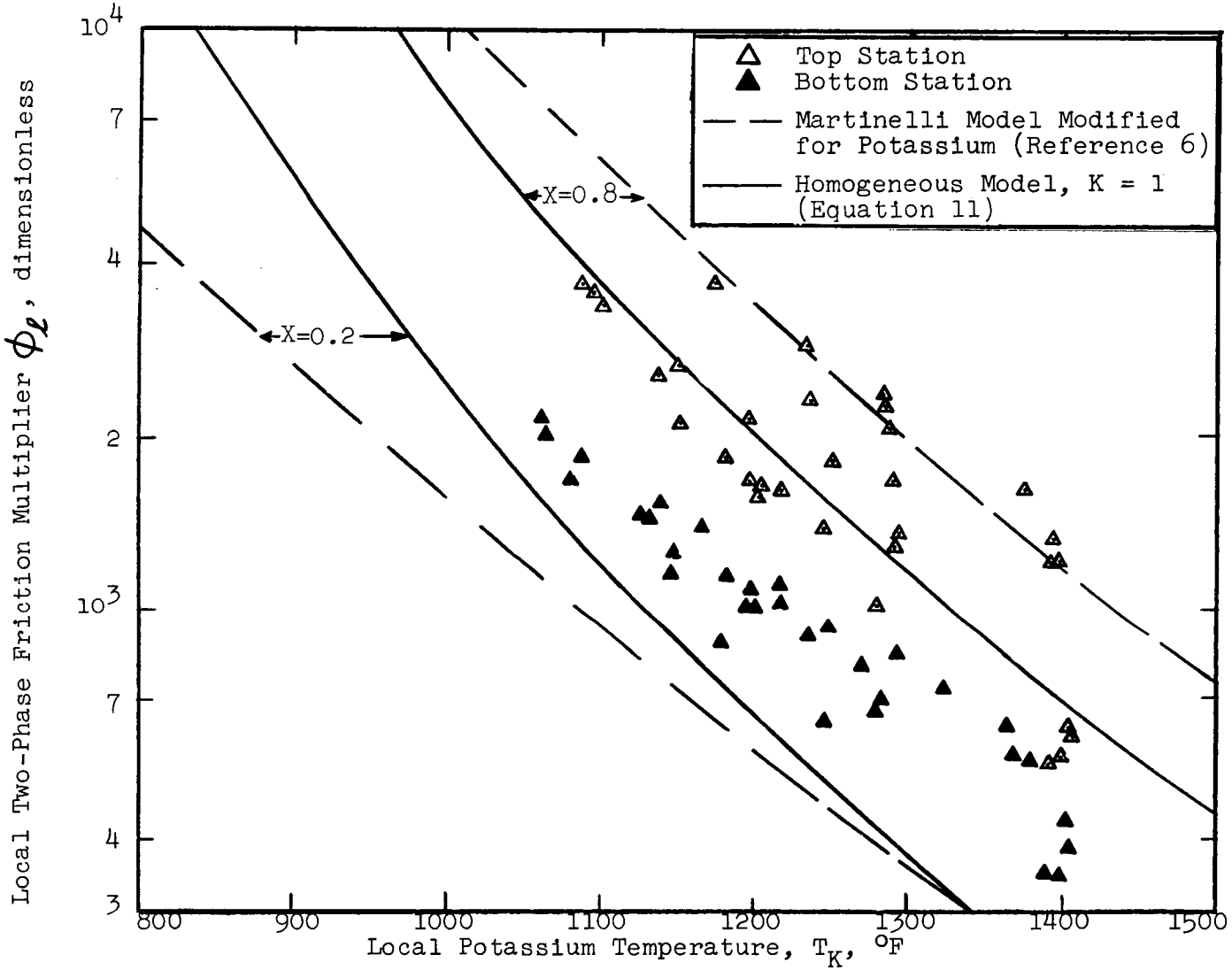

Figure 32. Local Two-Phase Friction Pressure Drop Multipliers As A Function of Potassium Temperature, Calculated From Test Set No. 4 Data (5/8-inch ID Tube with Helical Insert, $p/D_i = 6$) Using Eq. (19)

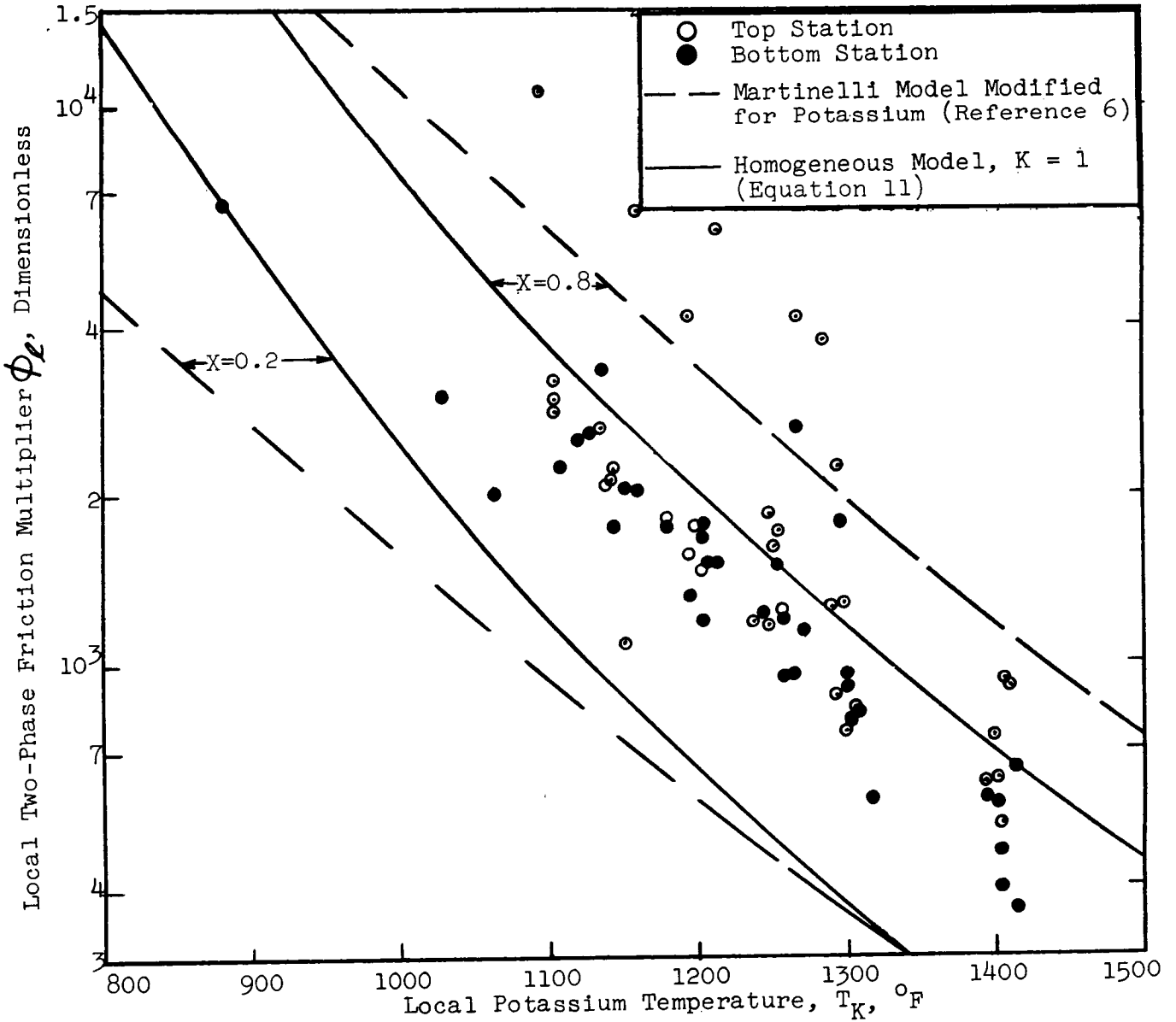

Figure 33. Local Two-Phase Friction Pressure Drop Multipliers As A Function of Potassium Temperature, Calculated From Test Set No. 5 Data (5/8-inch ID Tube with 1/4-inch OD Tubular Insert) Using Eq. (19)

VII STABILITY OF LIQUID LEVEL IN CONDENSER TUBE

During the condensing heat transfer tests the potassium liquid level was always maintained in the head-tank located about one-foot downstream of the condenser. An alternate mode of operation is to maintain the liquid level in the active heat transfer zone of the condenser. An investigation of the fluid temperature behavior and steadiness of operation when the liquid level was moved from the head-tank into the condenser was done at the end of Test Sets No. 4 and No. 5. Results from Test Set No. 5 (5/8-inch ID tube with instrumented 1/4-in OD tubular insert) are presented following. These results are essentially the same as those obtained in Test Set No. 4 (5/8-inch ID tube with instrumented helical insert, $p/D_i = 6$).

Prior to raising the liquid level from the head-tank into the condenser at the end of Test Set No. 5, the following steady-state conditions were established:

Boiler Power	25 KW
Average Condensing Heat Flux	120,000 Btu/hr-ft^2
Test Section Power	20 KW
Potassium Flow Rate	65 lb/hr
Vapor Inlet Temperature	1340°F

The test was started from these steady-state conditions by gradually reducing the liquid potassium pumping rate from the head-tank, while the boiler electrical power and the sodium flow rate were both held constant. Since the boiler power was held constant, the potassium vapor generation rate in the boiler and the potassium vapor flow rate into the condenser were nearly constant. Thus, with the liquid potassium flow rate having been reduced from the original steady-state value, the potassium vapor flow rate into the condenser became larger than the

liquid removal rate from the head-tank. The result of this unbalance in flow was to cause the liquid level to rise until it entered the condenser.

The results of this test are presented in Figure 34, which is composed of two segments of a continuous oscillograph recording made during the test. About one-hour had elapsed from the start of the test until the beginning of Segment-1 in Figure 34, by which time the liquid potassium pump flow rate had been reduced to 56 lb/hr. Entry of the liquid level into the condenser section is indicated in Segment-1 by the decrease in the potassium outlet temperature T_{K_O} from the initial 1339°F down to 1230°F over a period of several seconds.

The liquid level continued to move upward in the test section and about 30 seconds later it reached the insert thermocouple located 5-inches upstream of the condenser exit. The liquid level reaching this position is indicated by a reduction in the potassium temperature at that point, as shown in Segment-1.

A subsequent slight reduction in potassium liquid flow rate to 53 lb/hr at constant boiler power resulted in the liquid level moving gradually higher in the test section until it had passed the insert thermocouple located 10-inches upstream of the condenser exit, as shown in Segment-2. No further changes in the potassium liquid flow rate were made for one-hour and during this period the liquid level remained in the 5-inch long region of the test section between the insert thermocouple located 10-inches upstream of the condenser exit and the next higher insert thermocouple located 15-inches upstream of the exit.

The active condensing length during the last phase of the operation, measured from the potassium vapor inlet end of the test section, was between 21-inches and 26-inches long. The corresponding average condensing heat flux and potassium vapor flow rate at steady-state were about 150,000 Btu/hr-ft^2 and 53 lb/hr, compared to 120,000 Btu/hr-ft^2 and 65 lb/hr, respectively, at the start of the test. As shown in Segment-2 of Figure 34, the insert thermocouples

on each side of the liquid level (10-inches and 15-inches upstream of the condenser exit, respectively) indicate that the local potassium temperature was reduced about 140°F in the 5-inch long region in which the liquid level was located.

After the liquid level had been maintained in the upper position for one-hour, the potassium pump flow rate was increased to approximately the original value of 65 lbs/hr to lower the liquid level back into the head-tank. Throughout the entire test only the potassium pump flow rate was varied and all other system control variables, such as the boiler electrical power, the sodium flow rate and air flow rate to the sodium cooler, were left constant.

The following observations can be made from the test results shown in Figure 34:

(1) The liquid level was maintained in a steady position in the veritical condenser with only small fluctuations of fluid temperature and flow rate, as shown in Figure 34.

(2) A temperature differential in the potassium approximately equal to the difference between the potassium saturation temperature and the sodium inlet temperature was established over a 5-inch length of the condenser across the liquid level.

(3) The liquid level could be gradually moved from one position to another in the condenser by adjusting the potassium pump flow rate, without any significant fluctuations in temperature or flow rate other than the change in potassium axial temperature distribution associated with the change in potassium condensing and sub-cooled lengths.

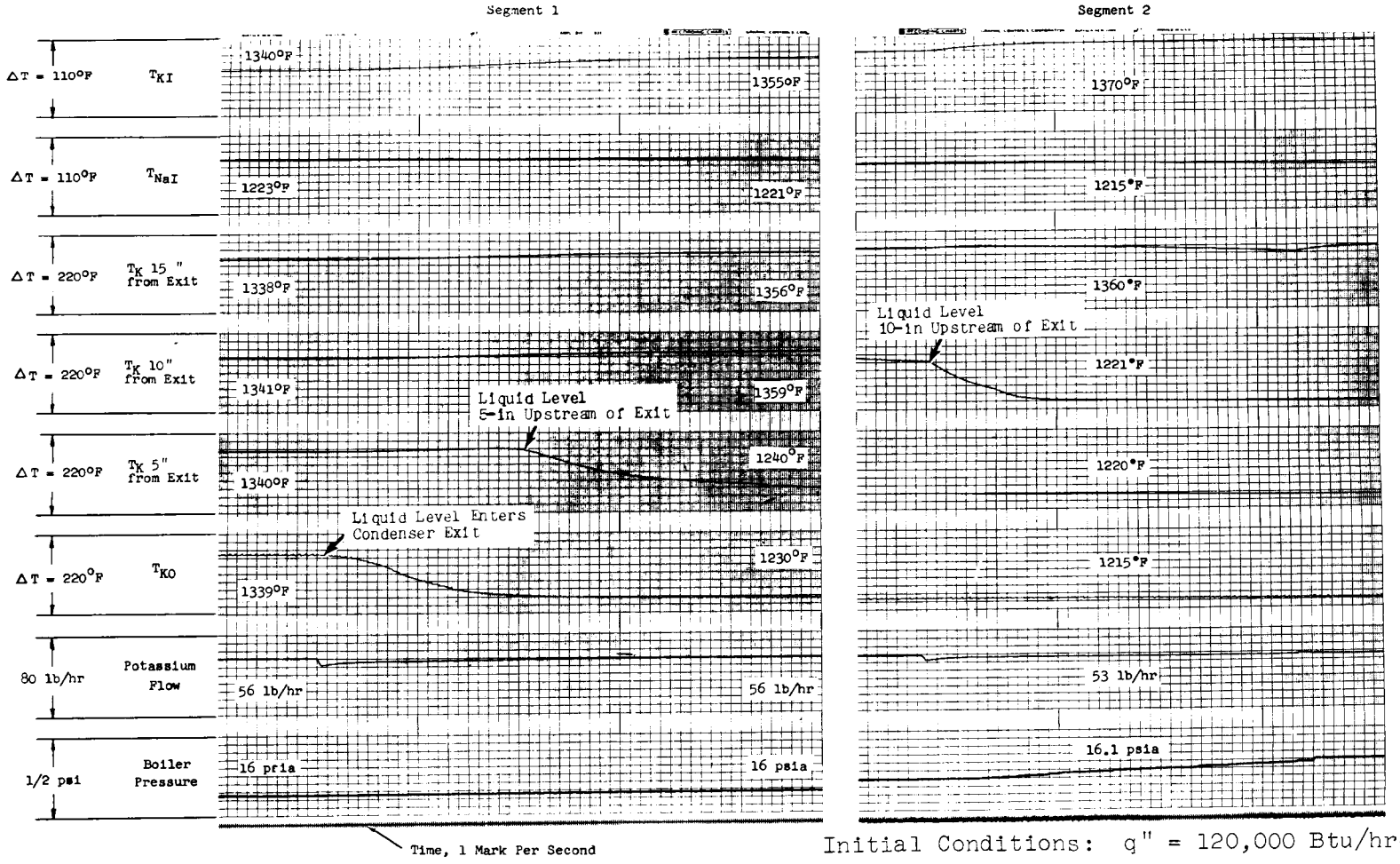

Initial Conditions: $q'' = 120{,}000$ Btu/hr-ft^2
$W_K = 65$ lb/hr
$T_K = 1340^\circ$F

Figure 34. Fluid Temperature Behavior In Condensing During Liquid Level Position Test With Tubular Insert In 5/8-inch ID Tube (Test Set No. 5)

VIII APPLICATION TO CONDENSER DESIGN

The forced convection potassium condensing heat transfer coefficient data presented in Section V are applicable to design of condensers in which the potassium is condensed inside tubes. This application is discussed briefly below, primarily in reference to a 7-tube NaK-cooled, shell-and-tube potassium condenser. This condenser, which is described in more detail in Reference 71, has a tube size, shell-side geometry, power per tube and operating conditions which are typical of those anticipated for space power system condensers.

The relationship between condensing heat transfer rate q_C, potassium condensing temperature T_K, the NaK cooling fluid inlet and outlet temperatures T_{NaK_I} and T_{NaK_O}, and the required condensing heat transfer area inside the tubes A_C is given by the following equation.

$$q_C = U_i A_C \frac{T_{NaK_O} - T_{NaK_I}}{\ell n \left(\frac{T_K - T_{NaK_I}}{T_K - T_{NaK_O}}\right)} \qquad (20)$$

The overall heat transfer coefficient U_i, based on the tube inside diameter, is calculated using

$$\frac{1}{U_i} = \frac{1}{h_c} + \frac{1}{h_w} + \frac{D_i}{D_o h_{NaK}} \qquad (21)$$

The wall heat transfer coefficient h_w in Equation (21) is given by

$$\frac{1}{h_w} = \frac{D_i}{2k_w} \ell n \left(\frac{D_o}{D_i}\right) \qquad (22)$$

and the condensing heat transfer area A_C in Equation (20) for uniform diameter tubes is given by

$$A_C = N\pi D_i L_C, \tag{23}$$

Consider the design of a 7-tube NaK-to-NaK condenser for the following assumed design conditions (Reference 71):

Condensing heat transfer rate	75 KW
Potassium saturation temperature	1300°F
NaK inlet temperature	1150°F
NaK outlet temperature	1250°F
Tube outside diameter	0.69-inch
Tube wall thickness	0.035-inch
Tube material	SS 316
Tube spacing-to-diameter ratio	1.3

For these conditions the NaK heat transfer coefficient on the shell-side h_{NaK}, the tube wall heat transfer coefficient h_w and the potassium condensing heat transfer coefficient h_c are estimated to be:

$$h_{NaK} = 6{,}000 \text{ Btu/hr-ft}^2\text{-°F}$$
$$h_w = 5{,}300 \text{ Btu/hr-ft}^2\text{-°F}$$
$$h_c = 15{,}000 \text{ Btu/hr-ft}^2\text{-°F}$$

The NaK heat transfer coefficient was calculated from the equation of Dwyer and Tu given in Reference 40, and the wall heat transfer coefficient was calculated using Equation (44). The potassium condensing heat transfer coefficient h_c = 15,000 Btu/hr-ft^2-°F is an assumed value based on the data from Test Set No. 5 (5/8-inch ID tube with instrumented 1/4-inch OD tubular insert). As shown in Figure 23 this value of h_c gives a reasonably good approximation of the Test Set No. 5 data over the temperature range from 1100°F to 1400°F (average deviation from the data less than ± 30%).

The corresponding overall heat transfer coefficient calculated using Equation (21) is U_i = 2470 Btu/hr-ft^2-°F. Using this value in Equation (20) together with the fluid temperatures listed above to obtain A_C, and substituting A_C into Equation (23) results in an estimated condensing length for the condenser of L_C = 1.0 foot. Estimates of the relative sensitivity of the calculated condensing length to uncertainties in the heat transfer coefficients are as follows.

If h_c were actually 7500 Btu/hr-ft^2-°F, or 50% lower than assumed, the overall heat transfer coefficient U_i would be 2120 Btu/hr-ft^2-°F, for which a condensing length of 1.17 feet would be calculated. A reduction of the average NaK temperature from 1200°F to 1185°F would cause the condenser to transfer the specified 75 KW in a 1-foot condensing length. If h_c were 22,500 Btu/hr-ft^2-°F, 50% higher than assumed originally, the overall heat transfer coefficient U_i would be 2620 Btu/hr-ft^2-°F and the corresponding calculated condensing length is 0.95-foot. An increase in average NaK temperature from 1200°F to 1205°F would cause the condenser to transfer the 75 KW in a 1-foot condensing length. This example illustrates the relative insensitivity of the condenser design to errors in the average condensing heat transfer coefficient.

Based on the data from Test Set No. 5 (Figure 23), a reasonably conservative design choice for the condensing potassium heat transfer coefficient is h_c = 10,000 Btu/hr-ft^2-°F. The calculated condensing length for the 7-tube condenser using this value is L_c = 1.12-feet, which is 12% longer than the length calculated using the approximate mean value for the Test Set No. 5 data of h_c = 15,000 Btu/hr-ft^2-°F.

The overall pressure change of the potassium across the condensing section $(P_O - P_I)_C$ can be calculated using Equation (24), derived in Section VI.

$$(P_O - P_I)_C = \frac{G^2}{\rho_f g_o} \left[\frac{\rho_f}{\rho_v} - 1 - \frac{fL_c}{2D} \phi_{l-O} \right] \qquad (24)$$

Use of the Martinelli flow model (Reference 31), modified for potassium (Reference 6) gives a reasonably good approximation of the overall two-phase friction pressure drop multiplier ϕ_{l-O}, as can be seen by comparison with the data from Test Sets No. 4 and 5 shown in Figure 30 and the data from Test Set No. 1 shown in Figure 31. The plots of ϕ_{l-O} versus potassium saturation temperature T_K for the modified Martinelli flow model in Figures 30 and 31 can be used directly to determine ϕ_{l-O} for design calculations.

IX CONCLUDING REMARKS

The condensing potassium heat transfer and pressure change results presented provide a reasonable basis for thermal design of potassium condensers. The data cover the range of condensing temperatures from 1100°F to 1400°F, local heat fluxes from 30,000 to 300,000 Btu/hr-ft^2, inlet vapor Mach numbers from 0.1 to near 1.0, and local vapor qualities of about 0.2 and 0.8, respectively.

Of the data presented, the condensing heat transfer coefficient data obtained with the instrumented helical and tubular inserts from Test Sets No. 4 and 5, respectively, are the most reliable, since for these tests the local potassium temperature was measured directly by thermocouples in the inserts (Figures 20-23).

The condensing tests were conducted with the potassium in vertical downflow in order to eliminate the gravity force normal to the tube wall. The good agreement between the data taken with a straight tubular insert (Test Set No. 5) and those taken with a helical insert (Test Set No. 4), for which the radial acceleration on the fluid ranged up to 100 g's, suggests that the effect of body forces such as gravity on the forced convection condensing heat transfer coefficient is small (Figure 22).

All of the condensing heat transfer and pressure change data were obtained with the potassium liquid level maintained downstream of the condenser. Subsequently, the liquid level was brought up into the active condensing section to investigate the stability of this alternate mode of operation.

The range of condensing temperatures tested, 1100°F to 1400°F, is anticipated to be the range of principal interest for design of space power systems using potassium as the working fluid. As discussed in Section V, there is some evidence that at temperatures lower than this range the condensing potassium heat transfer coefficients might be less than the values obtained from these tests (Figure 24).

Major conclusions indicated by the test results are as follows:

(1) The condensing potassium heat transfer coefficients are relatively high, typically in excess of 10,000 Btu/hr-ft^2-°F. The measured coefficients are nearly constant over the ranges of vapor saturation temperatures, mass velocities and heat fluxes tested (Figure 23).

(2) The measured condensing heat transfer coefficients decrease slightly with increased liquid film Reynolds number (Figures 20 and 21) and with decreased vapor quality (Figure 23).

(3) Although the measured local condensing heat transfer coefficients are high, they are lower than coefficients calculated by considering only the thermal resistance due to heat conduction through the liquid film. Treatment of the data using an analysis based on the concept of an additional thermal resistance at the vapor-liquid interface (Appendix G) results in an empirical value of the condensation coefficient of $\sigma_c = 0.2$ giving a reasonable correlation of the data (Figure 24).

(4) Overall two-phase friction pressure drop multipliers calculated using a homogeneous flow model (equal liquid and vapor velocities) and using the Martinelli model, modified for potassium, are in reasonably good agreement with measurements using the 5/8-inch ID test section with an instrumented helical insert ($p/D_i = 6$) and with an instrumented $\frac{1}{4}$-inch OD tubular insert. The modified Martinelli flow model gives the best agreement with the experimental data for the overall two-phase friction pressure drop multiplier ϕ_{l-o} (Figures 30 and 31).

(5) Test operation included conditions for which there was a net rise in the potassium pressure across the condenser and conditions for which there was a net pressure drop (Figures 28 and 29). There was no difference in stability of operation between these two kinds of conditions.

(6) There was no observed difference in stability of operation between having the potassium liquid level located in the active heat transfer section of the test condenser and having it located downstream of the condenser in the head-tank (Figure 34).

APPENDIX A

LIQUID HEAT TRANSFER RESULTS

At the beginning of the experimental program, liquid heat transfer tests were made to gain familiarity with the facility and the test section instrumentation. Local liquid potassium heat transfer coefficient data obtained from these tests are given in Table 11 and are plotted in Figure 35. A detailed listing of the experimental data from which these results were obtained is given in Reference 4. The data cover the following range of variables:

Reynolds Number, N_{Re}	19,000 to 84,000
Peclet Number, N_{Pe}	80 to 351
Prandtl Number, N_{Pr}	0.004
Potassium Temperature, T_K	700°F to 810°F

The test section geometry used for these liquid coefficient tests was the same as was subsequently used for Test Set No.1-B (5/8-inch ID tube without insert), shown in Figure 7. The potassium was in vertical upflow for the liquid coefficient tests and was cooled by sodium in cocurrent flow on the shell-side.

The local heat fluxes and bulk fluid temperatures at the measuring stations were calculated from energy balances using the measured flow rates and fluid inlet and outlet temperatures. The overall heat transfer coefficient for the test section was assumed to be constant for the energy balance analysis. The error introduced by this assumption was small since more than half of the thermal resistance between the two fluids was due to the thick-walled nickel tube. The inner and outer tube wall temperatures were determined by a least-squares procedure to fit the calculated heat fluxes and the measured temperatures inside the tube wall at the measuring stations to the integrated Fourier heat conduction equation, as described in Appendix E.

The local liquid potassium heat transfer coefficient h_K at each measuring station was then calculated from the inner wall heat flux q/A_i, the inner wall surface temperature T_{wi} and the local potassium bulk fluid temperature T_K using Equation (A-1).

$$h_K = \frac{q/A_i}{T_K - T_{wi}} \qquad \text{(A-1)}$$

Potassium fluid property values given in Reference 66 were used for these calculations.

Equations (A-2), (A-3) and (A-4) are plotted in Figure 35 for comparison with the data.

$$N_{Nu} = 5.0 + 0.025\ N_{Pe}^{0.8} \qquad \text{(A-2)}$$

$$N_{Nu} = 0.625\ N_{Pe}^{0.4} \qquad \text{(A-3)}$$

$$N_{Nu} = 3.66 + 0.0055\ N_{Pe} \qquad \text{(A-4)}$$

The experimental results are all below values calculated using the theoretical Equation (A-2) of Seban and Shimazaki (Reference 50). The experimental values are generally less than those calculated using the empirical Equation (A-3) of Lubarsky and Kaufman (Reference 47), but the general trend with Peclet number appears to be about the same as that given by Equation (A-3). The author's empirical Equation (A-4), which is similar in form to Equation (A-2), provides a reasonably good fit to the data for Peclet numbers above about 150. At lower Peclet numbers the data fall below values calculated from Equation (A-4).

The data obtained at the bottom measuring station ($\ell/D_i = 19$) are believed to be more reliable than those obtained at the top measuring station ($\ell/D_i = 38$), for the following reasons:

(1) The difference between the potassium bulk temperature and the wall temperature was greater at the bottom measuring station, thereby making the coefficient determinations at the bottom station less sensitive to thermocouple error.

(2) Four tube-wall thermocouples were functioning at the bottom measuring station during the liquid coefficient tests, whereas only three thermocouples were functioning at the top measuring station, which allowed a more reliable determination of the inner wall temperature at the bottom measuring station to be made.

Thus, due to these uncertainties the small dependence on ℓ/D_i indicated by the data in Figure 35 is not necessarily true.

For runs 1-28 (Table 11)a maximum error in the experimental Nusselt numbers of $\pm$ 15% is estimated. A slightly larger error is possible for data runs 29-31, due to the fact that at the low Peclet numbers for these runs ($N_{Pe} < 120$) the difference between the measured sodium and potassium temperatures was small, less than 2°F at the test section outlet. For the rest of the data ($N_{Pe} \geq 120$) the smallest difference between the measured fluid temperatures at the test section outlet was 4.5°F.

The sodium Reynolds number was maintained in the range from 21,000 to 29,000. No trend in the potassium Nusselt number as a function of sodium flow rate is discernible in the data, which indicates that the dependence of the sodium heat transfer coefficient on Reynolds number was small over this range. An average sodium Nusselt number of 5.3 was obtained for the sodium Peclet number range of 113 to 156. The measured data varied from this average value with a standard deviation of 31%. Agreement between the average experimental value of the sodium Nusselt number of 5.3 and the corresponding value of 5.6 calculated using the equation of Dwyer and Tu for an annulus (Reference 63) is good.

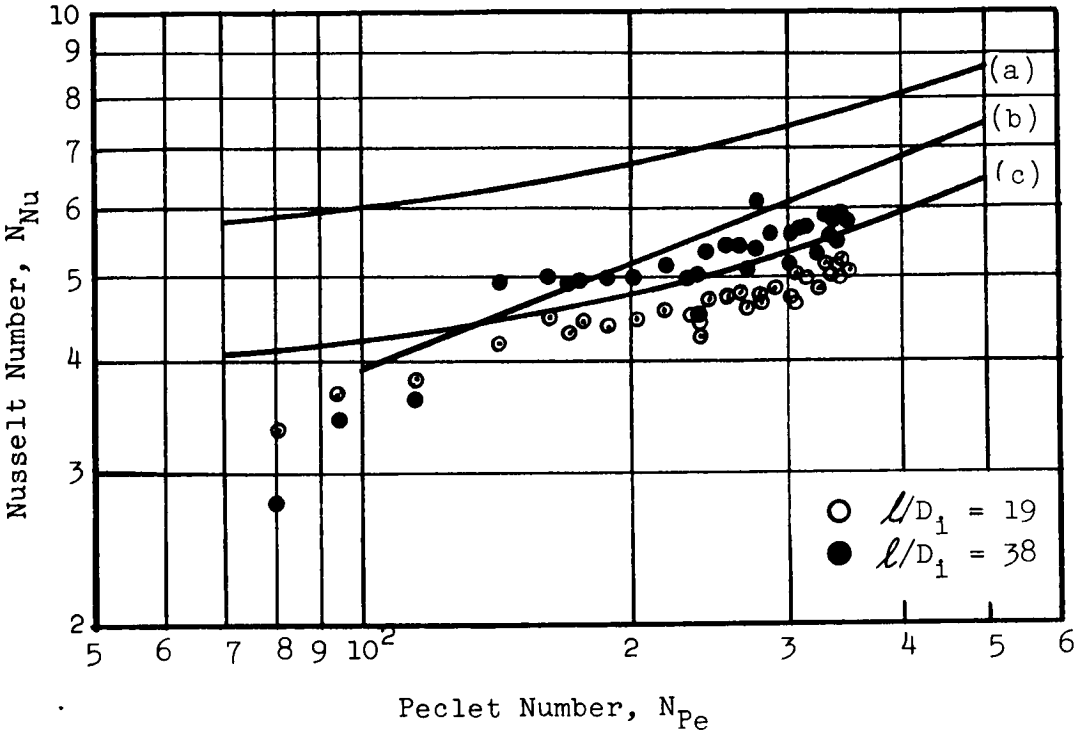

Curve-a: Equation A-2, Seban and Shimazaki (Reference 50)

Curve-b: Equation A-3, Lubarsky and Kaufman (Reference 47)

Curve-c: Equation A-4, author's correlation

Figure 35. Liquid Potassium Heat Transfer Data Obtained in 5/8-inch ID Tube at 700°F to 810°F.

APPENDIX B

ELECTROMAGNETIC FLOWMETER CALIBRATION

Electromagnetic flowmeters were used in both the sodium loop and the potassium loop. Both flowmeters were used for the liquid heat transfer coefficient tests described in Appendix A. For the condensing tests, however, the potassium loop flowmeter was not used, due to the small potassium flow rates in condensing, and the potassium flow rate was determined instead by energy balance across the test section using the measured sodium flow rate.

The equation for calculation of the flow rate of an electrical conducting fluid from the emf generated by an electromagnetic flowmeter, from Reference 67, is:

$$W/\rho_f E' = \frac{10^4 D_i K_E}{3.18 F K_1 K_2 K_3} \qquad \text{(B-1)}$$

where

$$K_i = \frac{2\left(\frac{D_i}{D_o}\right)}{1 + \left(\frac{D_i}{D_o}\right)^2 + R'\left[1 - \left(\frac{D_i}{D_o}\right)^2\right]} \qquad \text{(B-2)}$$

The constant K_2 in Equation (B-1) is a correction for end-effects and is equal to 0.989 (Reference 67). The factor K_3 is a function of the magnet temperature and dimensions and for these experiments was between 0.99 and 1.0. The pertinent dimensions and magnetic flow ratings of the two electromagnetic flowmeters at room temperature are as follows:

Flowmeter	D_i, inch	D_o, inch	F, gauss
Potassium	0.618	0.841	1989
Sodium	0.610	0.843	2019

At the beginning of the liquid heat transfer coefficient tests described in Appendix A a discrepancy in heat balance across the test section between the potassium and sodium sides was found. The discrepancy was that the indicated heat transfer rate from the potassium was about 15% higher than the indicated heat transfer rate to the sodium. It was therefore decided to calibrate the potassium electromagnetic flowmeter in-place in the loop and to then calibrate the sodium flowmeter relative to the potassium flowmeter.

A calorimetric method was chosen for the calibration. The thermal calorimeter used is illustrated in Figure 36. An immersion heater was used for heat input to the calorimeter to assure that all of the heat input to the calorimeter went into potassium sensible heat. To determine the potassium flow rate, three parameters have to be known:

(1) Heat input to the calorimeter, q, Btu/sec

(2) Specific heat of liquid potassium, c_{p_K}, Btu/lb-°F

(3) The potassium temperature increase across the calorimeter due to the heat input, $(T_{K_O} - T_{K_I})$, °F

The heat input to the calorimeter was measured by a standard single-phase wattmeter having full scale ranges of 500, 1000, and 2000 watts and an accuracy of $\pm$ 1/4% of full scale. The calorimeter heat loss and the systematic temperature measurement error between the inlet and outlet potassium thermocouples were determined by a technique similar to that used in the sodium thermocouple calibrations, described in Appendix C.

With zero heat input to the calorimeter, the potassium loses heat to the surroundings as a function of the temperatures of the calorimeter chamber and the surroundings. For the condition of zero heat input to the calorimeter (case-1) the heat loss from the calorimeter is given by:

$$q_{L1} = (Wc_p)_{K1} (T_{K_I} - T_{K_O} + \Delta)_1 \qquad \text{(B-3)}$$

where Δ is the systematic temperature measurement error between the inlet and outlet potassium thermocouples. With heat input q_{ca} to the calorimeter (case-2) an energy balance gives:

$$q_{ca} - q_{L2} = (Wc_p)_{K2} (T_{K_O} - T_{K_I} - \Delta)_2 \qquad \text{(B-4)}$$

Measurements with and without heat input q_{ca} were made at the same average potassium temperature, for which the calorimeter chamber temperatures and corresponding heat losses q_L were thus also the same. With this condition imposed q_{ca} can be calculated from the following Equation (B-5), which is obtained by combining Equations (B-3) and (B-4) with $q_{L1} = q_{L2}$.

$$q_{ca} = \left[(T_{K_O} - T_{K_I} - \Delta)_2 + \frac{(Wc_p)_{K1}}{(Wc_p)_{K2}} (T_{K_I} - T_{K_O} + \Delta)_1 \right] (Wc_p)_{K2} \qquad \text{(B-5)}$$

The potassium electromagnetic flowmeter was used to adjust the flow during the calibrations so that $(Wc_p)_{K1} = (Wc_p)_{K2}$. With this condition, together with the assumption that the systematic temperature measurement error between the inlet and outlet potassium thermocouples Δ was independent of the calorimeter heat input ($\Delta_1 = \Delta_2$), Equation (B-5) reduces to

$$W_{K2} = \frac{q_{ca}}{c_{p\,K2} \left[(T_{K_O} - T_{K_I})_2 + (T_{K1} - T_{K0})_1 \right]} \qquad \text{(B-6)}$$

Equation (B-6) was employed to determine the potassium flow rate using measured temperatures and heat input to the thermal calorimeter. For assumed errors of $\pm$ 0.5% in the calorimeter heat input q_{ca}, $\pm$ 2.2% in the potassium specific heat c_{pK} and $\pm$ 1.6% in the measured potassium temperature differences $(T_{K_O} - T_{K_I})_2$ and $(T_{K_I} - T_{K_O})_1$, the estimated standard error in the calculation of flow rate using Equation (B-6) is $\pm$ 3.1%.

Flow rates calculated from Equation (B-6) were used as the basis for calibration of the potassium electromagnetic flowmeter over the following ranges of calorimeter conditions:

Potassium flow rate	0.14 to 0.31 lbs/sec
Potassium Temperature Difference	11.5°F to 43.4°F
Average Potassium Temperature	600°F to 700°F
Calorimeter heat input	0.76 to 1.6 Btu/sec

Four sets of calibrations resulted in an average ratio of the calorimeter to electromagnetic flowmeter flow rates of 1.145 with a standard error of $\pm$ 1.3%. Multiplication of the flow rate indicated by the electromagnetic flowmeter by the factor 1.145 brought the test section liquid-liquid heat balances between the potassium and sodium sides into agreement within a standard error of $\pm$ 6.7%.

The test section heat balance error was calculated from Equation (B-7).

$$\text{Error} = 1 - \frac{q_L + q_{Na}}{q_K} \qquad \text{(B-7)}$$

The test section heat loss q_L was determined during the calibration of the sodium thermocouples, as discussed in Appendix C. The heat transfer rate from the potassium and the net heat transfer rate to the sodium were calculated from fluid temperature and flow rate measurements made during liquid operation using Equations (B-8) and (B-9), respectively.

$$q_K = W_K \, c_{pKM} \, (T_{K_I} - T_{K_O}) \qquad \text{(B-8)}$$

$$q_{Na} = W_{Na} \, c_{pNaM} \, (T_{Na_O} - T_{Na_I}) \qquad \text{(B-9)}$$

The fluid temperatures used in Equations (B-8) and (B-9) were corrected values based on the thermocouple calibrations discussed in Appendix C. The potassium flow rates W_K were corrected values based on the thermal calorimeter calibration results discussed above. The sodium flow rates used were uncorrected values obtained directly from the electromagnetic flowmeter output together with Equation (B-1). Reference 68 was used for the mean values c_{pM} of the sodium and potassium specific heats at test section temperatures.

The standard error in the test section heat balance calculated using Equation (B-7) was $\pm$ 6.7%. The heat balance error includes the error in sodium flow rate determination and errors from other sources. The heat balance error being small indicates that the sodium flow rate error was also small. On this basis, the sodium flow rates obtained from the electromagnetic flowmeter output together with Equation (B-1) were used directly, without further correction, for the condensing data reductions. The potassium flow rates for the condensing tests were determined by energy balance across the test section using the measured sodium flow rates (Appendix E).

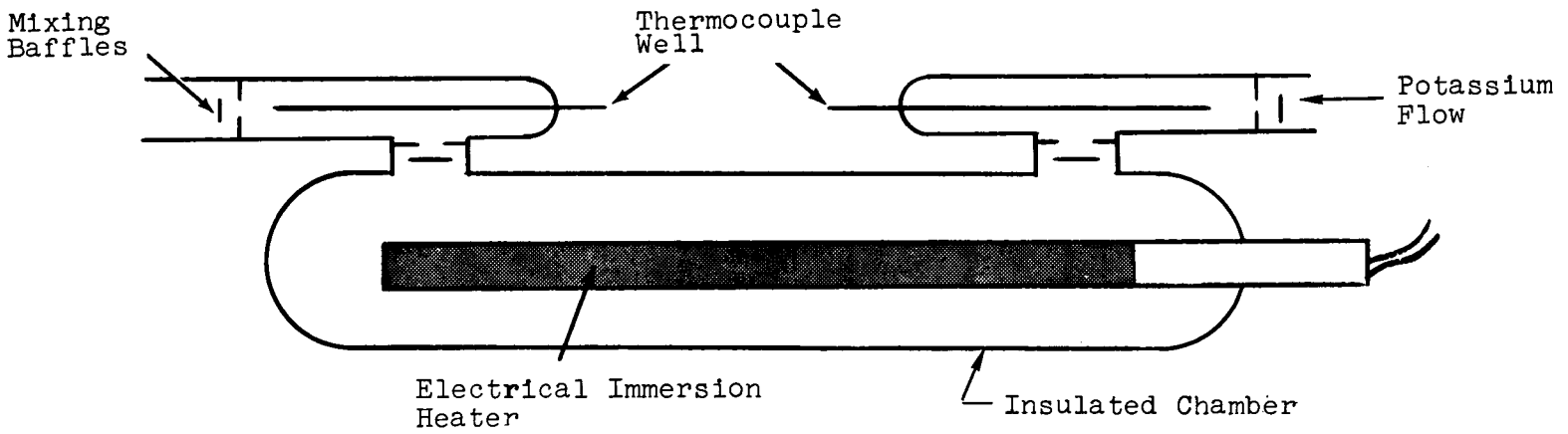

Figure 36. Thermal Calorimeter Used For Potassium Flowmeter Calibration.

APPENDIX C

THERMOCOUPLE CALIBRATION

Stainless steel sheathed, capped, 0.040-inch diameter, chromel-alumel thermocouples were used, due to their stability and relatively high emf output in the 1100°F to 1400°F temperature range. The high output of the chromel-alumel thermocouples, approximately 23 microvolts/°F, minimized temperature errors due to instrumentation noise, which was generally less than ± 3 microvolts.

Since the condensing heat transfer coefficients for potassium are high, in the order of 10,000 Btu/hr-ft^2-°F, accurate calibrations of the test section thermocouples were necessary. For calculation of the condensing heat transfer coefficient the difference between the vapor and wall temperatures is needed. Therefore, in-place calibrations of all test section thermocouples relative to each other were done.

Initial calibrations indicated inhomogeneities in the chromel-alumel sheathed thermocouples, which might have been caused by bending the thermocouples during installation. These inhomogeneities were detected by moving a soldering iron at about 700°F along the exposed thermocouple length after installation and observing the change in thermocouple output. All thermocouples which indicated greater than 50 microvolts (2°F) output change during the homogeneity check were replaced. In addition an individual ice junction was provided for each thermocouple to reduce errors caused by junction emf's

For intercalibration of the sodium inlet and outlet well thermocouples, sodium fluid temperature measurements were obtained at one temperature and two different sodium flow rates, with the potassium loop evacuated and with no heating of the test section (Reference 4). From these data the test section heat loss and the individual thermocouple corrections were determined independently as functions of average sodium temperature, as shown below. For two runs under the above conditions at two different flow rates, Equations C-1 and C-2 are applicable:

$$q_{L1} = (W\ c_p)_{Na1}\ (T_{Na_I} - T_{Na_O} + \Delta)_1 \qquad \text{(C-1)}$$

$$q_{L2} = (W\ c_p)_{Na2}\ (T_{Na_I} - T_{Na_O} + \Delta)_2 \qquad \text{(C-2)}$$

where Δ is the required correction between the sodium inlet and outlet thermocouples.

At the same average sodium temperature the average shell temperatures and, consequently, the test section heat losses will be the same for both runs, i.e., $q_{L1} = q_{L2}$. Also, if each thermocouple has a systematic correction which is independent of flow rate, the systematic thermocouple correction between the sodium inlet and outlet thermocouples can be obtained from Equation A-3.

$$\Delta = \frac{(T_{Na_I} - T_{Na_O})_1 - (T_{Na_I} - T_{Na_O})_2}{1 - \frac{(W\ c_p)_{Na1}}{(W\ c_p)_{Na2}}} + (T_{Na_O} - T_{Na_I})_1 \qquad \text{(C-3)}$$

The assumption of thermocouple corrections independent of flow rate is reasonable for the test section geometry used.

This method of calibration yields only relative calibrations between the inlet and outlet sodium well thermocouples. The correction, Δ, was applied to thermocouple readings used in the calculation of the amount of heat transferred to the sodium from the potassium during condensing tests. The test section heat loss was simultaneously determined during these thermocouple calibration runs.

In a similar manner , an attempt was made to determine relative calibrations between the potassium inlet and outlet well thermocouples. However, these calibrations were unsuccessful, probably due to the lack of fluid mixing at the test section inlet and outlet on the potassium side. Therefore, to obtain relative calibrations between the potassium fluid thermocouples and the nickel tube wall thermocouples, a different procedure was used.

For calibration of the potassium thermocouples, the test section annulus was evacuated and potassium vapor was passed through the test section while the test section shell was maintained at the potassium vapor temperature by use of electrical heating. The small amount of vapor passing through the test section from the boiler was condensed by heat losses in the head-tank below the condenser. Test section thermocouple readings were obtained under these conditions for each test geometry at 1200°F and 1300°F, both before and after the heat transfer tests. From these data a systematic correction for each test section thermocouple relative to a selected standard thermocouple was obtained as a linear function of temperature. For the last two test sets (Test Sets No. 4 and 5), the maximum thermocouple correction relative to the standard thermocouple was less than 3°F. Agreement between the thermocouple corrections determined before and after condensing operation was generally better than 1°F.

APPENDIX D

TEMPERATURE FIELD DISTORTION DUE TO THE THERMOCOUPLE HOLES IN THE THICK-WALL NICKEL CONDENSER TUBE

An analogue using teledeltos paper was used to determine the magnitude of the temperature field distortion caused by the axial thermocouple holes in the thick walled nickel tube of the test section. A flux plot was made on a six-times enlarged cross-section of the test section geometry. After the teledeltos paper was cut to size, it was checked for uniformity of resistance in the vicinity of the thermocouple holes before the holes were cut. The maximum deviation of the measured potential from the calculated values was $\pm$ 0.3%, with an applied potential difference of 10 volts between the inner and outer radii.

The flux plot determined from the analogue is shown in Figure 37. Maximum, minimum and average potentials measured around the circumference of each hole are listed in Table 12 together with the values calculated for the undistorted geometry at the radial position of each hole center. The calculated and measured values agree within a maximum error of 3.5%. On the basis of this small error, the temperatures indicated by the wall thermocouples were assumed for the data reductions to be equal to the temperature at the radial position of the respective thermocouple hole centers.

The noncircular holes shown in Figure 37 simulate those used in the first test section built, which was subsequently discarded. All the other test sections had drilled circular thermocouple holes. This slight difference in shape of the thermocouple holes between what is shown in Figure 37 and those used for the condensing tests would not have enough effect on the temperature field to alter the principal conclusion of this study, that the effect of the thermocouple holes on the measured wall temperature distributions is negligible.

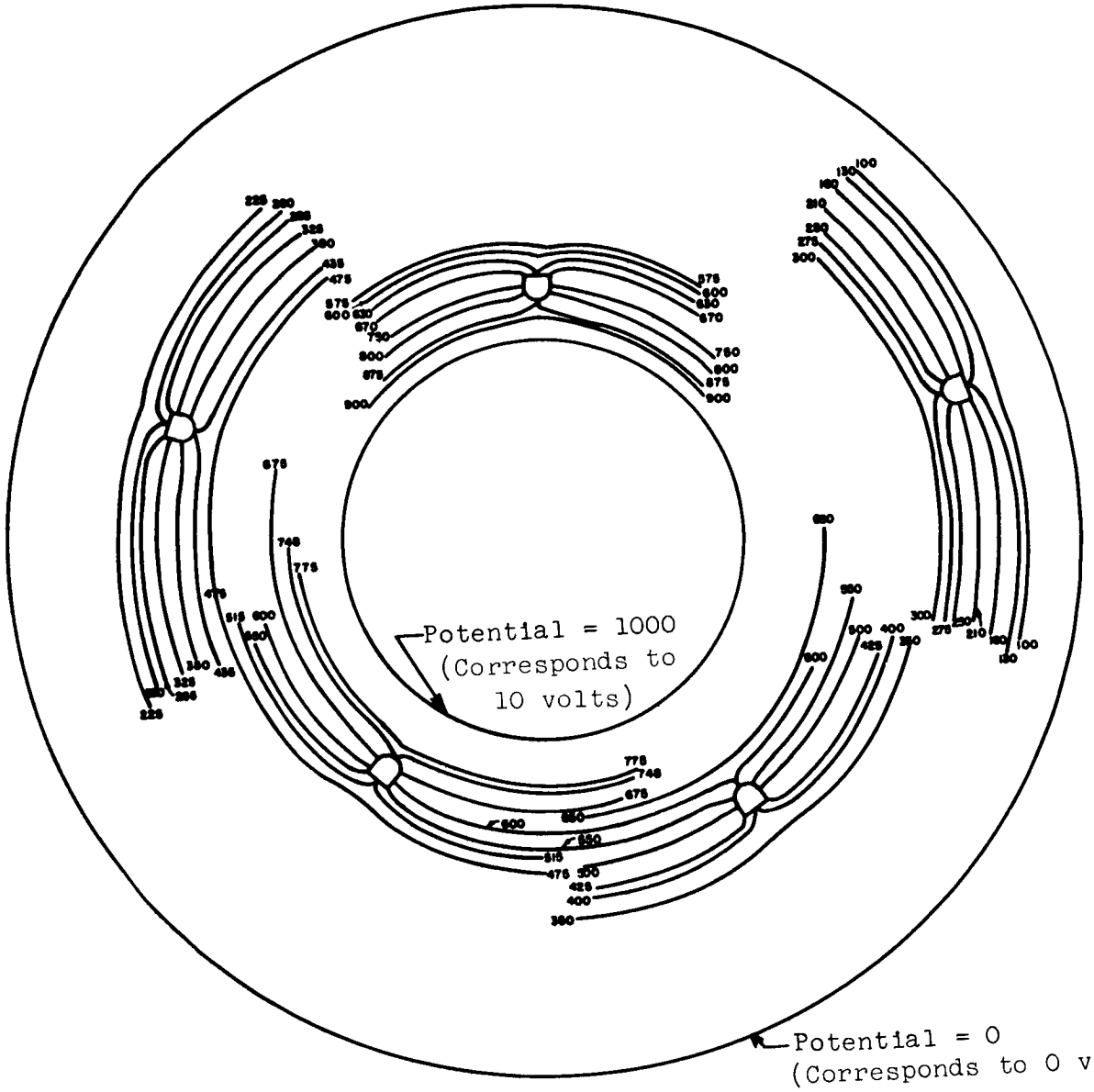

Figure 37. Flux Plot Showing Analogue of Temperature Field In Thick-Walled Nickel Condenser Tube.

APPENDIX E

CONDENSING DATA REDUCTION PROCEDURES

Fluid Properties

The potassium thermodynamic properties used for reduction of the condensing data were obtained from Reference 69. Specific heats for liquid sodium and liquid potassium were taken from Reference 68. Other sodium and potassium liquid transport properties used for the data reductions were obtained from Reference 66.

Potassium Flow Rate

In general, the potassium flow rates used for the condensing tests were too small to measure accurately with the electromagnetic flowmeter. For this reason the potassium flow rates for the condensing tests were determined indirectly by calculated energy balance across the test section using the measured sodium flow rate and measured sodium inlet and outlet temperatures, as follows.

Assuming that the potassium entered the test section as saturated vapor and that the effect of subcooling of the liquid film at the test section outlet was negligible, the potassium flow rate W_K was calculated from

$$W_K = \frac{q_K}{\lambda} \qquad \text{(E-1)}$$

By an energy balance across the test section the heat transfer rate from the potassium q_K was calculated from

$$q_K = q_{Na} + q_L \qquad \text{(E-2)}$$

Combining Equations (E-1) and (E-2) gives for the potassium flow rate

$$W_K = \frac{1}{\lambda} (q_{Na} + q_L) \qquad \text{(E-3)}$$

The test section heat loss rate q_L was determined by test, as described in Appendix C. The net heat transfer rate to the sodium q_{Na} was calculated from

$$q_{Na} = W_{Na}\, Cp_{Na}\, (T_{Na_O} - T_{Na_I}) \qquad \text{(E-4)}$$

The sodium temperature difference in Equation (E-4) was determined using measured bulk fluid inlet and outlet temperatures, corrected for relative thermocouple errors as described in Appendix C. The sodium flow rate was calculated from the sodium loop electromagnetic flowmeter output using Equation (B-1), as discussed in Appendix B.

Local Wall Temperature and Heat Flux

The local temperatures at the inner surface of the condenser tube wall T_{wi} and the local heat fluxes q_i'' were determined from temperature measurements using thermocouples located inside the wall at the top and bottom measuring stations, respectively. The arrangement of the wall thermocouples is described in Section III.

The Fourier heat conduction equation (Reference 12), Equation (E-5),

$$T_w = T_{wi} - q_i'' \frac{R_i}{k_w} \ln\left(\frac{R}{R_i}\right) \qquad \text{(E-5)}$$

was fitted to the measured internal wall temperatures T_W by a least-squares fit procedure for each data run. The local temperature at the inner surface of the wall was then calculated from the fitted Equation (E-5), as illustrated for two typical cases in Figure 16. The calculations were done using the following matrix equation, Equation (E-6), derived from Equation (E-5) to express the inner wall surface temperature T_{Wi} in terms of the least-squares fit to the measured internal wall temperature T_{wj} at the respective radial positions R_j.

$$T_{wi} = \frac{1}{\theta} \begin{vmatrix} \sum_{1}^{N_o} T_{wj} & \sum_{1}^{N_o} \ln\left(\frac{R_j}{R_i}\right) \\ \sum_{1}^{N_o} T_{wj} \ln\left(\frac{R_j}{R_i}\right) & \sum_{1}^{N_o} \left[\ln\left(\frac{R_j}{R_i}\right)\right]^2 \end{vmatrix} \qquad \text{(E-6)}$$

where

$$\theta = \begin{vmatrix} N_o & \sum_{1}^{N_o} \ln\left(\frac{R_j}{R_i}\right) \\ \sum_{1}^{N_o} \ln\left(\frac{R_j}{R_i}\right) & \sum_{1}^{N_o} \left[\ln\left(\frac{R_j}{R_i}\right)\right]^2 \end{vmatrix} \qquad \text{(E-7)}$$

Inside wall temperatures T_{wj} were normally measured at five different locations inside the wall at both measuring stations, for which the summation limit in Equations (E-6) and (E-7) is $N_o = 5$.

The local heat flux at the inner wall surface was calculated for each case using Equation (E-8), derived from Equation (E-5) to express the local inner wall surface heat flux q_i'' in terms of the least-squares fit to the measured internal wall temperatures T_{wj} at R_j,

$$q_i'' = \frac{\bar{k}_w}{R_i \theta} \begin{vmatrix} N_o & \sum_{1}^{N_o} T_{wj} \\ \sum_{1}^{N_o} \ln\left(\frac{R_j}{R_i}\right) & \sum_{1}^{N_o} T_{wj} \ln\left(\frac{R_j}{R_i}\right) \end{vmatrix} \qquad \text{(E-8)}$$

in which θ is given by Equation (E-7).

The mean value of the tube wall thermal conductivity $\bar{k}_w$ used for these calculations was evaluated for each case at the mean wall temperature $\bar{T}_w$, which was calculated using

$$\bar{T}_w = \frac{1}{N_o} \sum_{1}^{N_o} T_{wj} \qquad \text{(E-9)}$$

The thermal conductivities k_w of the INCO Nickel-270 condenser tube used were values measured by Battelle Memorial Institute, Columbus, Ohio, given in Figure 38.

Local Potassium Saturation Temperature

The local potassium temperature axial distributions were measured directly using the insert thermocouples for Test Sets No. 4 and 5. The local potassium temperature at the measuring stations for Test Sets No. 1, 2 and 3, for which no insert thermocouples were used, was determined by linear interpolation between bulk potassium temperature measurements at the test section inlet and outlet. An examination of the dependence of the experimental condensing heat transfer coefficients on the potassium temperature distribution is given in Appendix H.

For Test Set No. 4 an instrumented helical insert ($p/D_i = 6$) was used. For the data from Test Set No. 4 the insert thermocouple temperatures were corrected by analysis to account for the radial pressure rise and corresponding saturation temperature rise in swirl flow to obtain the estimated saturation temperature at the tube wall. The analysis used is as follows.

In cylindrical co-ordinates the equation of motion is

$$\frac{dP}{dR} = \frac{\rho}{g_o} \frac{V_\theta^2}{R} \qquad \text{(E-10)}$$

With the assumption that the axial component of the velocity, V_z, is independent of the radius, Equation (E-11) is obtained.

$$\frac{dP}{dR} = \frac{\rho}{g_o} \left(\frac{2\pi V_z}{p}\right)^2 R \qquad \text{(E-11)}$$

If the liquid fraction in the two-phase mixture is neglected, and the density is assumed to be the vapor density, Equation (E-11) can be integrated to obtain Equation (E-12), which gives the difference between the pressure at the condensing surface, P_D, and the pressure at the insert centerbody P_{DCB}.

$$P_D - P_{DCB} = \left(\frac{XG}{2g_o}\right)^2 \rho_v \left(\frac{\pi}{P/D}\right)^2 \left[1 - \left(\frac{D_{CB}}{D_i}\right)^2\right] \qquad \text{(E-12)}$$

The temperature measured by the helical insert thermocouples was assumed to be the saturation temperature corresponding to the static pressure at the insert centerbody, P_{DCB}. The radial pressure difference due to the swirling flow, as calculated from Equation (E-12) was then added to P_{DCB} to give P_D, the pressure existing at the liquid-vapor interface. A corrected value of the potassium saturation temperature T_K corresponding to P_D was then determined and used to calculate the condensing heat transfer coefficient.

The effect of this correction was to decrease the experimental condensing heat transfer coefficients for the helical insert data of Test Set No. 4, as a result of increasing the vapor saturation temperature from the measured centerbody saturation temperature to that corresponding to the pressure at the liquid-vapor interface. With this procedure, potassium saturation temperature corrections up to 20°F were obtained. As indicated in Figure 22, reasonably good agreement between the data for the 5/8-inch ID tube with helical insert (Test Set No. 4) and the data for the tubular insert (Test Set No. 5) was obtained after application of the correction.

Condensing Heat Transfer Coefficient

Experimental values of the local condensing heat transfer coefficient h_c were calculated for each measuring station using Equation (E-13).

$$h_c = \frac{q''_i}{(T_K - T_{wi})} \qquad \text{(E-13)}$$

and the values of T_{wi} and q''_i obtained from Equations (E-6) and (E-8). The corresponding Nusselt condensing ratio N_{Nuc} and the liquid film Reynolds number N_{Ref} used in the correlations in Section V were calculated from Equations (E-14) and (E-15), respectively.

$$N_{Nuc} = \frac{h_c}{k} \left(\frac{\nu^2}{g}\right)^{1/3} \qquad \text{(E-14)}$$

$$N_{Ref} = \frac{4W_K (1-X)}{\pi D_i \mu} \qquad \text{(E-15)}$$

Fluid properties used in Equations (E-14) and (E-15) were those of the saturated liquid (Reference 66).

Local Vapor Quality

For Test Set No. 5 (5/8-inch ID tube with instrumented 1/4-inch OD tubular insert) the local vapor quality at the measuring stations, listed in Table 3 and used in Equation (E-15), were calculated by energy balance using the measured potassium temperature distribution, inlet and exit sodium temperature, sodium flow rate, and the experimental condensing heat transfer coefficients. The procedure used for this calculation was to first estimate a value for the overall heat transfer coefficient using calculated values of the shell-side sodium heat transfer coefficient and tube wall heat transfer coefficient together with the measured condensing heat transfer coefficient. Then, the heat flux and sodium temperature distributions were calculated using the estimated overall heat transfer coefficient, the measured potassium temperature distribution and the sodium exit temperature. The calculation proceeds step-wise from sodium exit to inlet. The difference between the calculated and measured value of the sodium

inlet temperature is used as the closure criterion. If agreement within about $\frac{1}{2}$°F is not obtained on the first iteration the value of the overall heat transfer coefficient is adjusted and the procedure repeated. This process is continued until the measured and calculated sodium inlet temperature agree within about $\frac{1}{2}$°F. Finally, the vapor quality distribution was calculated by energy balance on the fluid using step-wise integration of the heat flux proceeding from the potassium vapor inlet.

The results of the calculation for one of the data runs is shown in Figure 39. As can be seen from Figure 39 the difference between the vapor quality calculated by energy balance and the quality estimated by linear interpolation is about 5% at both measuring stations. The measured potassium temperature distribution for the data shown in Figure 39 (Run No. 37), is one of the most non-linear obtained from Test Set No. 5 (Figure 17). Thus, the differences between the calculated quality and quality estimated by linear interpolation shown in Figure 39 should be among the largest for Test Set No. 5.

A similar procedure for calculating the local quality was attempted for the Test Set No. 4 data (5/8-inch ID tube with instrumented helical insert, $p/D_i = 6$), using an additional step in the analysis to correct for the effects of the swirl-flow on the saturation temperature at the wall. The results of the calculation for one of the data runs is shown in Figure 40. For this run the difference between the vapor quality calculated by energy balance and the quality estimated by linear interpolation is about 5% at the bottom measuring station and about 8% at the top measuring station. Since the required correction for swirl flow effects adds additional uncertainty to the local vapor quality calculations and since the differences between calculated qualities and qualities estimated by linear interpolation (Figure 40) are small, linear interpolation was used for estimating the local quality at the measuring stations for use in Equation (E-15) for the Test Set No. 4 data.

For the data of Test Sets No. 1, 2 and 3, the local quality at the measuring stations was estimated for use in Equation (E-15) by linear interpo-

lation. Based on the calculated quality comparisons shown in Figures 39 and 40 the estimated error in local vapor quality at the measuring stations is about 5%. The error in estimating the local vapor quality causes a small error in the calculation of the local liquid film Reynolds number. The error in the vapor quality estimates is not relevant in determination of the experimental condensing heat transfer coefficients.

It was assumed for the estimates of local vapor quality that the potassium enters the condenser as saturated vapor and exits as saturated liquid. The errors introduced by these approximations are assumed to be negligible. The piping from the boiler to the condenser was well-insulated to prevent any significant heat losses from the vapor. The potassium exit piping was similarly well-insulated. Estimates of the heat losses between the condenser exit and the liquid level in the head-tank downstream of the condenser (Figure 1) indicate that the vapor quality of the potassium at the condenser exit was less than 1%. The vapor inlet piping from the boiler to the condenser was well insulated to maintain the inlet vapor quality at about 100%.

Pressure Change

The pressure change data presented in Section VI were obtained from measurements of the two-phase potassium temperatures. The potassium pressures were assumed to be the saturation pressures corresponding to the measured local fluid temperatures. The fluid property data in Reference 69 were used for the pressure change data reductions.

Liquid Film Coefficient For Calculation Of Vapor Phase Resistance

The liquid-film heat transfer coefficient h_f, defined by Equation (5), was calculated using Dukler's model (Reference 28) for use in Equation (6) to obtain the vapor-phase resistance $1/h_v$ from the Test Set No. 5 data. The Nusselt condensing ratio, $(h_f/k_f)(\nu_f^2/g_o)^{1/3}$, calculated using Dukler's model is given in Figure 41 as a function of liquid-film Reynolds Number and τ_v^*, the dimensionless shear stress at the vapor-liquid interface.

The dimensionless shear stress τ_v^* is calculated using

$$\tau_v^* = \frac{\tau_v}{\rho_f \left(\nu_f^2/g_o\right)^{1/3}} \qquad \text{(E-16)}$$

for which the vapor shear stress τ_v is given by

$$\tau_v = \tfrac{1}{4} \left(D_i - D_{CB}\right) \left(\frac{dP}{d\ell}\right)_v \qquad \text{(E-17)}$$

The local pressure gradient of the vapor due to friction was estimated using

$$\left(\frac{dP}{d\ell}\right)_v = \frac{f_v \rho_v V_v^2}{2g_o \left(D_i - D_{CB}\right)} \qquad \text{(E-18)}$$

where

$$V_v = \frac{4 W_K X}{\pi \rho_v \left(D_i^2 - D_{CB}^2\right)} \qquad \text{(E-19)}$$

The vapor-phase friction factor was calculated from the Blasius smooth-tube equation (Reference 61),

$$f_v = \frac{0.316}{\left(N_{Rev}\right)^{\frac{1}{4}}} \qquad \text{(E-20)}$$

Although Dukler's thermal analysis of the condensing problem is in error for low Prandtl number fluids, as has been shown by Lee (Reference 27), the Dukler model accounts for shear at the vapor-liquid interface and appears to correlate liquid-film thickness data reasonably well (References 33, 34 and 35). For this reason Dukler's film thickness analysis was used for the calculations.

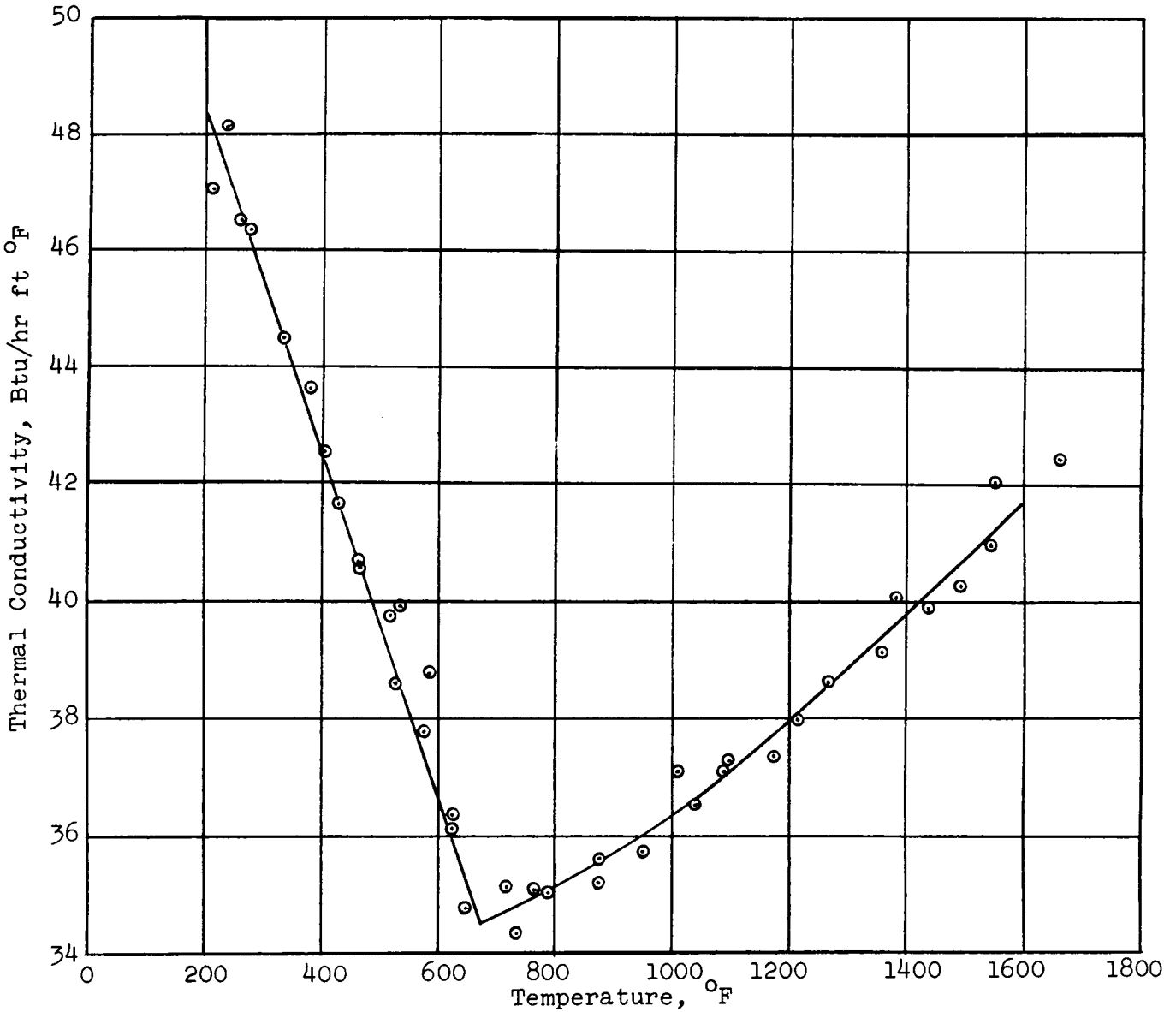

Figure 38. Thermal Conductivity of INCO Nickel 270 Used for Condenser Tube as Measured by BMI.

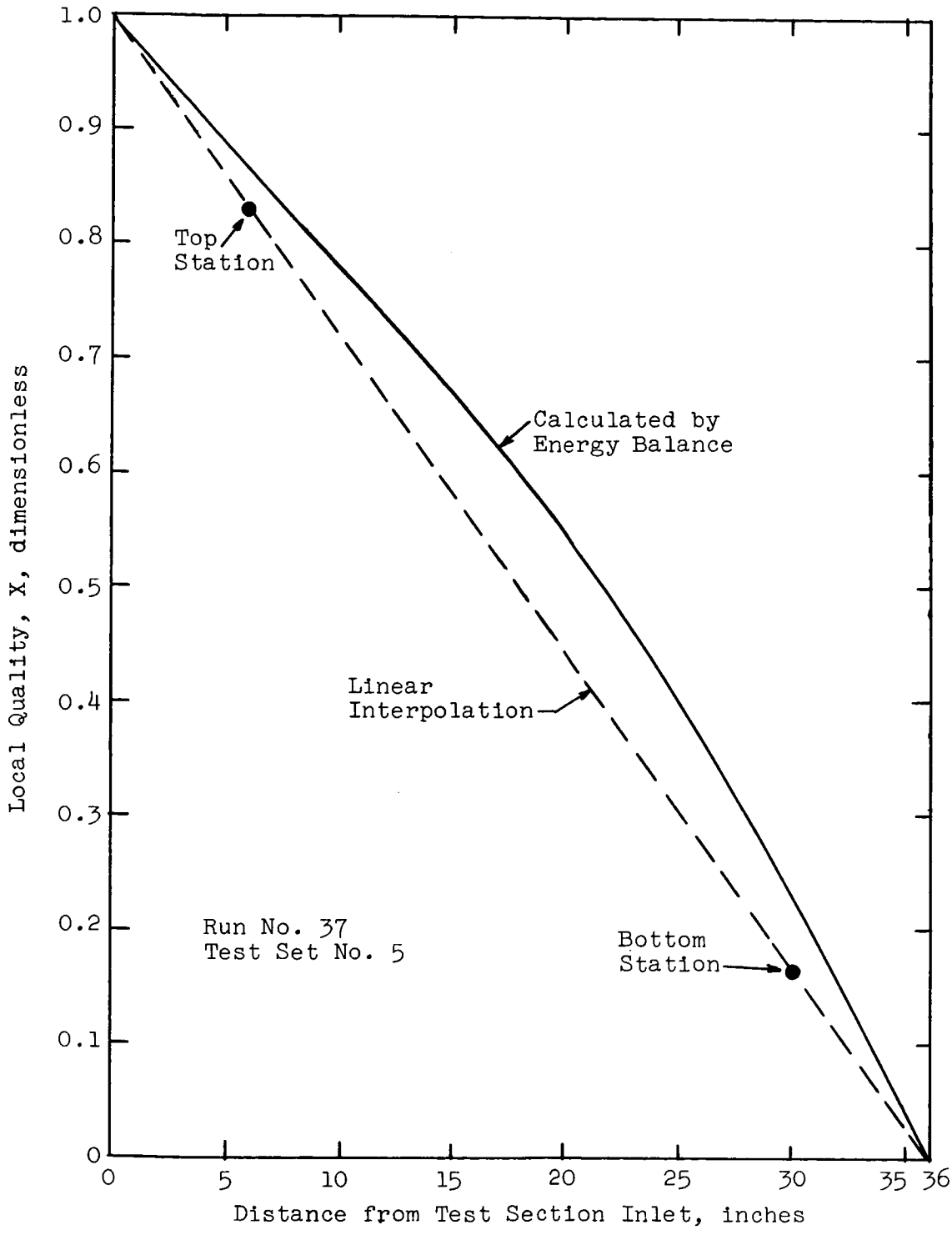

Figure 39. Calculated Potassium Quality Distribution Compared to Linear Interpolation for Run No. 37 of Test Set No. 5 (5/8-inch ID Tube with Instrumented 1/4-inch OD Tubular Insert)

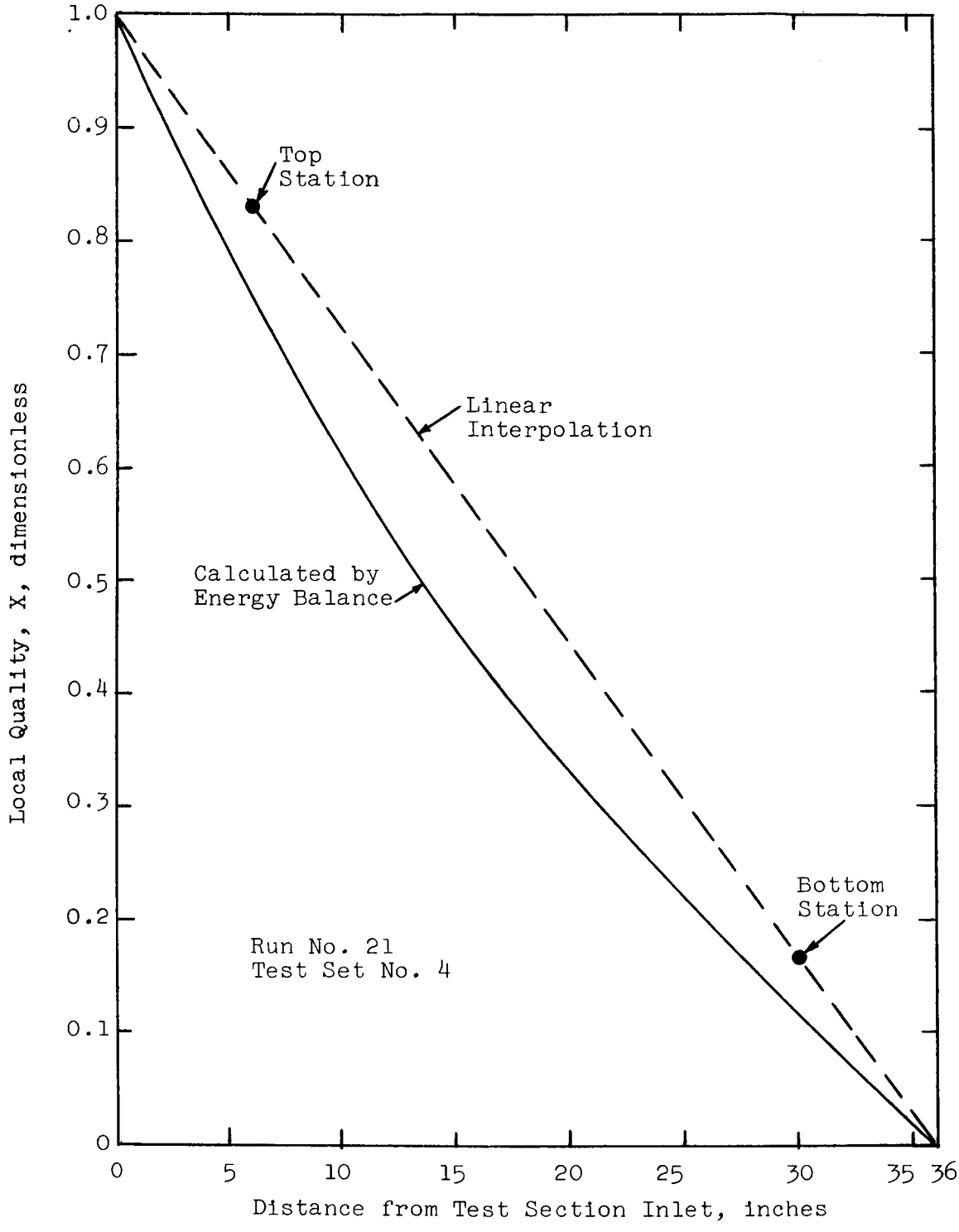

Figure 40. Calculated Potassium Quality Distribution Compared to Linear Interpolation for Run No. 21 of Test Set No. 4 (5/8-inch ID Tube with Instrumented Helical Insert, $p/D_1 = 6$)

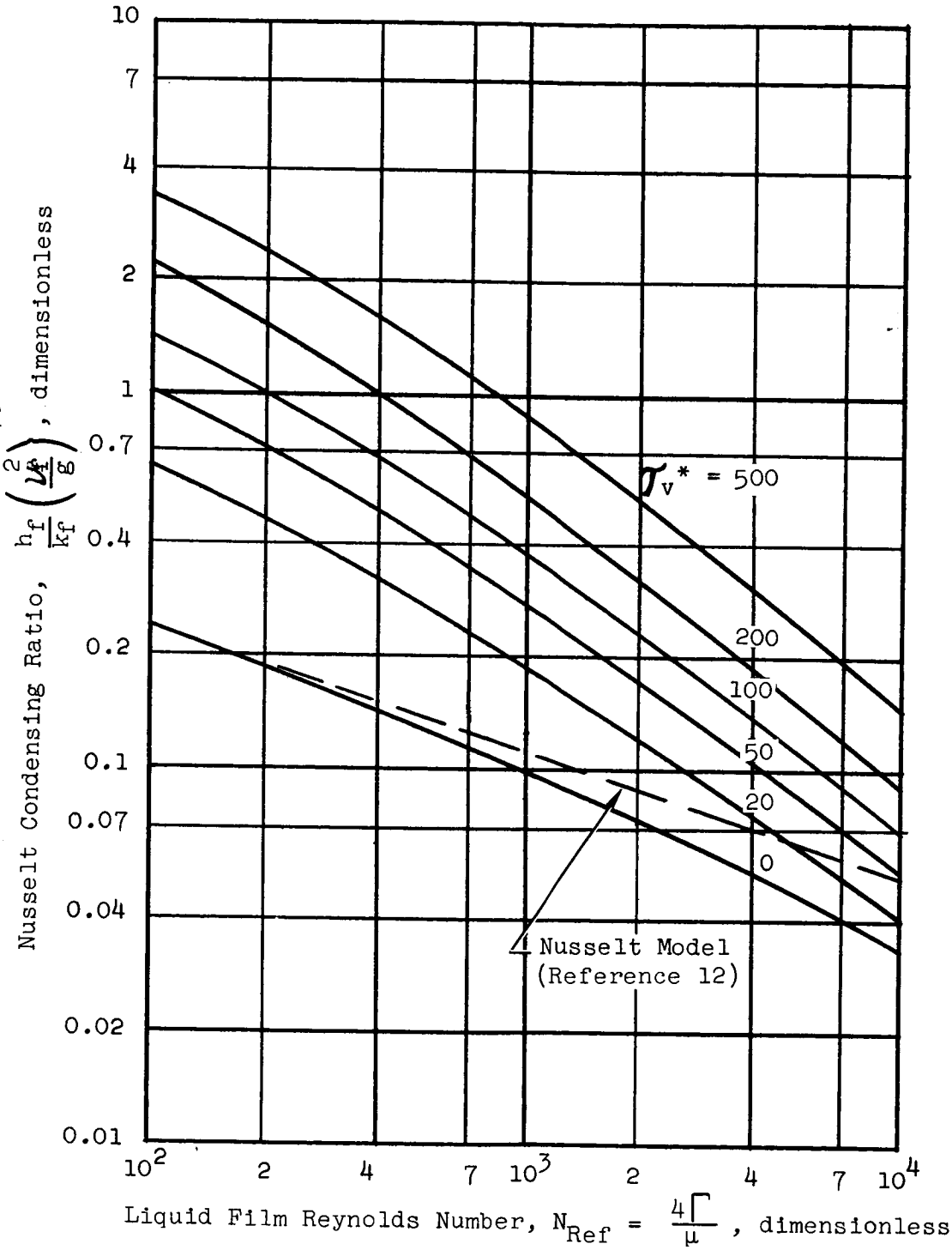

Figure 41. Nusselt Condensing Ratio Calculated Using Liquid Film Thickness Model of Dukler (Reference 28) and Eq. (5)

APPENDIX F

HEAT TRANSFER COEFFICIENT ERROR ANALYSIS

The error in the experimental local condensing heat transfer coefficients is a function of the errors in measurement of the following local quantities:

(1) Potassium saturation temperature

(2) Heat flux

(3) Tube inner wall temperature

An analysis of these measurement errors was done for the data of Test Set No. 5 (5/8-inch ID tube with instrumented 1/4-inch OD tubular insert).

Temperature Error - Two sources of temperature measurement error were considered, random measurement errors and errors due to thermocouple drift alone.

To determine the probable random error in the measurement of the potassium saturation temperature, readings from three of the insert thermocouples were considered. Three repetitive readings from each of the three thermocouples for three different groups of runs were used for the statistical analysis. The thermocouple identification numbers (T/C No.), the distance of the thermocouple from the condenser inlet (ℓ, inches) and the probable errors calculated from the thermocouple readings are listed below.

Insert T/C No.	ℓ, inches	Probable Error
23	1	$\pm$ 0.1°F
28	26	$\pm$ 0.4°F
29	31	$\pm$ 0.4°F

The identification numbers for the three repetitive runs in each data group, as listed in Reference 9, and the dates on which each data group used for these calculations were taken are: Runs 19, 20, 21, taken 2/27/65; Runs 25, 26, 27, taken 2/28/65; and Runs 28, 29, 30, taken 3/2/65. The average of the probable errors for these three thermocouples is $\pm$ 0.3°F, which was assumed to be the probable error in the potassium thermocouple temperatures E_{TK}.

The probable random errors for two of the nickel tube wall thermocouples, one at the top measuring station and one at the bottom measuring station, were also estimated from readings taken during these same runs. The thermocouple identification numbers (T/C No.), measuring station at which the thermocouples were located, the radial position of the thermocouples in the tube wall (R, inches) and the probable errors calculated from the thermocouple readings are listed below.

Wall T/C No.	Station	R, inches	Probable Error
11	Top	0.409	$\pm$ 0.4°F
16	Bottom	0.408	$\pm$ 0.3°F

The average of the probable errors for these two thermocouples is $\pm$ 0.3°F, which was assumed to be the probable error in the wall thermocouple temperatures E_{Tw}.

The thermocouple temperatures used were corrected values, based on the calibrations discussed in Appendix C. To make allowance for thermocouple drift with time, the thermocouple corrections used were the averages between the calibrations performed at the beginning of test operation and those performed at the end of test operation. The differences in indicated temperatures from the thermocouples between the before-test calibrations and the end-of-test calibrations were assumed to be drift. The absolute values of the drifts listed below were measured at 1300°F. The errors due to thermocouple drift were

assumed to be one-half the total drift between the before-test calibrations and the end-of-test calibrations.

	Thermocouple Number				
	11	16	23	28	29
Drift, °F	±1.6	±2.4	±1.0	±0.6	±0.4
Error, °F	±0.8	±1.2	±0.5	±0.3	±0.2

The probable error due to drift for the five thermocouples is assumed to be the average of the five individual errors. On this basis the probable error due to thermocouple drift E_d was calculated to be 0.6°F.

Heat Flux Error - The error in the heat flux q''_i is due to uncertainties in the tube wall thermal conductivity and uncertainty in the measured temperature gradient in the condenser tube wall (Appendix E). For this analysis these two error sources were assumed to have probable errors of 2% each, which results in an estimated probable error for the heat flux of $E_{q''} = 0.028\ q''_i$, Btu/hr-ft^2.

Wall Temperature Error - The probable error in the temperature at the tube wall inner surface T_{wi} was assumed for this analysis to be 1% of the total temperature drop across the nickel tube wall. Based on an estimated average heat transfer coefficient for conduction through the tube wall of 1300 Btu/hr-ft^2-°F, relative to the tube inner diameter (5/8-inch ID), the estimated error in the tube wall inner surface temperature is $E_{Twi} = 0.01\ q''_i/1300$, °F.

Condensing Coefficient Error - The probable error in the condensing heat transfer coefficient E_h was estimated from these component errors using Equation (F-1),

$$\frac{E_h}{h_c} = \left[\left(\frac{E_{q''}}{q''_i} \right)^2 + \left(\frac{\sqrt{E_{TK}^2 + E_d^2}}{T_K - T_{wi}} \right)^2 \left(\frac{\sqrt{E_{TW}^2 + E_d^2}}{T_K - T_{wj}} \right)^2 + \left(\frac{E_{Twi}}{T_K - T_{wi}} \right)^2 \right]^{\frac{1}{2}}, \quad \text{(F-1)}$$

for which, in summary, the component probable errors used were:

(1) E_d, thermocouple drift error = 0.6°F
(2) E_{TK}, potassium thermocouple error = 0.3°F
(3) E_{Tw}, wall thermocouple error = 0.3°F
(4) E_{Twi}, tube surface temperature error = 0.01 q''_i/1300°F
(5) E''_q, heat flux error = 0.028 q''_i, Btu/hr-ft^2

At typical test conditions of q''_i = 150,000 Btu/hr-ft^2 and ($T_K - T_{wi}$) = 15°F which corresponds to a condensing heat transfer coefficient h_c = 15,000 Btu/hr-ft^2-°F, a probable error in h_c of $\pm$ 15% was calculated using Equation (F-1). Assuming a random distribution of errors, this value corresponds to a standard error in h_c of $\pm$ 22% (Reference 70).

Figure 42 shows values of the probable error in the condensing heat transfer coefficient as a function of heat flux and potassium-to-wall temperature difference estimated using Equation (F-1). As shown in the Figure, the probable error decreases with increased temperature difference at constant heat flux, and increases with increased heat flux at constant temperature difference.

A similar error analysis was not performed for the data taken in the other Test Sets. It is believed that the data from Test Sets No. 1, 2 and 3, for which direct measurements of the local potassium temperature at the measuring stations were not made, have a larger error than the Test Set No. 5 data, due to additional errors involved in estimating the local potassium saturation temperature T_K, as discussed in Appendix H. The data from Test Set No. 4 (5/8-inch ID tube with instrumented helical insert, p/D_i = 6), for which the local potassium temperature was measured directly, should have approximately the same errors as estimated in this Appendix for Test Set No. 5 plus an additional uncertainty due to the correction for effects of swirl flow on the saturation temperature at the tube wall, as discussed in Appendix E.

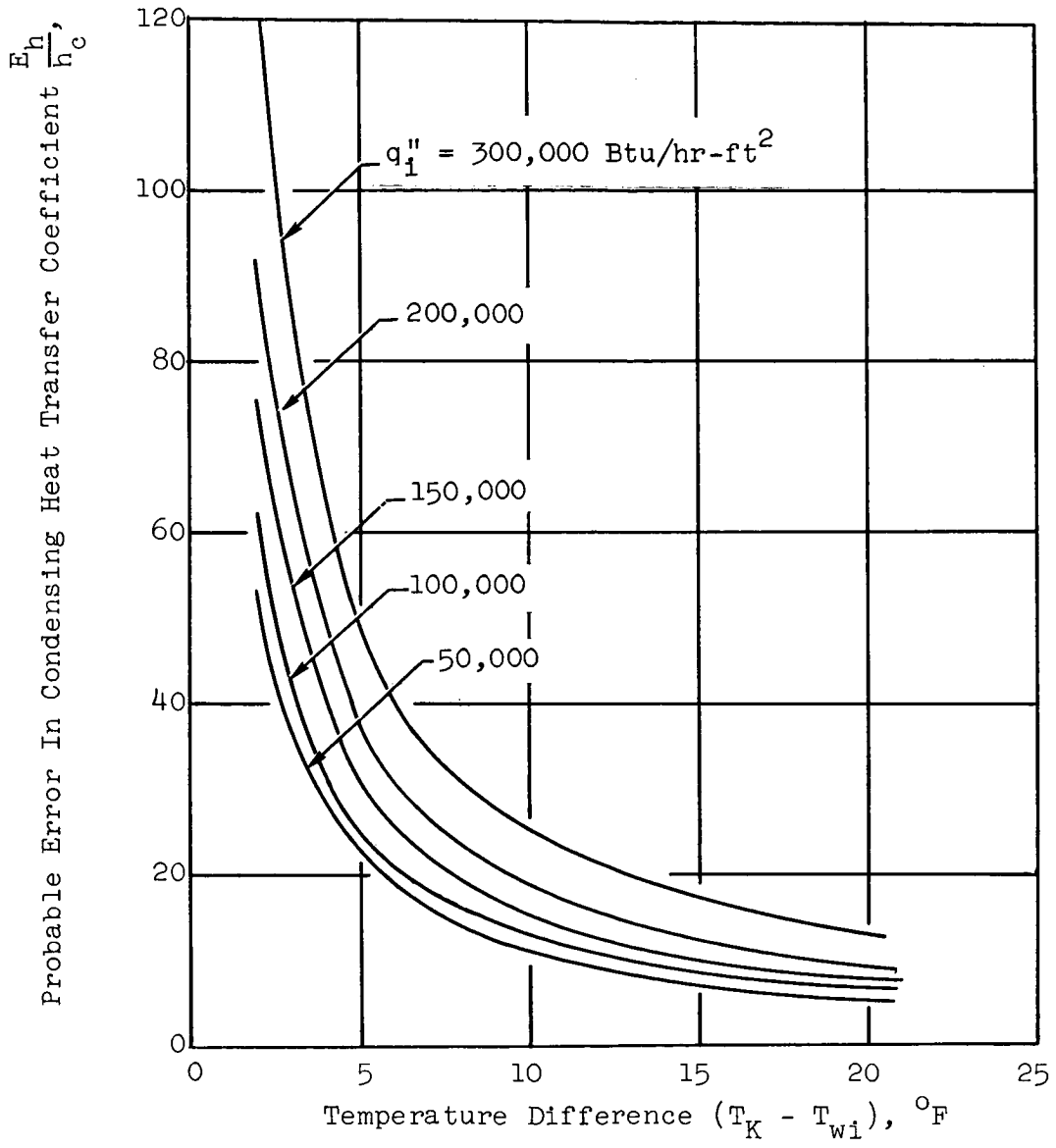

Figure 42. Estimated Probable Error In Condensing Heat Transfer Coefficient As Function Of Fluid-To-Wall Temperature Difference And Heat Flux For Test Set No. 5 Data (5/8-inch ID Tube With Instrumented 1/4-inch OD Tubular Insert)

APPENDIX G

ANALYSIS OF POTASSIUM VAPOR-PHASE THERMAL RESISTANCE

In order to compare with theory the values of the vapor-phase coefficient h_v obtained from the Test No. 5 data using Equation (6), an analysis was conducted based on a procedure suggested by the work of Schrage (Reference 32) and used by Rohsenow and Sukhatme (Reference 16). The analysis is as follows.

From kinetic gas theory (Reference 36), the mass flux of molecules impinging on a surface is given by

$$G_m = P \left(\frac{Mg_o}{2\pi \bar{R} T}\right)^{\frac{1}{2}} \qquad \text{(G-1)}$$

When equilibrium exists between a saturated vapor and its liquid, the mass flux of molecules leaving the liquid surface equals the mass flux of vapor molecules condensing on the liquid surface. That is, the net rate of heat transfer is zero. This equality is expressed by

$$P_v \left(\frac{Mg_o}{2\pi \bar{R}\, T_v}\right)^{\frac{1}{2}} = P_s \left(\frac{Mg_o}{2\pi \bar{R}\, T_s}\right)^{\frac{1}{2}} \qquad \text{(G-2)}$$

in which:

P_v = pressure of the saturated vapor
T_v = temperature of the saturated vapor
T_s = temperature of the liquid at the liquid-vapor interface
P_s = saturation pressure corresponding to T_s

When a net rate of mass transfer occurs, such as in condensing, a condition of

nonequilibrium exists at the vapor-liquid interface. For condensing, the net mass flux of molecules G_c leaving the vapor and condensing into the liquid can be expressed as

$$G_c = \sigma_c P_v \left(\frac{Mg_o}{2\pi \bar{R} T_v}\right)^{\frac{1}{2}} - \sigma_e P_s \left(\frac{Mg_o}{2\pi \bar{R} T_s}\right)^{\frac{1}{2}} \qquad \text{(G-3)}$$

where

σ_c = condensation coefficient, the mass flux of molecules from the vapor which actually condense divided by the mass flux predicted by Equation (G-1) for P_v and T_v.

σ_e = evaporation coefficient, the mass flux of molecules which actually leave the liquid surface divided by the mass flux predicted by Equation (G-1) for P_s and T_s.

It was assumed for the treatment of the Test Set No. 5 data that $\sigma_c = \sigma_e$. With this assumption Equation (G-3) reduces to Equation (G-4).

$$G_c = \sigma_c \left[P_v \left(\frac{Mg_o}{2\pi \bar{R} T_v}\right)^{\frac{1}{2}} - P_s \left(\frac{Mg_o}{2\pi \bar{R} T_s}\right)^{\frac{1}{2}} \right] \qquad \text{(G-4)}$$

Substituting from Equation (G-1) into Equation (G-4) gives

$$G_c = \sigma_c \left[G_{mv} - G_{ms} \right] \qquad \text{(G-5)}$$

Assuming that all of the heat transferred from the vapor to the liquid film is by condensation, an energy balance on a unit area of the heat transfer surface, using Equation (G-5), gives

$$q'' = \sigma_c \left[\lambda_v G_{mv} - \lambda_s G_{ms} \right]$$

$$= \sigma_c \Delta (\lambda G_m) \qquad \text{(G-6)}$$

where the difference Δ is between the two sets of pressure and temperature conditions P_v, T_v and P_s, T_s.

A vapor phase heat transfer coefficient h_v can be defined as

$$h_v = q''/\Delta T_v \qquad \text{(G-7)}$$

where q'' is the condensing heat flux and ΔT_v is the corresponding difference between the bulk vapor temperature T_v and the liquid surface temperature T_s.

Substituting into Equation (G-7) from Equation (G-6) for q'' results in

$$h_v = \sigma_c \frac{\Delta (\lambda G_m)}{\Delta T_v} \qquad \text{(G-8)}$$

For small values of the temperature difference ΔT_v, the latent heat of vaporization can be assumed to be constant and the righthand side of Equation (G-8) can be expressed as a derivative to give Equation (G-9)

$$h_v = \sigma_c \lambda \frac{dG_m}{dT_v} \qquad \text{(G-9)}$$

Substitution from Equation (G-1) into Equation (G-9) results in Equation (G-10) for the vapor-phase heat transfer coefficient.

$$h_v = \sigma_c \lambda \left[\frac{Mg_o}{2\pi \bar{R} T} \right]^{\frac{1}{2}} \left(\frac{dP}{dT} - \frac{P}{2T} \right) \qquad \text{(G-10)}$$

Equation (G-10) was used to calculate the vapor-phase heat transfer coefficients for comparison with the values obtained from the Test Set No. 5 data (Section V, Equation 7). Saturation properties for potassium from Reference 69 were used for these calculations.

Values of the vapor-phase coefficient for potassium as a function of saturation temperature with the condensation coefficient σ_c as a parameter, calculated using Equation (G-10), are shown in Figure 43. As can be seen from the Figure, the calculated vapor phase heat transfer coefficient increases with increased saturation temperature T_K and is proportional to the condensation coefficient σ_c.

It is interesting to compare the relative importance of the vapor-phase heat transfer coefficient for potassium with that of a higher Prandtl number fluid such as water. Figure 44 shows the vapor-phase heat transfer coefficients calculated for water and potassium, respectively, using Equation (G-10) with $\sigma_c = 1.0$. The corresponding liquid-film heat transfer coefficients calculated using Nusselts model (Reference 12) for an assumed liquid-film Reynolds number $N_{Ref} = 10^3$ are shown in the Figure for comparison.

Figure 44 shows that over the pressure range from 0.1 to 100 psia, the vapor phase heat transfer coefficient for water at $\sigma_c = 1.0$ is in the order of 10^2 to more than 10^4 times as large as the liquid film heat transfer coefficient. A value of $\sigma_c = 0.3$ has recently been reported for water (Reference 37). Thus, the vapor phase thermal resistance for water is very small relative to the thermal resistance due to conduction through the liquid film, even for condensation coefficients as small as $\sigma_c = 0.1$. In contrast, for potassium, even with condensation coefficients as large as $\sigma_c = 1.0$, the vapor phase coefficient is about equal to the liquid film coefficient at 1 psia ($T_{sat} = 990°F$) and is less than ten times the liquid film coefficient at 25 psia ($T_{sat} = 1500°F$).

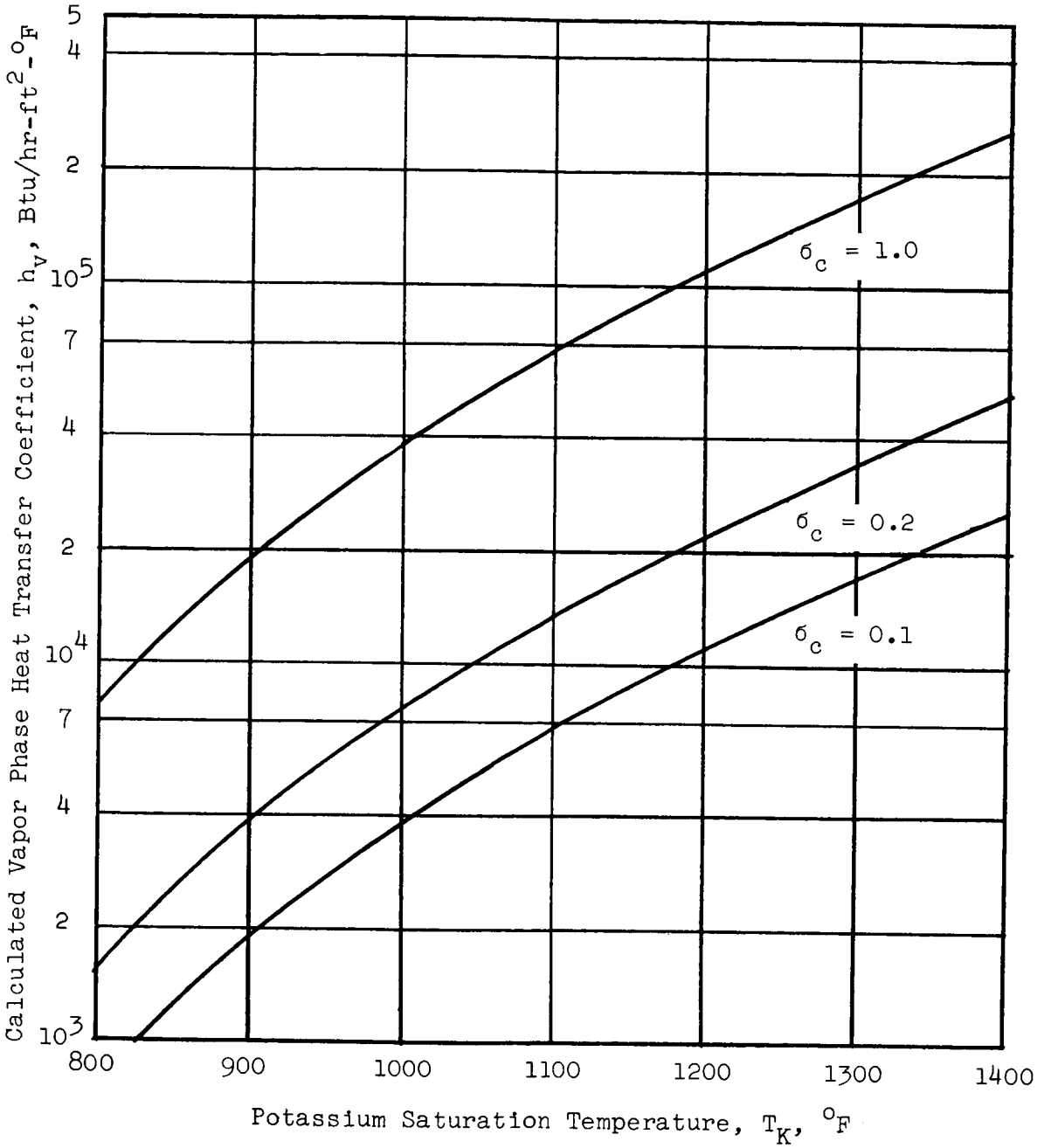

Figure 43. Vapor Phase Condensing Heat Transfer Coefficient Calculated For Potassium From Kinetic Theory of Gases Using Equation (7), For Various Values of σ_c.

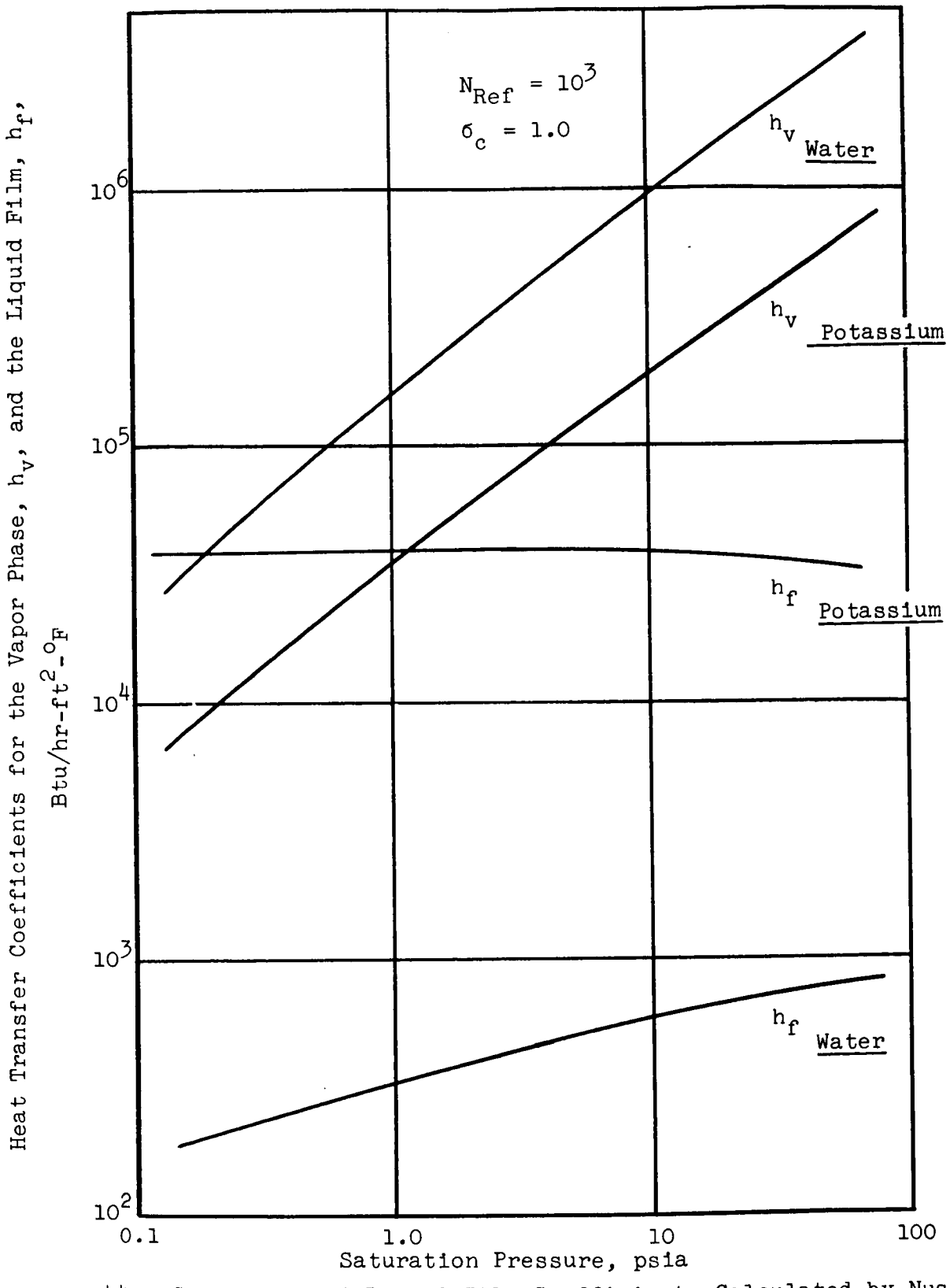

Figure 44. Comparison of Liquid Film Coefficients Calculated by Nusselt's Model (Reference 12) with Vapor Phase Coefficients Calculated by Equation (7) for Condensing Water and Condensing Potassium.

APPENDIX H

DEPENDENCE OF EXPERIMENTAL CONDENSING COEFFICIENTS ON POTASSIUM TEMPERATURE DISTRIBUTION

As indicated in Appendix E, linear interpolation between the bulk potassium temperatures measured at the condenser inlet and outlet, respectively, was used to estimate the local potassium temperature at the measuring stations for the data of Test Sets No. 1, 2 and 3. The effect on the heat transfer coefficient accuracy of the linear potassium temperature distribution approximation can be studied by comparing coefficients obtained from Test Set No. 5 (5/8-inch ID tube with instrumented 1/4-in. OD tubular insert), which are based on direct measurement of the local potassium temperature, with values calculated from the same data using linear interpolation to estimate the local potassium temperatures.

Figure 45-a shows the condensing heat transfer coefficient data from Test Set No. 5 obtained using the measured local potassium temperatures. These are the same data as presented in Figure 21 except that the three low-temperature data points (discussed in Section V) have been deleted for this comparison. The same data, but with the coefficients obtained using local potassium temperatures estimated by linear interpolation from measured condenser inlet and outlet bulk potassium temperatures, are shown for comparison in Figure 45-b.

Comparison of Figure 45-b with Figure 45-a indicates that using linear interpolation to estimate the local potassium temperature causes increased scatter of the heat transfer coefficients compared to the coefficients obtained using the measured local potassium temperatures. The increased scatter is particularly evident for the data taken at the top measuring station ($\ell/D_i = 10$).

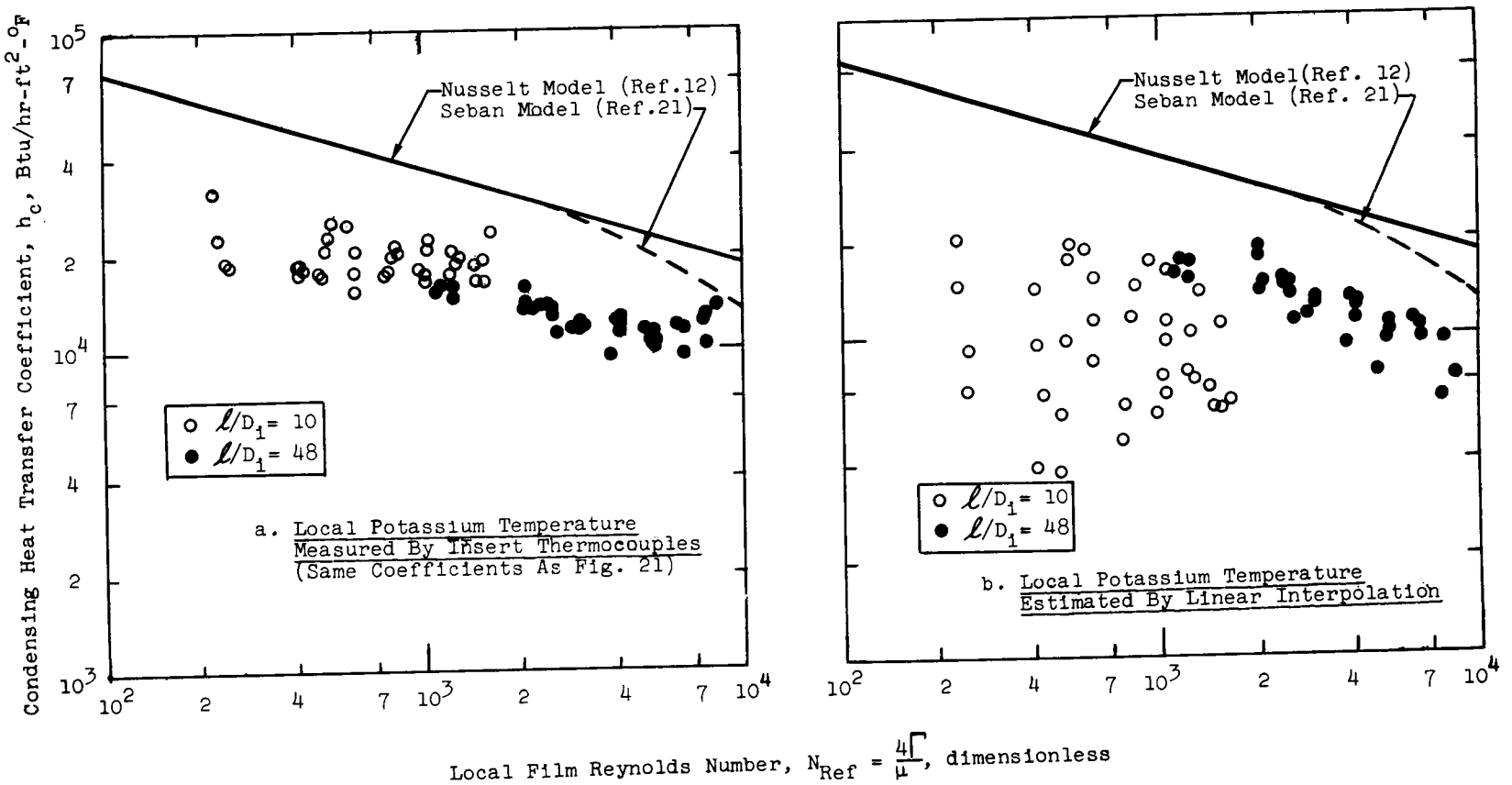

Figure 45. Local Condensing Heat Transfer Coefficients From Test Set No. 5 (5/8-inch ID Tube with Instrumented 1/4-inch OD Tubular Insert) Compared With Coefficients From Same Data Obtained Using Linear Interpolation For Estimating Local Potassium Temperature

TABLE 1

SUMMARY OF CONDENSING TESTS

Group-A — Test Set No. 1

Test Period: May 1963 (Reference 9)

Geometry: 5/8-inch ID tube, no insert

Range of total G, lbs/sec-ft^2:	3.3 to 4.0
Approximate local X:	0.65
Range of local T_{sat}, ^oF:	1157 to 1185
Range of local q", 10^5 Btu/hr-ft^2:	0.32 to 0.40
ℓ/D, from inlet	29

Group-B

Test Period: December 1963 (Reference 7)

Geometry: 5/8-inch ID tube, no insert

Range of total G, lbs/sec-ft^2:	1.4 to 1.6	
Range of local T_{sat}, ^oF:	1165 to 1258	
Measuring Station: ℓ/D, from inlet	Top 19	Bottom 38
Approximate local X	0.71	0.38
Range of local q", 10^5 Btu/hr-ft^2	0.17 to 0.19	0.23 to 0.26

Group-C

Test Period: July 1964 (Reference 7)

Geometry: 5/8-inch ID tube, no insert

Range of total G, lbs/sec-ft^2:	3.0 to 6.0	
Range of local T_{sat}, ^oF:	1130 to 1312	
Measuring Station: ℓ/D, from inlet	Top 13	Bottom 46
Approximate local X	0.85	0.28
Range of local q", 10^5 Btu/hr-ft^2	0.39 to 0.84	0.45 to 0.95

Group-D

Test Period: September 1964 (Reference 8)

Geometry: 5/8-inch ID tube, no insert

Range of Total G, lbs/sec-ft^2	1.2 to 11	
Range of local T_{sat}, ^oF:	1140 to 1457	
Measuring Station: ℓ/D, from inlet	Top 13	Bottom 45
Approximate local X	0.88	0.22
Range of local q", 10^5 Btu/hr-ft^2	0.21 to 1.2	0.07 to 1.6

Test Set No. 2

Test Period: December 1964 (Reference 10)

Geometry: 5/8-inch ID tube, tapered pin insert

Range of total G, lbs/sec-ft^2:	3.7 to 19.3	
Range of local T_{sat}, ^oF:	1198 to 1435	
Measuring Station: ℓ/D, from inlet	Top 10	Bottom 45
Approximate local X	0.86	0.26
Range of local q", 10^5 Btu/hr-ft^2	0.50 to 2.3	0.64 to 3.0

Test Set No. 3

Test Period: January 1965 (Reference 10)

Geometry: 3/8-inch ID tube, no insert

Range of total G, lbs/sec-ft^2	3.8 to 36.1	
Range of local T_{sat}, ^oF:	1143 to 1415	
Measuring Station: ℓ/D, from inlet	Top 21	Bottom 75
Approximate local X	0.80	0.25
Range of local q", 10^5 Btu/hr-ft^2	0.29 to 2.8	0.29 to 3.2

Test Set No. 4

Test Period: 2/3/65 to 2/9/65 (Reference 9)

Geometry: 5/8-inch ID tube, inst'd helical insert (P/D = 6)

Range of total G, lbs/sec-ft^2:	2.5 to 19	
Measuring Station: ℓ/D, from inlet	Top 10	Bottom 48
Range of local T_{sat}, ^oF	1088 to 1407	1062 to 1405
Approximate local X	0.83	0.17
Range of local q", 10^5 Btu/hr-ft^2	0.32 to 2.9	0.35 to 2.4

Test Set No. 5

Test Period: 2/27/65 to 3/3/65 (Reference 9)

Geometry: 5/8-inch ID tube, inst'd tubular insert (1/4-inch OD)

Range of Total G, lbs/sec-ft^2:	2.5 to 18	
Measuring Station: ℓ/D, from inlet	Top 10	Bottom 48
Range of local T_{sat}, ^oF	1094 to 1410	884 to 1414
Range of local X	0.83 to 0.89	0.16 to 0.21
Range of local q", 10^5 Btu/hr-ft^2	0.24 to 2.9	0.3 to 2.7

TABLE 2

CONDENSING HEAT TRANSFER DATA FROM TEST SET NO. 4

(5/8-inch ID Tube with Instrumented Helical Insert, $p/D_i = 6$)

							Top Station, $\ell/D_i = 10$, $X \approx 0.83$					Bottom Station, $\ell/D_i = 48$, $X \approx 0.17$				
Run No.	Date	Time	T_{KI} °F	W_K lb/hr	T_{KO} °F	T_K °F	T_{wi} °F	h_c Btu/hr-ft^2-°F	N_{Nuc}	N_{Ref}	q_i'' Btu/hr-ft^2	T_K °F	T_{wi} °F	h_c Btu/hr-ft^2-°F	N_{Nuc}	N_{Ref}	q_i'' Btu/hr-ft^2
1	2/3/65	2300	1183	23.4	1179	1182	1180	17,700	.0498	263.3	37,200	1179	1175	10,400	.0293	1315	39,400
2	2/4/65	0515	1247	21.0	1245	1247	1245	19,100	.0541	245.6	31,900	1245	1241	9,300	.0264	1227	35,400
3		1000	1154	40.5	1146	1154	1149	12,700	.0355	448.4	63,400	1146	1140	10,700	.0300	2236	66,100
4		1300	1221	38.8	1216	1221	1217	16,700	.0472	447.5	61,000	1217	1211	12,500	.0352	2235	68,900
5		1720	1295	35.8	1292	1294	1291	17,100	.0489	431.0	56,000	1292	1287	12,600	.0358	2154	65,700
6		2210	1399	29.6	1398	1399	1397	21,200	.0617	377.0	48,800	1399	1394	11,200	.0326	1885	54,100
7	2/5/65	0112	1392	46.7	1390	1391	1388	21,200	.0616	591.6	70,900	1391	1383	10,900	.0315	2956	83,400
8		0500	1282	53.4	1279	1282	1278	18,600	.0532	637.9	82,900	1278	1270	11,600	.0329	3186	94,700
9		0830	1206	57.9	1198	1207	1201	14,200	.0400	660.6	91,500	1197	1189	11,700	.0328	3292	98,000
10		1215	1103	54.5	1067	1111	1096	7,000	.0196	581.5	108,300	1065	1059	12,700	.0353	2844	80,500
11		1330	1145	50.0	1129	1146	1138	10,600	.0296	548.2	87,500	1128	1121	12,500	.0349	2721	83,600
12	2/6/65	0035	1202	47.5	1195	1202	1197	16,100	.0454	540.3	78,000	1194	1188	13,300	.0373	2695	85,600
13		1230	1210	57.0	1201	1210	1204	14,600	.0436	652.2	93,900	1200	1192	12,600	.0354	3249	101,200
14		0425	1204	61.8	1182	1202	1195	13,500	.0379	702.4	107,900	1181	1173	12,900	.0361	3477	105,800
15		0620	1258	69.8	1236	1255	1247	15,800	.0447	820.5	120,800	1234	1225	13,000	.0369	4064	122,000
16		0915	1295	69.4	1283	1293	1287	17,500	.0499	834.4	113,100	1283	1273	12,900	.0368	4153	124,100
17		1100	1407	61.5	1405	1407	1403	23,700	.0690	785.2	97,300	1405	1396	13,000	.0377	3922	115,400
18		1400	1405	83.1	1401	1405	1399	20,600	.0600	1060	126,800	1401	1388	12,100	.0351	5293	150,900
19		1645	1299	87.3	1270	1294	1285	15,600	.0446	1048	147,100	1269	1257	12,200	.0347	5180	149,200
20		1900	1252	87.7	1200	1244	1231	12,700	.0359	1022	159,400	1199	1188	11,900	.0334	4992	140,500
21		2200	1203	90.0	1058	1190	1166	8,800	.0247	1010	209,500	1065	1055	10,900	.0303	4689	108,700
22	2/7/65	0047	1257	107.5	1140	1245	1224	11,000	.0311	1250	227,900	1140	1130	14,900	.0417	5897	153,800
23		0250	1302	104.0	1249	1294	1280	14,800	.0422	1248	191,000	1249	1237	15,500	.0440	6101	178,600
24		0930	1403	107.5	1380	1399	1390	19,600	.0569	1367	178,600	1481	1368	15,600	.0451	6773	196,300
25		1400	1399	121.0	1370	1394	1382	16,800	.0490	1534	199,000	1369	1355	14,900	.0431	7584	214,800
26		1800	1305	121.0	1218	1293	1276	13,600	.0390	1449	234,600	1219	1206	15,500	.0437	6970	194,400
27		2110	1309	141.7	1167	1297	1274	13,000	.0373	1698	294,300	1167	1152	13,200	.0369	7913	198,100
28	2/8/65	0215	1404	131.8	1365	1397	1385	17,900	.0520	1672	220,200	1365	1351	16,000	.0463	8245	231,900
29		0418	1392	144.6	1324	1380	1364	15,900	.0460	1818	255,200	1324	1306	13,900	.0400	8852	240,500
30		1900	1141	34.9	1131	1141	1136	13,800	.0387	382.2	65,100	1130	1127	21,400	.0598	1902	65,700
31		2100	1108	37.7	1091	1108	1101	10,300	.0286	403.5	72,700	1089	1086	23,600	.0656	2001	66,600
32		2345	1092	21.4	1082	1091	1088	14,200	.0395	227.2	42,000	1081	1080	35,600	.0989	1131	38,200
33	2/9/65	0130	1152	18.8	1147	1151	1149	17,600	.0493	207.3	35,000	1147	1146	27,600	.0772	1034	35,800

TABLE 3

CONDENSING HEAT TRANSFER DATA FROM TEST SET NO. 5

(5/8-inch ID Tube with Instrumented 1/4-inch OD Tubular Insert)

Run No.	Date	Time	T_{KI} °F	W_K lb/hr	T_{KO} °F	Top Station, $\ell/D_i = 10$					Bottom Station, $\ell/D_i = 48$					
						T_K °F	T_{wi} °F	h_c Btu/hr-ft^2-°F	N_{Nuc} —	X —	N_{Ref} —	q''_i Btu/hr-ft^2	T_K °F	T_{wi} °F	h_c Btu/hr-ft^2-°F	N_{Nuc} —	X —	N_{Ref} —	q''_i Btu/hr-ft^2
1	2/27/65	0130	1106	23.0	1109	1104	1102	18,800	.0524	.88	174.4	31,100	1109	1106	15,000	.0417	.19	1209	43,800
2		0245	1143	22.6	1145	1142	1140	18,800	.0524	.88	175.7	30,600	1145	1142	15,700	.0438	.18	1231	41,400
3		0415	1195	20.3	1195	1194	1193	22,400	.0630	.88	162.7	27,400	1195	1193	15,900	.0447	.17	1153	35,100
4		0545	1257	18.9	1257	1257	1256	31,300	.0888	.89	144.2	24,200	1257	1255	15,200	.0433	.16	1128	30,400
5		1130	1253	34.5	1253	1252	1250	18,400	.0520	.88	286.4	46,900	1255	1250	13,300	.0378	.18	2007	62,000
6		1330	1200	36.1	1204	1199	1196	18,200	.0511	.88	290.0	48,200	1204	1200	15,900	.0447	.18	2035	68,000
7		1500	1141	38.4	1151	1139	1136	18,100	.0505	.88	297.7	51,100	1150	1144	13,600	.0379	.20	2048	76,800
8		1715	1110	38.1	1122	1105	1102	17,500	.0488	.88	288.3	48,200	1120	1115	13,900	.0388	.21	1965	78,600
9		1845	1111	44.7	1128	1104	1100	17,700	.0492	.88	338.4	55,800	1126	1119	13,800	.0384	.22	2287	96,200
10		2030	1148	43.9	1161	1145	1141	17,200	.0482	.88	341.2	58,300	1159	1153	13,900	.0388	.21	2324	91,100
11		2230	1196	44.2	1204	1195	1192	20,600	.0578	.87	384.0	61,700	1203	1197	13,300	.0374	.20	2433	86,000
12	2/28/65	0045	1301	42.6	1303	1301	1298	22,800	.0651	.87	393.7	59,000	1303	1297	12,800	.0366	.18	2547	76,300
13		0330	1404	41.0	1405	1404	1402	25,200	.0734	.87	399.8	54,900	1405	1399	11,100	.0324	.18	2583	68,900
14		0415	1402	45.8	1403	1402	1399	24,900	.0724	.87	446.0	62,000	1403	1396	11,600	.0338	.18	2882	78,300
15		0610	1307	51.2	1310	1307	1303	20,400	.0585	.87	474.3	71,300	1310	1302	12,000	.0345	.19	3032	92,400
16		0900	1239	53.0	1246	1238	1234	17,600	.0497	.88	436.0	72,500	1245	1237	12,100	.0343	.19	3026	98,800
17		1030	1205	53.8	1215	1204	1199	15,400	.0434	.88	434.0	72,800	1215	1206	11,800	.0331	.19	3020	104,000
18		1315	1185	69.1	1206	1180	1175	17,700	.0496	.88	548.8	90,300	1204	1192	12,100	.0340	.20	3802	139,400
19		1445	1249	69.8	1260	1248	1243	19,400	.0551	.87	625.7	97,000	1259	1248	12,200	.0345	.19	4018	132,500
20		1730	1295	69.5	1301	1294	1289	20,100	.0574	.87	639.8	97,400	1300	1290	12,300	.0353	.19	4096	128,500
21		2100	1394	65.0	1395	1393	1389	21,200	.0616	.87	630.8	90,200	1395	1385	11,100	.0323	.19	4029	113,600
22		2350	1400	82.3	1401	1399	1393	20,500	.0597	.87	801.4	116,800	1401	1387	10,200	.0296	.19	5119	145,900
23	3/1/65	0150	1301	86.9	1308	1302	1293	22,100	.0633	.87	801.6	120,400	1307	1292	10,500	.0301	.19	5140	157,400
24		0210	1294	86.8	1302	1290	1284	20,800	.0594	.87	797.7	119,300	1300	1286	11,200	.0321	.19	5116	159,800
25		0320	1254	87.2	1267	1248	1242	17,300	.0490	.87	782.7	121,300	1264	1248	10,500	.0298	.20	4976	166,400
26		0500	1210	86.0	1209	1194	1187	17,800	.0500	.84	919.0	135,000	1202	1187	11,500	.0323	.21	4668	169,200
27		0930	1260	104.9	1274	1255	1248	20,200	.0572	.87	945.1	149,000	1271	1254	11,700	.0334	.20	6012	202,500
28		1300	1309	107.2	1312	1300	1292	19,600	.0559	.87	989.1	148,500	1310	1293	11,600	.0331	.19	6352	197,600
29		1515	1412	102.7	1414	1410	1403	20,000	.0583	.87	1004.4	144,200	1414	1395	9,700	.0284	.19	6419	182,200
30		2045	1409	121.3	1416	1407	1396	16,400	.0478	.87	1184.9	170,600	1414	1392	10,400	.0302	.19	7588	217,800
31		2345	1306	123.2	1321	1293	1282	16,700	.0476	.86	1220.3	171,400	1314	1295	12,000	.0344	.20	7230	236,800
32	3/2/65	0130	1312	137.9	1308	1287	1276	23,300	.0665	.84	1555.8	219,000	1292	1272	13,600	.0387	.21	7893	264,700
33		0820	1292	131.3	1279	1266	1255	19,100	.0543	.83	1556.3	223,700	1261	1241	12,500	.0354	.21	7384	252,800
34		1330	1254	126.6	1119	1213	1198	18,400	.0519	.77	1969.1	291,500	1061	1023	3,300	.00906	.16	6668	124,300
35		1800	1193	108.3	1074	1160	1145	17,200	.0482	.78	1559.1	248,100	1027	996	3,500	.00963	.16	5561	106,000
36		2200	1157	96.7	884	1094	1077	16,700	.0464	.70	1816.6	282,600	884	846	1,200	.00326	.07	4793	45,200
37	3/3/65	0145	1161	68.8	1182	1151	1146	17,000	.0475	.87	581.9	91,600	1179	1164	9,500	.0267	.21	3681	138,990

TABLE 4

VAPOR PHASE COEFFICIENTS CALCULATED FROM TEST SET NO. 5 DATA

Run No.[1]	Top Station, ℓ/D_i = 10		Bottom Station, ℓ/D_i = 48	
	h_v Btu/hr-ft^2-°F[2]	σ_c[3] —	h_v Btu/hr-ft^2-°F[2]	σ_c[3] —
1	20,300	0.29	24,400	0.34
2	20,400	0.24	27,100	0.31
3	25,300	0.23	28,200	0.25
4	39,000	0.26	26,700	0.18
5	20,500	0.14	24,700	0.17
6	19,900	0.17	33,600	0.29
7	19,500	0.23	23,400	0.26
8	18,700	0.26	23,500	0.31
9	18,800	0.27	23,800	0.30
10	18,500	0.21	25,100	0.27
11	22,700	0.20	24,700	0.21
12	26,500	0.15	25,400	0.14
13	31,600	0.12	20,600	0.079
14	30,800	0.12	23,300	0.090
15	23,300	0.13	24,100	0.13
16	19,200	0.14	22,900	0.16
17	16,600	0.14	20,900	0.17
18	19,000	0.18	23,400	0.20
19	21,300	0.15	26,000	0.17
20	22,500	0.13	28,600	0.16
21	24,900	0.099	24,800	0.098
22	23,900	0.093	22,600	0.087
23	24,900	0.14	22,000	0.12
24	23,200	0.14	25,200	0.14
25	18,700	0.13	20,500	0.13
26	19,000	0.17	21,800	0.19
27	22,000	0.15	27,700	0.18
28	21,600	0.12	29,600	0.16
29	22,900	0.086	23,000	0.085
30	18,400	0.070	30,100	0.11
31	18,000	0.10	35,600	0.19
32	26,000	0.15	52,000	0.30
33	20,800	0.13	33,300	0.22
34	19,800	0.16	3,600	0.066
35	18,200	0.19	3,800	0.086
36	17,400	0.26	1,200	0.072
37	18,100	0.20	14,900	0.14

(1) Operating conditions for each run are given in Table 3

(2) h_v calculated from data in Table 3 using Equation (6)

(3) σ_c^v calculated from h_v data using Equation (7)

TABLE 5

CONDENSING HEAT TRANSFER DATA FROM TEST SET NO. 1

(5/8-inch ID Tube without Insert)

GROUP-A

(ℓ/D_1 = 29, X ≈ 0.65)

Run No.	Date	Time	T_{KI} °F	T_K °F	h_c Btu/hr-ft²-°F	N_{Nuc}	N_{Ref}	q_1'' Btu/hr-ft²	W_K lbs/hr.
1	5/17/63	0810	1153	1157	10,770	.0301	556.6	32,570	25.7
2	5/17/63	0845	1170	1173	11,170	.0313	639.5	33,960	27.1
3	5/17/63	0907	1175	1178	11,320	.0317	692.4	34,810	27.6
4	5/17/63	0935	1181	1183	11,200	.0314	730.5	35,070	27.9
5	5/17/63	1030	1176	1179	10,770	.0302	750.4	36,780	29.4
6	5/17/63	1045	1173	1176	10,870	.0305	746.9	37,060	29.4
7	5/17/63	1115	1170	1173	11,600	.0325	754.4	37,930	29.5
8	5/17/63	1140	1170	1173	11,370	.0318	767.6	37,680	29.5
9	5/17/63	1210	1174	1178	11,420	.0320	767.8	37,200	29.0
10	5/17/63	1311	1178	1182	8,740	.0245	820.7	39,000	30.3
11	5/17/63	1411	1182	1185	7,980	.0224	838.0	39,360	30.6

GROUP-B

					Top Station, ℓ/D_1 = 19, X ≈ 0.71				Bottom Station, ℓ/D_1 = 38, X ≈ 0.38				
Run No.	Date	Time	T_{KI} °F	W_K lbs/hr.	T_K °F	h_c Btu/hr-ft²-°F	N_{Nuc}	N_{Ref}	q_1'' Btu/hr-ft²	T_K °F	h_c Btu/hr-ft²-°F	N_{Nuc}	N_{Ref}	q_1'' Btu/hr-ft²
1	12/6/63	2300	1165	12.1	1166	8879	.0249	226.5	18,720	1166	11,560	.0324	494.8	25,550
2	12/7/63	0020	1202	11.1	1203	8749	.0246	224.1	17,200	1203	11,530	.0324	476.8	23,200
3	12/7/63	0130	1236	10.9	1236	11270	.0319	227.1	17,530	1236	13,420	.0380	480.2	22,910
4	12/7/63	0220	1257	11.6	1258	10543	.0299	246.2	18,380	1258	13,000	.0369	519.0	24,210
5	12/7/63	0230	1257	11.8	1257	10008	.0284	250.1	18,420	1257	13,740	.0390	528.4	24,850

GROUP-C

					Top Station, ℓ/D_1 = 13, X≈0.85					Bottom Station, ℓ/D_1 = 46, X ≈ 0.28				
Run No.	Date	Time	T_{KI} °F	W_K lbs/hr.	T_K °F	h_c Btu/hr-ft²-°F	N_{Nuc}	N_{Ref}	q_1'' Btu/hr-ft²	T_K °F	h_c Btu/hr-ft²-°F	N_{Nuc}	N_{Ref}	q_1'' Btu/hr-ft²
1	7/21/64	1945	1135	33.2	1138	20960	.0585	293.4	57,170	1146	18,180	.0508	1525	74,570
2	7/21/64	2000	1130	32.1	1133	16810	.0469	280.9	55,290	1140	17,570	.0491	1469	73,340
3	7/22/64	0234	1158	26.4	1160	12270	.0343	272.4	45,420	1164	13,840	.0387	1268	57,160
4	7/22/64	0845	1249	22.9	1249	13220	.0375	292.7	40,230	1251	12,520	.0355	1208	45,740
5	7/22/64	0945	1270	39.9	1271	14250	.0405	490.3	70,420	1273	11,410	.0325	2104	82,850
6	7/22/64	1100	1239	39.8	1240	11900	.0337	472.4	71,470	1243	11,800	.0334	2055	87,110
7	7/22/64	1235	1214	40.1	1216	18530	.0522	442.5	71,500	1222	15,270	.0430	2014	88,980
8	7/22/64	1630	1311	46.0	1312	20730	.0594	586.2	83,750	1315	12,540	.0359	2493	94,800

TABLE 6

CONDENSING HEAT TRANSFER DATA FROM TEST SET NO. 2

(5/8-inch ID Tube with Non-Instrumented Tapered Pin Insert)

Run No.	Date	Time	T_{KI} °F	W_K lbs/hr.	Top Station, $\ell/D_1 = 10$, $X \approx 0.86$					Bottom Station, $\ell/D_1 = 45$, $X \approx 0.26$				
					T_K °F	h_c Btu/hr-ft^2-°F	N_{Nuc}	N_{Ref}	q''_i Btu/hr-ft^2	T_K °F	h_c Btu/hr-ft^2-°F	N_{Nuc}	N_{Ref}	q''_i Btu/hr-ft
1	12/ 7/64	1000	1198	41.7	1198	-34,980	-.0983	372.4	61,180	1202	46,680	.1312	2,080	77,560
2		1300	1292	45.0	1292	- 8,240	-.0235	451.4	67,760	1256	-2,480	-.0070	2,379	85,550
3		1900	1398	55.3	1383	- 5,920	-.0172	-710.0	87,180	1326	-1,610	-.0046	2,047	111,800
4	12/ 8/64	0745	1299	57.1	1299	-142,000	-.4060	567.4	85,620	1301	43,770	.1252	3,055	108,800
5		1300	1200	58.8	1201	-31,570	-.0887	502.4	87,810	1207	74,190	.2086	2,908	115,300
6		1830	1200	71.9	1202	-82,530	-.2319	626.3	108,100	1208	70,160	.1973	3,573	143,800
7		2215	1293	72.3	1293	-188,320	-.5378	698.0	107,100	1297	39,470	.1128	3,831	138,700
8	12/ 9/64	0245	1420	67.2	1420	85,530	.2501	718.8	100,650	1421	34,440	.1007	3,838	130,200
9		1930	1395	88.8	1395	146,920	.4269	942.2	132,400	1395	32,030	.0931	5,014	168,500
10	12/10/64	0020	1267	90.2	1268	-56,080	-.1594	848.0	136,700	1273	47,410	.1349	4,701	176,500
11		0500	1198	89.4	1199	30,910	.0868	860.6	140,000	1199	19,560	.0549	4,537	175,300
12		1130	1292	109.6	1293	-58,610	-.1674	1075	170,700	1296	36,870	.1053	5,831	213,500
13		1715	1402	107.2	1402	110,750	.3222	1137	163,400	1403	30,280	.0881	6,067	207,400
14		2200	1400	120.1	1400	361,720	1.0519	1273	184,600	1401	34,390	.1000	6,791	233,800
15	12/11/64	0220	1342	121.0	1342	-1,064,680	-3.0661	1226	187,500	1345	32,770	.0944	6,624	236,700
16		1030	1263	107.6	1265	-41,790	-.1188	1021	173,900	1269	35,610	.1013	5,616	217,400
17		1540	1250	74.7	1252	-45,690	-.1295	681.2	118,900	1257	47,920	.1360	3,839	153,200
18		1645	1238	61.4	1239	-88,320	-.2498	562.2	98,760	1243	58,170	.1647	3,140	128,600
19		1815	1230	48.1	1231	-59,980	-.1694	440.9	78,830	1234	102,860	.2907	2,450	102,300
20		1920	1228	38.7	1228	-87,680	-.2475	360.6	64,950	1231	90,490	.2556	1,976	83,410
21		2020	1228	32.0	1229	-158,150	-.4465	304.6	54,890	1231	108,700	.3070	1,643	69,780
22		2100	1215	28.8	1214	-96,750	-.2725	272.1	50,650	1216	187,160	.5272	1,468	64,250
23	12/12/64	1430	1412	145.2	1413	-891,400	-2.6018	1527	225,800	1417	27,520	.0804	8,246	286,800
24		1100	1432	139.4	1433	64,660	.1902	1489	218,100	1435	38,680	.1136	7,995	278,100

TABLE 7

CONDENSING HEAT TRANSFER DATA FROM TEST SET NO. 3

(3/8-inch ID Tube without Insert)

Run No.	Date	Time	T_{KI} °F	W_K lbs/hr.	Top Station, $\ell/D_1 = 21$, $X \approx 0.80$					Bottom Station, $\ell/D_1 = 45$, $X \approx 0.25$				
					T_K °F	h_c Btu/hr-ft²-°F	N_{Nuc} --	N_{Ref} --	q_1'' Btu/hr-ft²	T_K °F	h_c Btu/hr-ft -°F	N_{Nuc} --	N_{Ref} --	q_1'' Btu/hr-ft²
1	1/10/65	1200	1190	22.1	1192	4,410	.0124	457.9	56,320	1195	28,460	.0799	1,854	80,350
2*		1500	1193	27.2	1193	2,060	.0058	640.9	63,920	1193	13,520	.0379	2,357	103,900
3		1800	1243	24.5	1245	12,900	.0365	512.2	67,200	1248	58,700	.1663	2,104	83,810
4		2000	1303	24.8	1304	75,420	.2158	565.2	71,090	1306	81,340	.2328	2,236	79,840
5	1/11/65	0230	1398	26.4	1398	-171,840	-.4996	666.1	77,880	1399	41,790	.1215	2,531	80,930
6		0900	1245	32.7	1247	7,610	.0215	685.8	84,840	1252	43,330	.1228	2,816	114,000
7*		1530	1214	32.4	1209	1,330	.0037	823.7	76,040	1197	7,380	.0207	2,868	124,600
8*		2045	1254	40.7	1237	1,330	.0038	796.7	116,460	1198	3,130	.0088	3,378	135,100
9	1/12/65	0200	1302	40.4	1305	19,750	.0565	887.5	109,660	1309	58,290	.1669	3,610	135,100
10		0430	1394	45.3	1395	419,550	1.2190	1108	128,000	1397	62,550	.1818	4,306	143,800
11		0800	1405	61.0	1407	-345,960	-1.0079	1492	172,900	1410	49,550	.1445	5,830	194,600
12		1445	1307	48.1	1310	17,290	.0495	1070	130,950	1315	49,930	.1431	4,326	163,100
13		1630	1310	55.3	1311	9,530	.0273	1316	150,500	1314	23,890	.0685	5,063	187,200
14*		2030	1320	64.3	1301	2,550	.0073	1539	202,300	1254	3,960	.0112	5,720	198,900
15	1/13/65	0240	1414	76.9	1415	-683,670	1.9966	1910	218,700	1418	40,040	.0117	7,402	244,900
16*		0445	1415	99.4	1412	11,590	.0338	2664	276,700	1405	18,490	.0538	9,722	316,200
17		1600	1361	65.5	1363	67,710	.1957	1565	184,100	1366	38,700	.1119	6,122	211,300
18		2000	1358	47.5	1360	128,160	.3702	1113	132,800	1363	71,170	.2057	4,410	153,900
19		2245	1357	30.6	1357	-502,450	-1.4506	741.9	87,310	1359	57,670	.1665	2,866	95,730
20	1/14/65	0030	1304	31.4	1305	42,740	.1223	708.0	86,360	1308	63,980	.1831	2,826	101,100
21		0440	1299	18.1	1299	314,440	.8988	432.7	51,530	1299	51,730	.1479	1,645	54,900
22		0630	1259	20.5	1260	37,290	.1058	450.4	58,110	1261	55,670	.1581	1,798	66,850
23		0730	1250	14.7	1250	116,470	.3301	327.6	41,760	1252	51,400	.1457	1,287	44,850
24		0900	1198	15.1	1198	16,890	.0474	309.0	41,420	1200	39,690	.1115	1,265	48,980
25		1300	1206	18.3	1207	13,740	.0386	368.4	50,300	1209	46,230	.1301	1,534	62,380
26		1430	1152	16.2	1153	5,640	.0158	303.3	42,060	1157	23,200	.0649	1,301	57,880
27		1715	1143	10.6	1143	9,330	.0261	229.4	28,990	1143	25,460	.0711	875.5	33,320
28		1930	1186	18.4	1186	7,700	.0216	373.3	48,700	1190	32,620	.0915	1,532	63,150
29		2130	1235	28.1	1237	7,650	.0216	601.0	75,480	1241	37,880	.1072	2,426	99,850
30	1/15/65	0830	1295	50.3	1296	8,190	.0234	1169	134,330	1300	32,420	.0927	4,544	174,530

* Data calculation not valid for Runs No. 2, 7, 8, 14 and 16 due to subcooled liquid at potassium outlet

TABLE 8

TWO-PHASE FRICTION PRESSURE DROP MULTIPLIERS OBTAINED FROM TEST SET NO. 4 DATA
(5/8-inch ID Tube With Instrumented Helical Insert, $p/D_i = 6$)

Run No.(1)	T_{KI} °F	T_{KO} °F	W_K lbs/hr.	V_I ft/sec.	(P_I-P_O) psi	ϕ_{1-0}(2)	ϕ_ℓ(3) Top Station	ϕ_ℓ(3) Bottom Station
1	1182.8	1179.1	23.3	380	.105	1319	1854	873
2	1247.1	1245.1	21.0	234	.078	954	1379	639
3	1155.6	1145.9	40.6	783	.231	1622	2124	1268
4	1221.8	1216.1	38.8	501	.208	1156	1625	1026
5	1295.8	1292.4	35.8	306	.168	823	1359	835
6	1399.6	1398.4	29.6	150	.091	510	559	346
7	1391.7	1390.4	46.7	246	.099	466	543	347
8	1282.4	1278.6	53.4	490	.177	811	1025	662
9	1207.7	1198.2	57.9	812	.300	1258	1580	1012
10	1109.9	1067.2	54.5	1418	.705	2462	3544	2018
11	1146.9	1128.8	50.0	1020	.401	1832	2552	1461
12	1203.0	1195.4	47.5	684	.234	1256	1682	1007
13	1211.3	1200.9	57.0	783	.334	1259	1654	1011
14	1207.0	1182.3	61.8	870	.746	1518	2153	1135
15	1260.0	1235.5	69.8	725	.967	1275	1807	895
16	1295.8	1283.3	69.4	593	.618	965	1297	694
17	1407.6	1405.1	61.5	300	.198	485	607	384
18	1405.4	1401.1	83.1	410	.341	520	625	431
19	1301.0	1269.6	87.3	725	1.49	1164	1674	799
20	1255.5	1199.9	87.6	933	2.00	1522	2303	1082
21	1212.5	1058.0	89.9	1225	3.45	2196	3697	2144
22	1267.0	1140.1	107.5	1074	4.07	1778	2889	1535
23	1306.5	1249.0	104	839	2.63	1317	2066	931
24	1405.2	1380.5	107.5	531	1.87	837	1205	545
25	1401.3	1370.0	121	608	2.30	859	1216	556
26	1310.3	1218.4	121	957	3.96	1425	2275	1111
27	1321.0	1166.9	142	1063	6.08	1529	2358	1393
28	1407	1364.9	131.5	644	3.10	923	1328	623
29	1395.5	1323.7	144.6	747	4.74	1102	1620	725
30	1142.4	1130.9	34.8	731	.253	1807	2570	1443
31	1110.4	1091.2	37.7	978	.362	2272	3370	1836
32	1093.2	1081.8	21.4	624	.187	2426	3684	1694
33	1152.5	1147.0	18.8	369	.130	1736	2665	1150

(1) Operating conditions for each run are given in Table 2
(2) ϕ_{1-0} calculated from data using Equation (14)
(3) ϕ_ℓ calculated from data using Equation (19)

TABLE 9

TWO-PHASE FRICTION PRESSURE DROP MULTIPLIERS OBTAINED FROM TEST SET NO. 5 DATA
(5/8-inch ID Tube with Instrumented 1/4-inch OD Tubular Insert)

Run No.(1)	T_{KI} °F	T_{KO} °F	W_K lbs/hr.	V_I ft/sec.	(P_O-P_I) psi	ϕ_{l-o}(2)	ϕ_l(3) Top Station	ϕ_l(3) Bottom Station
1	1106.2	1109.1	23.0	585	.053	2419	2821	2262
2	1143.1	1144.8	22.7	453	.039	1896	2118	1742
3	1194.7	1195.2	20.3	294	.015	1391	1539	1315
4	1257.4	1257.4	18.9	190	0	1025	1231	945
5	1252.7	1253.3	34.5	356	.033	1125	1608	1494
6	1200.8	1203.6	36.1	503	.088	1433	1778	1764
7	1142.3	1151.2	38.4	710	.206	1939	2108	2044
8	1112.6	1122.0	38.1	928	.184	2513	2979	2516
9	1112.7	1128.5	44.7	1089	.316	2494	3207	2578
10	1149.4	1160.9	43.9	841	.280	1871	2228	2024
11	1197.2	1204.2	44.2	630	.219	1376	1548	1500
12	1301.3	1303.4	42.7	338	.109	763	755	795
13	1404.4	1404.9	41.0	194	.040	492	515	397
14	1402.4	1402.8	45.8	219	.032	544	622	461
15	1307.1	1309.9	51.1	392	.145	783	837	820
16	1238.8	1245.5	53.0	592	.259	1108	1180	1221
17	1206.1	1215.4	53.9	728	.305	1374	1472	1506
18	1186.8	1205.9	69.1	1048	.582	1627	1814	1691
19	1250.0	1260.0	69.8	731	.410	1124	1169	1201
20	1295.2	1301.0	69.6	569	.289	899	878	954
21	1393.8	1395.1	65.0	323	.099	587	609	574
22	1400.4	1401.3	82.3	396	.071	656	741	561
23	1302.4	1308.1	87.0	685	.295	997	1278	834
24	1296.0	1301.5	86.9	707	.276	1049	1258	902
25	1256.2	1267.2	87.3	883	.465	1238	1840	959
26	1211.3	1209.2	86.0	1126	-.069	1999	4154	1191
27	1260.4	1274.4	105.0	1038	.611	1286	1708	1139
28	1312.0	1311.8	107.2	802	-.011	1190	2626	3395
29	1413.2	1413.7	102.7	466	.041	680	906	646
30	1410.5	1416.0	121.3	557	.454	588	935	362
31	1309.8	1320.8	123.1	931	.598	1036	2233	572
32	1312.0	1308.0	138.0	1011	-.429	1338	3790	179
33	1296.5	1278.7	131.0	1064	-.853	1589	4149	263
34	1264.0	1119.1	126.6	1226	-.438	2950	5946	2000
35	1198.0	1074.3	108.3	1535	-2.75	3369	6431	3007
36	1167.0	884.4	96.7	1657	-3.48	4380	10,747	6703
37	1162.3	1182.0	68.8	1214	.527	2024	1081	1778

(1) Operating Conditions for each run are given in Table 3
(2) ϕ_{l-o} calculated from data using Equation (14)
(3) ϕ_l calculated from data using Equation (19)

TABLE 10

TWO-PHASE FRICTION PRESSURE DROP MULTIPLIERS
OBTAINED FROM TEST SET NO. 1 DATA
(5/8-inch ID Tube Without Insert)

Run No. (1)	T_{KI} °F	T_{KO} °F	W_K lbs/hr	V_I ft/sec	(P_O-P_I) psi	ϕ_{1-0} (2)
Group A						
1	1153.4	1161.0	25.7	410	.176	1657
2	1170.0	1176.8	27.1	395	.176	1517
3	1175.3	1181.7	27.6	385	.169	1560
4	1180.7	1186.5	27.8	380	.158	1601
5	1175.5	1182.6	29.4	410	.188	1618
6	1173.2	1180.5	29.4	415	.191	1635
7	1169.4	1177.3	29.5	430	.202	1627
8	1169.7	1177.4	29.5	430	.199	1646
9	1174.5	1181.7	29.0	405	.189	1572
10	1178.5	1185.4	30.3	415	.187	1690
11	1181.7	1188.4	30.6	410	.183	1690
Group C						
1	1135.0	1148.5	33.2	600	.290	2306
2	1130.2	1143.6	32.1	595	.284	2330
3	1158.1	1165.8	26.3	410	.187	1518
4	1248.9	1250.6	22.9	205	.068	1052
5	1269.6	1274.6	39.7	315	.214	894
6	1238.6	1244.9	40	375	.234	1190
7	1214.3	1223.2	40.2	440	.292	1271
8	1311.4	1315.7	46.0	295	.228	734

(1) Operating conditions for each run are given in Table 5

(2) ϕ_{1-0} calculated from data using Equation (14)

TABLE 11

LIQUID POTASSIUM HEAT TRANSFER DATA*

	Bottom Station, $\ell/D_i = 19$				Top Station, $\ell/D_i = 38$		
Run No.	N_{Pe}	(T_K-T_{wi}) °F	$q_i, \frac{10^4 Btu}{hr\text{-}ft^2}$	N_{Nu}	(T_K-T_{wi}) °F	$q_i, \frac{10^4 Btu}{hr\text{-}ft^2}$	N_{Nu}
1	351	12.7	2.87	5.09	6.85	1.77	5.79
2	340	12.2	2.76	5.10	6.49	1.68	5.81
3	315	11.9	2.65	4.97	6.18	1.57	5.68
4	289	12.0	2.60	4.86	5.98	1.50	5.58
5	264	10.3	2.22	4.79	5.02	1.22	5.42
6	244	10.4	2.19	4.69	4.87	1.17	5.33
7	219	10.7	2.19	4.57	4.75	1.10	5.15
8	188	10.8	2.13	4.39	4.41	0.99	5.00
9	171	11.0	2.11	4.28	4.17	0.92	4.90
10	143	10.8	2.04	4.19	3.51	0.78	4.93
11	162	9.8	1.97	4.49	3.64	0.82	4.99
12	176	10.0	1.98	4.43	4.00	0.89	4.93
13	202	9.8	1.96	4.48	4.30	0.96	4.99
14	233	9.8	1.97	4.53	4.73	1.05	4.98
15	256	9.4	1.99	4.77	4.57	1.10	5.41
16	278	9.3	1.98	4.78	3.19	1.14	5.34
17	308	9.5	2.11	5.04	5.01	1.26	5.66
18	331	9.4	2.15	5.17	5.10	1.32	5.83
19	345	9.4	2.16	5.24	5.16	1.34	5.90
20	341	14.4	3.13	5.00	8.18	1.97	5.49
21	324	14.4	3.05	4.84	8.14	1.89	5.30
22	302	14.6	3.02	4.72	8.06	1.83	5.17
23	270	15.1	3.04	4.59	7.82	1.76	5.11
24	239	15.2	2.86	4.25	7.86	1.58	4.51
25	238	14.9	2.95	4.45	7.18	1.61	5.00
26	279	14.4	2.99	4.67	6.63	1.74	6.11
27	305	14.6	3.00	4.65	7.38	1.82	5.60
28	336	14.4	3.19	5.02	7.94	1.97	5.59
29	115	6.6	1.12	3.82	2.29	0.37	3.62
30	94	6.1	1.00	3.67	1.76	0.26	3.43
31	80	6.4	0.94	3.33	1.73	0.21	2.75

*Obtained with test section geometry of Test Set No. 1-B (Figure 7), 5/8-inch ID thick-wall nickel tube, potassium in vertical up-flow cooled by sodium in cocurrent flow.

TABLE 12

RESULTS FROM FLUX-PLOT ANALOGUE OF TEMPERATURE FIELD IN THICK-WALL NICKEL CONDENSER TUBE(1)

T/C Hole No.	Radius, inch	Calc'd. Potential(2)	Potential From Flux Plot Analogue(3)		
			Maximum	Minimum	Average
R_i	0.313	1000	1000	1000	1000
1	0.398	758	875	630	753
2	0.449	637	748	515	632
3	0.518	494	600	400	500
4	0.601	346	435	260	348
5	0.698	196	275	130	203

(1) Potentials are normalized to a value of 1,000 at the inner surface (radius R_i) corresponding to 10-volts in the analogue test.

(2) Calculation based on tube wall without thermocouple holes.

(3) See Figure 36.

REFERENCES

1. "Alkali Metals Boiling and Condensing Investigations", Quarterly Report 2-3, Contract NAS 3-2528, General Electric Company - SPPS, April 20, 1963

2. "Alkali Metals Boiling and Condensing Investigations", Quarterly Report 4, Contract NAS 3-2528, General Electric Company - SPPS, July 25, 1963.

3. "Alkali Metals Boiling and Condensing Investigations", Quarterly Report 5, Contract NAS 3-2528, General Electric Company - SPPS, January 6, 1964.

4. "Alkali Metals Boiling and Condensing Investigations", Quarterly Report 6, Contract NAS 3-2528, General Electric Company - SPPS, April 20, 1964, NASA-CR-54037.

5. "Alkali Metals Boiling and Condensing Investigations", Quarterly Report 7, Contract NAS 3-2528, General Electric Company - SPPS, April 20, 1964, NASA-CR-54038.

6. "Alkali Metals Boiling and Condensing Investigations", Quarterly Report 8, Contract NAS 3-2528, General Electric Company - SPPS, July 20, 1964, NASA-CR-54138.

7. "Alkali Metals Boiling and Condensing Investigations", Quarterly Report 9, Contract NAS 3-2528, General Electric Company - SPPS, October 20, 1964, NASA-CR-54215.

8. "Alkali Metals Boiling and Condensing Investigations", Quarterly Report 10, Contract NAS 3-2528, General Electric Company - SPPS, January 20, 1965, NASA-CR-54308.

9. "Alkali Metals Boiling and Condensing Investigations", Quarterly Report 11, Contract NAS 3-2528, General Electric Company - SPPS, April 20, 1965, NASA-CR-54405.

10. "Alkali Metals Boiling and Condensing Investigations", Quarterly Report 12, Contract NAS 3-2528, General Electric Company - SPPS, July 23, 1965, NASA-CR-54739.

11. "Alkali Metals Boiling and Condensing Investigations", Quarterly Report 13, Contract NAS 3-2528, General Electric Company - SPPS, October 20, 1965, NASA-CR-54890.

12. McAdams, W.H., Heat Transmission, 3rd Edition, McGraw Hill Inc., New York, New York, 1954.

13. Misra, B., and Bonilla, C.F., "Heat Transfer in the Condensation of Metal Vapors: Mercury and Sodium Up to Atmospheric Pressure", Chem. Eng. Prog., Symposium Series, Vol. 52, No. 18, July 1965.

14. Gel'man, L.I., "Heat Exchange by Drop Condensation of Mercury Vapor", Teploenergetika, Vol. 5, No. 3, 1958 pp. 47-50.

15. Cohn, P.D., "Heat Transfer Coefficients for Condensation of Liquid Metal Vapors Inside a Vertical Tube", MSc Thesis, Dept. of Chem. Eng., Oregon State College, July 1959.

16. Sukhatme, S.P., and Rohsenow, W.M., "Heat Transfer During Film Condensation of a Liquid Metal Vapor", Technical Report No. 9167-27, Dept. of Mech. Eng., MIT, April 1964.

17. Roth, J.A., "Experimental Determination of Overall Heat Transfer Coefficients for Condensing Sodium (1140°F to 1840°F)", Proceedings of 1962 High Temperature Liquid-Metal Heat Transfer Technology Meeting, Brookhaven National Laboratory, May 1962, pp. 276-285.

18. Roth, J.A., "Condensation of Sodium and Rubidium at Low Heat Fluxes", Report No. ASD-TDR-62-738, October 1962.

19. Engelbrecht, J.C., "Heat Transfer Coefficients in the Boiling and Condensation of Liquid Metals: Potassium and Rubidium", MSc. Thesis, Dept. of Chem. Eng., Columbia University, October 1961.

20. Brooks, R.D., and Sawochka, S.G., "Alkali Metal Two-Phase Heat Transfer for Space Power: Present Status", Progress in Astronautics and Aeronautics, Vol. 11, Academic Press, 1963.

21. Seban, R.A., "Remarks on Film Condensation with Turbulent Flow", Trans. ASME, Vol. 76, 1954, p. 299.

22. Rohsenow, W.M., "Heat Transfer and Temperature Distribution in Laminar Film Condensation", Trans. ASME, Vol. 78, pp. 1645-1648, 1956.

23. Rohsenow, W.M., Weber, J.H., and Ling, A.J., "Effect of Vapor Velocity of Laminar and Turbulent Film Condensation", Trans. ASME, Vol. 78, pp. 1637-1643, 1956.

24. Sparrow, E.M., and Gregg, J.L., "Laminar Condensation Heat Transfer on a Horizontal Cylinder", Trans. ASME, Series C, J. Heat Trans., Vol. 81, No. 4, pp. 291-296, November 1959.

25. Koh, J.C.Y., Sparrow, E.M., and Hartnett, J.P., "The Two-Phase Boundary Layer in Laminar Film Condensation", Int. J. Heat Mass Trans. Vol. 2, pp. 69-82, 1961.

26. Chen, M.M., "An Analytical Study of Laminar Film Condensation: Part I - Flat Plates, and Part 2 - Single and Multiple Horizontal Tubes", Trans. ASME, Series C., J. Heat Trans., Vol. 83, No. 1, pp. 48-54 and pp. 55-60, February, 1961.

27. Lee, Jon, "Turbulent Film Condensation", AIChE Journal, pp. 540-544, July 19, 1964, Vol. 10, No. 4.

28. Dukler, A.E., "Fluid Mechanics and Heat Transfer in Vertical Falling-Film Systems", Chem. Eng. Prog. Symposium Series, No. 30, Vol. 56, 1960.

29. Koh, J.C.Y., "Film Condensation in Forced Convection Boundary Layer Flow", Int. J. Heat Mass Trans., Vol. 5, pp. 941-954, 1962.

30. Wilhelm, D.J., "Condensation of Metal Vapors: Mercury and the Kinetic Theory of Condensation", ANL-6948, October 1964.

31. Martinelli, R.C. and Nelson, D.B., "Prediction of Pressure Drop During Forced-Circulated Boiling of Water", Trans. ASME, pp. 695-702, August 1948.

32. Schrage, R.W., A Theoretical Study of Interphase Mass Transfer, Columbia University Press, New York, 1953.

33. Dukler, A.E., "Comparison of Theoretical and Experimental Film Thickness", Jour. Amer. Rocket Soc., Vol. 31, No. 1, pp. 86-87, January 1961.

34. Wilkes, J.O., and Nedderman, R.M., "The Measurement of Velocities in Thin Films of Liquid", Chem. Eng. Sci., Vol. 17, pp. 177-187, 1962.

35. Portalske, S., "Studies of Falling Liquid Film Flow; Film Thickness on a Smooth Vertical Plate", Chem. Eng. Sci., Vol. 18, pp. 787-804, 1963.

36. Jeans, J., "An Introduction to the Kinetic Theory of Gases", Cambridge University Press, 1940.

37. Jamieson, D.T., "Condensation Coefficient of Water", Advances In Thermophysical Properties at Extreme Temperatures and Pressures, ASME, 1965, pp. 230-236.

38. Sawochka, S.G., "Heat Transfer During the Condensation of Potassium", Ph.D. Thesis, Department of Chemical Engineering, University of Cincinnati, 1965.

39. Fauske, H.F., "Contribution to the Theory of Two-Phase, One-Component Critical Flow", ANL-6633, October 1962.

40. Dwyer, O.E., and P.S. Tu, "Analytical Study of Heat Transfer Rates for Parallel Flow of Liquid Metals Through Tube Bundles", Chemical Engineering Progress Symposium Series, Vol. 56, No. 30, 1960.

41. Borishanskiy, V.M., and Fursova, E.V., "Heat Transfer in Longitudinal Flow of Sodium Through a Bank of Tubes", Atomnoya Energiya, Vol. 14, No. 6, 1963, p. 584.

42. Gutierrez, O.A., Sekas, N.J., Acker, L.W., Fenn, D.B., "Potassium Condensing Tests of Horizontal Convection and Radiative Multitube Condensers Operating at 1250°F to 1500°F", Presented at AIAA Rankine Cycle Specialist's Conference, October 1965.

43. Deissler, R.G., "Analytical and Experimental Investigation of Adiabatic Turbulent Flow in Smooth Tubes", NACA Technical Note 2138, 1950.

44. Von Karman, T., "The Analogy Between Fluid Friction and Heat Transfer", Trans. ASME, Vol. 61, 1939, pp. 705-710.

45. Carpenter, E.F., and Coburn, A.P., "The Effect of Vapor Velocity on Condensation Inside Tubes", General Discussion on Heat Transfer, London, England, Sept. 11-13, 1951, U.S. Section 1.

46. Sawochka, S.G., and Schleef, D.J., "Liquid Heat Transfer Coefficients for Potassium During Vertical Upflow Inside a Tube", Paper No. 64-WA/HT-19, ASME, 1964.

47. Lubarsky, B., and Kaufman, S.J., "Review of Experimental Investigations of Liquid-Metal Heat Transfer", Report 1270, NASA, 1956

48. Kutateladze, S.S., et al., "Liquid-Metal Heat Transfer Media", Consultants Bureau, Inc., New York, New York, 1959, pp. 23-28.

49. Martinelli, R.C., "Heat Transfer to Molten Metals", Trans. ASME, Vol. 69, 1947, pp. 947-959.

50. Seban, R.A., and Shimazaki, T.T., "Heat Transfer to a Fluid Flowing Turbulently in a Smooth Pipe with Walls at Constant Temperature", Trans. ASME, Vol. 73, 1951, pp. 803-809.

51. Isakoff, S.E., and Drew, T.B., "Heat and Momentum Transfer in Turbulent Flow of Mercury", General Discussions on Heat Transfer, London, September 1961, ASME-IME, 1952, pp. 405-409.

52. Subbotin, V.I., et al., "Turbulent Heat Transfer in a Flow of Liquid Metals", Int. J. Heat Mass Transfer, Vol. 4, 1961 pp. 79-87.

53. Schmidt, E.H.W., and Jung, E., "Measurements of the Thermal Contact Resistance from Stainless Steel to Liquid Sodium", Modern Developments in Heat Transfer, Academic Press, New York, New York, 1963.

54. Pirogov, M.S., "Heat Transfer to Sodium in the Region of Small Peclet Numbers", Teploenergetika, No. 3, 1961, pp. 62-64.

55. Lyon, R.N., "Liquid Metal Heat Transfer Coefficients", Chem. Eng. Prog. Vol. 47, 1951, pp. 75-79.

56. Trefethen, L., "Measurement of Mean Fluid Temperatures", Trans. ASME, Vol. 78, 1956, pp. 1207-1212

57. Hall, W.B., and Jenkins, A.E., "Heat Transfer Experiments with Sodium and Sodium Potassium Alloy", J. Nuclear Energy, Vol. 1, 1955, pp. 244-263.

58. Johnson, H.A., Hartnett, J.P., and Clabaugh, W.J., "Heat Transfer to Lead-Bismuth and Mercury in Laminar and Transition Pipe Flow", Paper No. 53-A-188, ASME, 1953.

59. Johnson, H.A., Clabaugh, W.J., and Hartnett, J.P., "Heat Transfer to Mercury in Turbulent Pipe Flow", Paper No. 53-A-189, ASME, 1953.

60. Lubarsky, B., "Experimental Investigations of Forced Convection Heat-Transfer Characteristics of Lead-Bismuth Eutectic", RM E51G02, NASA, 1951

61. Rohsenow, W.M., and Choi, H.Y., "Heat, Mass, and Momentum Transfer," Prentice-Hall, Inc., Englewood Cliffs, New Jersey, 1961.

62. Stein, R.P., "Heat Transfer Coefficients in Liquid Metal Co-current Flow Double Pipe Heat Exchangers", Presented at the Third Annual High-Temperature Liquid-Metal Heat Transfer Technology Conference, September 4-6, 1963, Oak Ridge National Laboratory.

63. Dwyer, O.E., and Tu, P.S., "Unilateral Heat Transfer to Liquid Metals Flowing in Annuli", Nuclear Science and Engineering, Vol. 15, 1963, pp. 58-68.

64. Martinelli, R.C., et al., "Heat Transfer and Pressure Drop for Fluid Flowing in Viscous Region Through Vertical Pipes", Trans. AIChE, Vol. 38, No. 3, 1942, pp. 493-530.

65. Kokorev, L.S., and Ryapsov, V.N., "Turbulent Heat Transfer During the Flow of a Heating Medium of Small Prandtl Number Along a Tube", International Chemical Engineering, Vol. 2, 1962, pp. 514-519.

66. "Properties of Inorganic Energy - Conversion and Heat Transfer Fluids for Space Applications", WADD Technical Report 61-96, November 1961.

67. Jackson, C.B., "Liquid-Metals Handbook (Sodium-NaK Supplement), AEC Third Edition, 1955.

68. Lemmon, A.W., Deem, H.W., Hall, E.H., and Walling, J.R., "The Thermodynamic and Transport Properties of Potassium", Battelle Memorial Institute, Presented at ORNL, Liquid Metals Conference, September 1963.

69. Ewing, C.T., et al., "High Temperature Properties of Sodium and Potassium", Report 6094, USNRL, February 1964.

70. Beers, Y., "Introduction to the Theory of Error" Addison-Wesley Inc., Reading, Mass., 1957.

71. Tippets, F.E., Peterson, J.R., and Sawochka, S.G., "Potassium Multiple-Tube Test Condenser Design Study", Topical Report, Contract NAS 3-2528, General Electric Company - SPPS. 1966, NASA-CR-72137.

DISTRIBUTION FOR TOPICAL REPORTS
CONTRACT NAS 3-2528

NASA
Washington, D.C. 20546
ATTN: William H. Woodward (RN)

NASA
Washington, D.C. 20546
ATTN: Dr. Fred Schulman (RN)

NASA
Washington, D.C. 20546
ATTN: J. J. Lynch (RNP)

NASA
Washington, D.C. 20546
ATTN: S. V. Manson (RNP)

NASA
Washington, D.C. 20546
ATTN: George C. Deutsch (RR)

NASA
Goddard Space Flight Center
Greenbelt, Maryland 20771
ATTN: Librarian

NASA
Langley Research Center
Hampton, Virginia 23365
ATTN: Librarian

NASA
Lewis Research Center
21000 Brookpark Road
Cleveland, Ohio 44135
ATTN: Librarian M.S. 3-7

NASA
Lewis Research Center
21000 Brookpark Road
Cleveland, Ohio 44135
ATTN: Dr. Bernard Lubarsky M.S. 500-201

NASA
Lewis Research Center
21000 Brookpark Road
Cleveland, Ohio 44135
ATTN: Seymour Lieblein M.S. 7-1

NASA
Lewis Research Center
21000 Brookpark Road
Cleveland, Ohio 44135
ATTN: Solomon Weiss M.S. 54-1

NASA
Lewis Research Center
21000 Brookpark Road
Cleveland, Ohio 44135
ATTN: Warren H. Lowdermilk M.S. 106-1

NASA
Lewis Research Center
21000 Brookpark Road
Cleveland, Ohio 44135
ATTN: Dr. Louis Rosenblum M.S. 106-1

NASA
Lewis Research Center
21000 Brookpark Road
Cleveland, Ohio 44135
ATTN: Robert Siegel M.S. 49-2

NASA
Lewis Research Center
21000 Brookpark Road
Cleveland, Ohio 44135
ATTN: Robert Y. Wong M.S. 5-9

NASA
Manned Spacecraft Center
Houston, Texas 77001
ATTN: Librarian

NASA
George C. Marshall Space Flight Center
Huntsville, Alabama 35812
ATTN: Librarian

NASA
George C. Marshall Space Flight Center
Huntsville, Alabama 35812
ATTN: Ernst Stuhlinger

Contract NAS 3-2528

NASA
George C. Marshall Space Flight Center
Huntsville, Alabama 35812
ATTN: Russell H. Shelton

NASA
Lewis Research Center
21000 Brookpark Road
Cleveland, Ohio 44135
ATTN: I. I. Pinkel M.S. 86-5

NASA
Lewis Research Center
21000 Brookpark Road
Cleveland, Ohio 44135
ATTN: J. E. Dilley (500-309)

NASA
Lewis Research Center
21000 Brookpark Road
Cleveland, Ohio 44135
ATTN: Patent Counsel M.S. 77-1

NASA
Lewis Research Center
21000 Brookpark Road
Cleveland, Ohio 44135
ATTN: Harold J. Christenson M.S. 5-3

NASA
Lewis Research Center
21000 Brookpark Road
Cleveland, Ohio 44135
ATTN: Robert G. Dorsch M.S. 11-1

NASA
Lewis Research Center
21000 Brookpark Road
Cleveland, Ohio 44135
ATTN: Robert E. English M.S. 86-1

NASA
Lewis Research Center
21000 Brookpark Road
Cleveland, Ohio 44135
ATTN: James P. Lewis M.S. 11-1

NASA
Jet Propulsion Laboratory
4800 Oak Grove Drive
Pasadena, California 91103
ATTN: D. R. Bartz

NASA
Westerns Operations Office
150 Pico Boulevard
Santa Monica, California 90406
ATTN: John Keeler

NASA
Lewis Research Center
21000 Brookpark Road
Cleveland, Ohio 44135
ATTN: Daniel Bernatowicz M.S. 100-1

NASA
Lewis Research Center
21000 Brookpark Road
Cleveland, Ohio 44135
ATTN: Ruth N. Weltmann M.S. 500-201 (6)

NASA
Lewis Research Center
21000 Brookpark Road
Cleveland, Ohio 44135
ATTN: H. G. Hurrell M.S. 100-1

NASA
Jet Propulsion Laboratory
4800 Oak Grove Drive
Pasadena, California 91103
ATTN: Librarian

NASA
Lewis Research Center
21000 Brookpark Road
Cleveland, Ohio 44135
ATTN: D. Namkoong M.S. 86-1

NASA
Lewis Research Center
21000 Brookpark Road
Cleveland, Ohio 44135
ATTN: L. Gertsma M.S. 86-1

Contract NAS 3-2528

NASA
Lewis Research Center
21000 Brookpark Road
Cleveland, Ohio 44135
ATTN: Robert L. Cummings M.S. 500-309

NASA
Lewis Research Center
21000 Brookpark Road
Cleveland, Ohio 44135
ATTN: U. H. Von Glahn

NASA
Lewis Research Center
21000 Brookpark Road
Cleveland, Ohio 44135
ATTN: N. D. Sanders

NASA
Lewis Research Center
21000 Brookpark Road
Cleveland, Ohio 44135
ATTN: V. H. Gray

NASA
Lewis Research Center
21000 Brookpark Road
Cleveland, Ohio 44135
ATTN: E. R. Furman

NASA
Lewis Research Center
21000 Brookpark Road
Cleveland, Ohio 44135
ATTN: M. U. Gutstein

Air Force Systems Command
Aeronauticsl Systems Division
Wright-Patterson Air Force Base, Ohio 45433
ATTN: R. J. Benzing (ASRCNL)

Air Force Systems Command
Aeronautical Systems Division
Wright-Patterson Air Force Base, Ohio 45433
ATTN: Bernard Chasman (ASRCEA)

Air Force Systems Command
Aeronautical Systems Division
Wright Patterson Air Force Base, Ohio 45433
ATTN: George E. Thompson (ASRMFP-1)

U.S. Atomic Energy Commission
Technical Reports Library
Washington, D.C. 20545
ATTN: J. M. O'Leary (2)

U.S. Atomic Energy Commission
Washington, D.C. 20545
ATTN: R. M. Scroggins

U.S. Atomic Energy Commission
Reactor Experiment Branch
Washington, D.C. 20545
ATTN: T. W. McIntosh

Argonne National Laboratory
Library Services, Dept. 203-CE125
9700 South Cass Avenue
Argonne, Illinois 60439
ATTN: Report Section

Argonne National Laboratory
9700 South Cass Avenue
Argonne, Illinois 60440
ATTN: John F. Marchaterre

Brookhaven National Laboratory
Upton, Long Island, New York 11973
ATTN: Librarian

Oak Ridge National Laboratory
Oak Ridge, Tennessee 37831
ATTN: Herbert W. Hoffman

Oak Ridge National Laboratory
Oak Ridge, Tennessee 37831
ATTN: W. D. Manly

U.S. Naval Research Laboratory
Washington, D.C. 20390
ATTN: C. T. Ewing

Contract NAS 3-2528

Columbia University
Department of Chemical Engineering
New York, New York 10027
ATTN: Dr. Charles F. Bonilla

Massachusetts Institute of Technology
Cambridge, Massachusetts 02139
ATTN: Dr. Warren M. Rohsenow

University of Michigan
Department of Chemical and
Metallurgical Engineering
Ann Arbor, Michigan 48103
ATTN: Dr. Richard E. Balzhiser

Southern Methodist University
Engineering School
Dallas, Texas 75222
ATTN: Dr. Harold A. Blum

University of Wisconsin
Madison, Wisconsin 53706
ATTN: Dr. Max W. Carbon

Advanced Technology Laboratories
Division of American Standard
369 Whisman Road
Mountain View, California 94040
ATTN: Library

Aerojet-General Corporation
P.O. Box 296
Azusa, California 91702
ATTN: Librarian (2)

Aerojet-General Nucleonics
P.O. Box 77
San Ramon, California 94583
ATTN: Librarian (2)

Aerojet-General Nucleonics
P.O. Box 77
San Ramon, California 94583
ATTN: Mr. Ken Johnson

AiResearch Manufacturing Company
Sky Harbor Airport
402 South 36th Street
Phoenix, Arizona 85009
ATTN: Librarian (2)

AiResearch Manufacturing Company
Sky Harbor Airport
402 South 36th Street
Phoenix, Arizona 85009
ATTN: E. A. Kovacevich

AiResearch Manufacturing Company
9851-9951 Sepulveda Blvd.
Los Angeles, California 90045
ATTN: Librarian

AiResearch Manufacturing Company
9851-9951 Sepulveda Blvd.
Los Angeles, California 90045
ATTN: James J. Killackey

Atomics International
8900 DeSoto Avenue
Canoga Park, California 91303
ATTN: Louis Bernath

Avco
Research & Advanced Development Department
201 Lowell Street
Wilmington, Massachusetts 01800
Attn: Librarian

Babcock and Wilcox Company
Research Center
Alliance, Ohio
ATTN: W. Markert, Jr.

Battelle Memorial Institute
505 King Avenue
Columbus, Ohio 43201
ATTN: Alexis W. Lemmon, Jr.

Contract NAS 3-2528

Curtiss-Wright Corporation
Wright Aero Division
Wood Ridge, New Jersey 07075
ATTN: S. Lombardo

Electro-Optical Systems, Inc.
Advanced Power Systems Division
Pasadena, California
ATTN: Joseph Neustein

General Motors Corporation
Allison Division
Indianapolis, Indiana 46206
Attn: Librarian

Geoscience Ltd.
8686 Dunaway Drive
La Jolla, California 92037
ATTN: H. F. Poppendiek

Hughes Aircraft Company
Engineering Division
Culver City, California 90230
ATTN: Tom B. Carvey, Jr.

Southwest Research Institute
8500 Culebra Road
San Antonio, Texas 78206
ATTN: Dr. W. D. Weatherford, Jr.

Marquardt Aircraft Company
P.O. Box 2013
Van Nuys, California
ATTN: Librarian

Materials Research Corporation
Orangeburg, New York
ATTN: Vernon E. Adler

The Martin Company
Nuclear Division
P.O. Box 5042
Baltimore, Maryland 21220
ATTN: Librarian

MSA Research Corporation
Callery, Pennsylvania 16024
ATTN: Frederick Tepper

Plasmadyne Corporation
3839 South Main Street
Santa Anna, California
ATTN: Librarian

Pratt & Whitney Aircraft
400 Main Street
East Hartford, Connecticut 06108
ATTN: Librarian (2)

Pratt & Whitney Aircraft
400 Main Street
East Hartford, Connecticut 06108
ATTN: Richard Curry

Pratt & Whitney
400 Main Street
East Hartford, Connecticut 06108
ATTN: Eugene Szetela

Rocketdyne
Canoga Park, California 91303
ATTN: Librarian

Sunstrand Denver
2480 West 70th Street
Denver, Colorado 80221
ATTN: Librarian

Thompson-Ramo-Wooldridge, Inc.
New Devices Laboratories
7209 Platt Avenue
Cleveland, Ohio 44115
ATTN: Librarian

Thompson-Ramo-Wooldridge, Inc.
New Devices Laboratories
7209 Platt Avenue
Cleveland, Ohio 44115
ATTN: A. Ziobro

Union Carbide Nuclear Company
P.O. Box X
Oak Ridge, Tennessee 37831
ATTN: X-10 Laboratory Records
Department (2)

Contract NAS 3-2528

United Nuclear Corporation
Development Division
5 New Street
White Plains, New York
ATTN: Librarian

Westinghouse Electric Corporation
Astronuclear Laboratory
P.O. Box 10864
Pittsburgh, Pennsylvania 15236
ATTN: Librarian

Westinghouse Electric Corporation
Aero-Space Department
Lima, Ohio 45801
ATTN: Librarian

California Institute of Technology
Jet Propulsion Laboratory
4800 Oak Grove Drive
Pasadena, California 91103
ATTN: Mr. Gerald M. Kikin

General Electric Company
3325 Wilshire Blvd.
Los Angeles, California 90005
ATTN: A. L. Clarkson

Research Institute of Temple University
4150 Henry Avenue
Philadelphia, Pennsylvania 19144
ATTN: A. V. Grosse

Professor W. E. Hilding
Department of Mechanical Engineering
University of Connecticut
Storrs, Connecticut 06268

Reactor Engineering Argonne Materials
Laboratory
Argonne, Illinois 60440
ATTN: Ralph P. Stein

Knolls Atomic Power Laboratory
P.O. Box 1072
Schenectady, New York 12301
ATTN: Document Librarian

General Electric Company
P.O. Box 100
Richland, Washington 99352
ATTN: Technical Information Operation
Dr. T. T. Claudson

Professor George A. Brown
Engineering Projects Laboratory
Massachusetts Institute of Technology
Research Laboratory of Electronics
Cambridge, Massachusetts 02139

General Dynamics Corporation
General Atomic Division
P.O. Box 608
San Diego, California 92112
ATTN: Library (2)

Mr. Rudolph Rust
Jet Propulsion Laboratory
4800 Oak Grove Drive
Pasadena, California

Paul D. Cohn
Battelle-Northwest
P.O. Box 999
713 Bldg., 700 Area
Richland, Washington 99352

Oak Ridge National Laboratory
P.O. Box Y
Oak Ridge, Tennessee 37831
ATTN: R. E. MacPherson

Dr. James Hadley
Head, Reactor Division
Lawrence Radiation Laboratory
Livermore, California (2)

Curtiss-Wright Corporation
Wright Aero Division
Wood-Ridge, New Jersey 07075
ATTN: W.A.D. Librarian

North Carolina State University
Department of Chemical Engineering
Raleigh, North Carolina 27601
ATTN: Prof. J. K. Ferrell

Contract NAS 3-2528

North American Aviation, Inc.
Atomics International
P.O. Box 309
Canoga Park, California 91304
ATTN: Director, Liquid Metals
Information Center

General Electric Company
175 Curtner Avenue
San Jose, California
ATTN: D. H. Imhoff

General Electric Company
175 Curtner Avenue
San Jose, California
ATTN: Dr. S. Levy

General Electric Company
175 Curtner Avenue
San Jose, California
ATTN: Dr. E. L. Zebroski